CA1
DTC 801
82
P631
c.2

**MARTEC Limited**

OCEAN SCIENCE &
ENGINEERING CONSULTANTS

FINAL REPORT

# PROPELLER/ICE INTERACTION: A PARAMETRIC STUDY OF PROPELLERS OPERATING IN AN ICE ENVIRONMENT

TP 4021E

Library and Information Centre / Centre de Documentation (GSLA)
RECEIVED - REÇU LE
SEP 8 1983
Transport Canada / Transports Canada

December 1982

By:

M.E. Norwood
C.G. DesRochers
J.L. Warner

Prepared for:

TRANSPORTATION DEVELOPMENT CENTRE
1000 Sherbrooke Street, West
Montreal, Quebec
H3A 2R3

Submitted by:

MARTEC LIMITED
5670 Spring Garden Road
Halifax, Nova Scotia
B3J 1H6

PROJECT TEAM

J.L. Warner
M.E. Norwood
C.G. DesRochers

The contents of this report reflect the views of the Contractor and not necesssarily the official views of the Transportation Development Centre.

# REPORT DOCUMENTATION FORM

| 1. Transport Canada Report No | 2 TDC Project No | 3. Recipient's Catalogue No |
|---|---|---|
| TP 4021E | | |

| 4 Title and Subtitle | 5 Report Date |
|---|---|
| Propeller/Ice Interaction: A Parametric Study of Propellers Operating in an Ice Environment | December 1982 |
| | 6. Performing Organization Report No |
| 7. Author(s) | 8 Transport Canada File No |
| M.E. Norwood, C.G. DesRochers and J.L. Warner | |
| 9 Performing Organization Name and Address | 10 DSS File No |
| Martec Limited<br>5670 Spring Garden Road<br>Halifax, Nova Scotia<br>B3J 1H6 | 10SD.T8200-1-1557 |
| | 11 DSS or Transport Canada Contract No |
| | 1SD81-00129 |
| 12 Sponsoring Agency Name and Address | 13 Type of Report and Period Covered |
| Transportation Development Centre (TDC)<br>Suite 2421<br>1000 Sherbrooke Street West<br>Montreal, Quebec H3A 2R3 | Final Dec. 1981 - Sept. 1982 |
| | 14 Sponsoring Agency Code |
| 15 Supplementary Notes | 16 TDC Project Officer |
| | I.M. Bayly |

17 Abstract

A parametric study of propellers operating in an ice environment is presented. A typical modern icebreaker propeller is analyzed. The finite element method is used to model the propeller blade. Simplified loading definitions are used. Results of studies carried out to assess the sensitivities to a number of geometric parametric variations, using a nominal loading of uniformly distributed pressure over a depth of the blade, are presented. Stress distribution patterns and critical points of failure are looked at. The effect of chord-wise distribution of pressure due to blade/ice interaction forces are investigated. The most sensitive geometric parameters affecting stress levels were found to be blade diameter, blade thickness and section size. Also, it was found that stress distribution patterns and areas of critical stress depend largely on the assumed pressure distribution representing the blade/ice interaction forces. Consequently, the need for further work on a realistic description of propeller/ice interaction forces is indicated.

| 18 Key Words | 19 Distribution Statement |
|---|---|
| Propeller/ice interaction, parametric study, blade stresses, finite element method | |

| 20 Security Classification (of this report) | 21 Security Classification (of this page) | 22 No of Pages | 23 Price |
|---|---|---|---|
| Nil | Nil | 131 | Nil |

TDC 001 (7/83)

# FORMULE DE DOCUMENTATION POUR RAPPORT

| 1 N° du rapport Transports Canada | 2 N° de l'étude — CDT | 3 N° de catalogue du destinataire |
|---|---|---|
| TP 4021E | | |

| 4 Titre et sous-titre | 5 Date du rapport |
|---|---|
| Interaction entre hélice et glace: étude paramétrique d'helices fonctionnant dans un milieu glacé. | December 1982 |
| | 6 N° du rapport de l'organisme exécutant |

| 7 Auteur(s) | 8 N° de dossier Transports Canada |
|---|---|
| M.E. Norwood, C.G. DesRochers and J.L. Warner | |

| 9 Nom et adresse de l'organisme exécutant | 10 N° de dossier — ASC |
|---|---|
| Martec Limited<br>5670 Spring Garden Road<br>Halifax, Nova Scotia<br>B3J 1H6 | 10SD.T8200-1-1557 |
| | 11 N° de contrat — ASC ou Transports Canada |
| | 1SD81-00129 |

| 12 Nom et adresse de l'organisme parrain | 13 Genre de rapport et période visée |
|---|---|
| Transportation Development Centre (TDC)<br>Suite 2421<br>1000 Sherbrooke Street West<br>Montreal, Quebec H3A 2R3 | Final Dec. 1981 - Sept. 1982 |
| | 14 Code de l'organisme parrain |

| 15 Remarques additionnelles | 16 Agent de projet — CDT |
|---|---|
| | I.M. Bayly |

17 Resume


Une étude paramétrique se penche sur le comportement d'une hélice dans un milieu contaminé par la glace. La méthode d'éléments finis est utilisée pour représenter une hélice typique de brise-glaces modernes. La distribution des forces sur la surface de la lame d'une hélice est décrite d'une façon simple. Pour une pression uniforme exercée sur une certaine longueur de la lame, on détermine l'importance de plusieurs paramètres géométriques. La distribution du stress, ainsi que des points critiques pour le bris sont examinées. L'effet d'une distribution latérale non-uniforme de la pression est aussi étudié. Les paramètres les plus importants au niveau des stress sonts le diamètre, l'épaisseur et la surface de coupe de la lame. On conclus également que la distribution du stress et des zones critiques dépend en grande partie de la distribution des forces choisies pour représenter l'intéraction entre la glace et l'hélice. Il semble donc nécessaire d'approfondir la recherche sur les forces d'intéraction entre hélice et glace.


| 18 Mots-clés | 19 Diffusion |
|---|---|
| Interaction hélice/glace, étude paramétrique, méthode d'éléments finis | |

| 20 Classification de sécurité (de ce rapport) | 21 Classification de sécurité (de cette page) | 22 Nombre de pages | 23 Prix |
|---|---|---|---|
| Nil | Nil | 131 | Nil |

CDT/TDC 79-005

# TABLE OF CONTENTS


| | Page |
|---|---|
| Table of Contents | i |
| List of Tables | ii |
| List of Figures | iii |
| 1. Introduction | 1 |
| 2. Finite Element Model | 2 |
| 3. Outline of Parametric Study | 4 |
| 4. Summary of Results | 6 |
| 4.1 Sensitivity Analysis of Geometric Parameters | 6 |
| 4.2 Effect of Various Loading Formulations | 9 |
| 5. Discussion and Conclusion | 11 |
| Tables | 12 |
| Figures | 17 |
| References | |
| Nomenclature | |

# LIST OF TABLES


| | | Page |
|---|---|---|
| Table 1 | Geometric Parameters Considered in Sensitivity Analysis | 12 |
| Table 2 | Summary of Results from Analysis of Existing Blade | 13 |
| Table 3 | Summary of Results from Sensitivity Analysis of Geometric Parameters | 14 |
| Table 4 | Change in Maximum Stress (MPa) Due to 10% Variation in Parameters | 16 |

# LIST OF FIGURES


| | | Page |
|---|---|---|
| Figure 1 | Finite Element Idealization | 17 |
| Figure 2 | Computer Plots of Blade Geometry | 18 |
| Figure 3 | Finite Element Analysis Using 20-Noded Solid Elements | 20 |
| Figure 4 | Finite Element Analysis Using Thick/Thin Shell Elements | 21 |
| Figure 5 | Blade Loading | 22 |
| Figure 6 | Types of Pressure Distribution Considered | 23 |
| Figures 7 to 9 | Principal Stress Contours for Existing Blade - Load Case Type A | 24 |
| Figures 10 to 12 | Principal Stress Directions for Existing Blade - Load Case Type A | 27 |
| Figures 13 to 18 | Radial and Tangential Stress Contours for Existing Blade - Load Case Type A | 30 |
| Figures 19 to 24 | Principal Stress Contours for Variations in Rake | 36 |
| Figure 25 | Effect of Rake on Maximum Stress | 42 |
| Figures 26 to 31 | Principal Stress Contours for Variations in Skew | 43 |
| Figure 32 | Effect of Skew on Maximum Stress | 49 |
| Figures 33 to 38 | Principal Stress Contours for Rotations about Spindle Axis | 50 |
| Figure 39 | Effect of Rotation about Spindle Axis on Maximum Stress | 56 |
| Figures 40 to 45 | Principal Stress Contours for Variations P/D Ratios | 57 |
| Figure 46 | Effect of P/D Ratio on Maximum Stress | 63 |
| Figures 47 to 58 | Principal Stress Contours for Variations in Chord Thickness | 64 |

LIST OF FIGURES (Continued)


| | | Page |
|---|---|---|
| Figure 59 | Effect of Blade Thickness on Maximum Stress | 76 |
| Figures 60 to 65 | Principal Stress Contours for Variations in Chord and Maximum Thickness | 77 |
| Figure 66 | Effect of Length and Maximum Thickness of Chord on Maximum Stress | 83 |
| Figures 67 to 72 | Principal Stress Contours for Variations in Blade Diameter | 84 |
| Figure 73 | Effect of Blade Diameter on Maximum Stress | 90 |
| Figure 74 | Maximum Stress versus Cutting Depth for Various Blade Diameters | 91 |
| Figure 75 | Maximum Stress versus Blade Diameter for Various Cutting Depths | 92 |
| Figures 76 to 81 | Principal Stress Contours for Variations in Hub Diameter | 93 |
| Figure 82 | Effect of Hub Diameter on Maximum Stress | 99 |
| Figures 83 to 88 | Principal Stress Contours for Variations in Both Blade and Hub Diameters | 100 |
| Figures 89 to 91 | Change in Maximum Stress vs. Variation in Parameter | 106 |
| Figures 92 to 97 | Principal Stress Contours for Existing Blade - Load Case Types B and C | 109 |
| Figures 98 to 103 | Principal Stress Directions for Existing Blade - Load Case Types B and C | 115 |
| Figure 104 | Variation of Maximum Stress with Cutting Depth | 121 |

## 1. Introduction

This report describes work carried out under DSS/TDC Contract No. 1SD81-00129 on the stress analysis of modern icebreaker propellers subjected to propeller/ice interaction forces. The aim has been to employ the finite element of structural analysis to this complex problem, with the objective of developing a reliable technique to be used in establishing ice class rules which will enable effective design and regulation of propellers for Arctic service.

The work plan for the project has been divided into two parts, i.e. (i) a parametric study of propellers operating in an ice environment using simplified loading definitions, and (ii) an investigation into the problem of predicting propeller/ice interaction forces, considering stress and fracture patterns in the ice milling process. This report describes the work relating to the parametric study; the work relating to the predicting of propeller/ice interaction forces is presented in another report (Reference 1).

The intended scope of the parametric study is as follows:

(i) Analyze a typical modern icebreaker propeller using a nominal loading of uniformly distributed pressure over a depth of the blade immersed in a block of ice.

(ii) Carry out studies to assess sensitivities to a number of geometric parameter variations.

(iii) Study the effect of more realistic blade loading formulations (if identified) on stress distribution patterns and critical points of failure.

The Department of National Defence/Martec finite element stress analysis program for marine propellers (Reference 2) has been used in the parametric study. A brief summary of the method and a description of the finite element model used in the analysis are given in Section 2.

An outline of the parametric study is given in Section 3 and the results are summarized in Section 4.

## 2. Finite Element Model

The finite element method is a computer analysis technique which provides numerical solutions to problems in structural mechanics. The special advantages of the method lie in its ability to represent highly irregular and complex structures and loading situations. This makes it ideal for the analysis of propellers operating in an ice environment.

The basis of the finite element method is the representation of a structure by an assemblage of subdivisions called finite elements. These elements are inconnected at joints which are called nodes (or nodal points). Functions are chosen to relate the displacements within each element to the displacements at the nodes. Equilibrium equations relating nodal displacements to nodal forces are formed. The equilibrium equations are solved to obtain unknown nodal point displacements resulting from applied nodal forces. Once determined, the nodal point displacements are used to compute reaction forces and element stresses.

The fineness of the element mesh (i.e. the number of elements) depends to a large extent on the type of element used. Over the years, propeller analysts have used elements ranging from simple flat two-dimensional elements to more advanced curved three-dimensional elements. Results indicate quite clearly that curved three-dimensional elements permit the use of much coarser meshes, thus minimizing problem size and, consequently, computer costs.

The DND/Martec program offers two types of curved three-dimensional elements for modelling propellers, i.e. a 20-noded solid element and an eight-noded thick/thin shell element. These elements are shown in Figure 1(a). The 20-noded solid element has three degrees-of-freedom per node (translations in x, y and z) for a total of 60 degrees-of-freedom. The thick/thin shell element has five degrees of freedom per node (translations in x, y and z plus two local rotations), but because it has only eight nodes, it has a total of 40 degrees-of-freedom. The elements are identical with respect to geometry.

Because of the fact that the thick/thin shell element has fewer degrees-of-freedom than the 20-noded solid element, it is more economical to use. Unfortunately, in areas of large thickness, it cannot be expected to yield results as accurate as the 20-noded solid element. However, the element does avoid the assumption that normals remain normal after deformations, thus permitting shear deformation (an important feature in thick shell situtations).

The CCGS Pierre Radisson/Franklin propeller (Reference 3) was selected as the typical icebreaker propeller to be analyzed. The finite element model of the blade and root is shown in Figure 1(b). A total of 20 elements were used, 16 for the blade and 4 for the root area containing the fillet. The hub below the fillet was assumed to be infinitely stiff. This three-dimensional model was generated by special pre-processing routines contained in the DND/Martec program. The geometric description of the propeller was entered in the form of blade radius, section offsets,

section pitch angles, rake and skew obtained from Reference 3. This information was transformed by the program into three-dimensional spacial coordinates. Computer plots describing the blade geometry are given in Figure 2.

For the purpose of selecting the type of element which should be used in the parametric study, the blade was first modelled using 20-noded solid elements and then using thick/thin shell elements, the former requiring a total of 188 nodes (564 degrees-of-freedom), and the latter requiring a total of 79 nodes (395 degrees-of-freedom). Computer results for the two analyses are shown in Figures 3 and 4. As can be seen, the results are reasonably close. However, the cost of doing an analysis using 20-noded elements was found to be about four times the cost of an analysis using thick/thin shell elements. Consequently, the thick/thin shell element was selected for the parametric study.

## 3. Outline of Parametric Study

The parametric study has involved: (i) a sensitivity analysis of geometric parameters using a nominal loading of a uniformly distributed pressure over various depths of blade immersion in ice, and (ii) a study of the effect of more realistic blade loading formulations on stress distribution patterns and critical points of failure.

For the sensitivity analysis of geometric parameters, effects of variations in skew, rake, pitch, thickness, section size, blade diameter, and hub diameter were considered. The nature of the variations is given in Table 1. Each new configuration was analyzed for 3 cutting depths. Blade loading was applied as shown in Figure 5. Maximum stresses, maximum displacements, and pressure resultants ($F_x$, $F_y$, $F_z$, $M_x$, $M_y$, and $M_z$, see Figure 5) were recorded. Stress distributions in the form of stress contour plots were obtained. The results are presented in Section 4.

In the coordinate system shown in Figure 5, the y axis represents the spindle axis of the blade, the spindle axis being the axis about which the blade pivots during pitch changes. The z axis corresponds to the shaft axis of rotation. Therefore, the pressure resultants $F_z$, $M_y$ and $M_z$ relate to, respectively, thrust, spindle torque and shaft torque.

As a first step toward determining the effects of more realistic blade loading formulations on stress distribution patterns and critical points of failure, two different types of pressure distribution were considered. They represent the cases when: (i) a uniform pressure distribution is assumed to act only on the leading edge area of the blade; and (ii) a uniform pressure distribution is assumed to act only on the trailing edge area of the blade. The unmodified CCGS Pierre Radisson/Franklin blade was used in this investigation. The loadings are shown in Figure 6. The results are presented in Section 4.

The different loadings used in the study are shown in Figure 6. In all, three different cutting depths were considered, using three different chordwise pressure distributions for each cutting depth. L1, L2 and L3 refer to the cutting depths of 0.17 R, 0.33 R and 0.50 R, respectively. Type A refers to a uniform chordwise distribution, Type B refers to the case where chordwise pressure is concentrated at the leading edge, and Type C refers to the case where chordwise pressure is concentrated at the trailing edge.

During full scale trials in ice of the CCGS Pierre Radisson, a forward thrust of 725,211 pounds (2.566 MNt) was measured during one of the most significant propeller milling incidents recorded (see Reference 4). For a cutting depth of 1 m, a uniform pressure of 1.83 MPa is required to produce this thrust. Ice induced thrust depends largely on the crushing strength of the ice, which, unfortunately, is very difficult to define. Salinity, depth, age and strain rate are some of the factors affecting the strength of ice. Reference 5 states that in current U.S. Coast Guard work, the crushing strength of ice is typically taken as 2.6

MPa. However, tests show that typical values for the uniaxial compressive strength of ice fall within the range of 1 to 10 MPa (eg. References 6 and 7).

The problem of defining a suitable criteria for establishing the crushing strength of ice was not within the scope of the present investigation. Consequently, it was decided to use a pressure of 1.83 MPa for all uniform chordwise pressure distributions (i.e. load cases L1-A, L2-A and L3-A). Furthermore, in order to provide insight on the importance of assumed pressure loading on stress levels when the thrust is known (eg. measured), constant thrust for a particular cutting depth was maintained. This was achieved by using a pressure of 7.36 MPa for pressure distribution Types B and C.

Stresses are linearily proportional to the applied pressure. Hence, the results presented in Section 4 can be used to compute stresses for any value of applied pressure.

## 4. Summary of Results

### 4.1 Sensitivity Analysis of Geometric Parameters

First, the unmodified CCGS Pierre Radisson/Franklin blade was analyzed for load cases L1-A, L2-A and L3-A (see Figure 6). A pressure of 1.83 MPa was used for all three cases.

The results are summarized in Table 2. Contour plots of primary principal stresses are shown in Figures 7, 8 and 9. Principal stress directions are shown in Figures 10 to 12. Contour plots of radial and tangential stresses are shown in Figures 13 to 18.

The maximum stress was found to occur at the top of the blade root fillet, the direction of the stress varying very little with changes in the cutting depth. The stress distribution for this loading case is roughly symmetrical about the 50% chord (mid-chord) line for all three cutting depths.

After the analysis of the unmodified blade was completed, the configuration of the blade was changed in accordance with Table 1. Each new configuration was analyzed for load cases L1-A, L2-A and L3-A. Again, a pressure of 1.83 MPa was used for each case.

#### Rake

The rake was varied from a value of zero to 514.8 mm which is twice the rake of the existing blade.

The results of the analysis are summarized in Table 3. Contour plots of the primary principal stresses are shown in Figures 19 to 24. A plot of the rake versus maximum stress is shown in Figure 25.

The effect of rake variation was found to be relatively small, amounting to a zero to six percent decrease in stress for the range of rakes considered. There was no significant change in the distribution of the stresses, and the maximum stress remained near the root fillet.

#### Skew

The skew was varied from a value of zero to twice that of the existing blade.

The results of the analysis are summarized in Table 3. Contour plots of the primary principal stresses are shown in Figures 26 to 31. Figure 32 shows a plot of skew versus maximum stress.

As the skew was increased, the value of maximum stress increased significantly, and the location of maximum stress moved towards the trailing edge of the blade.

Pitch

Two different methods were employed to study the effects of varying pitch.

The first consisted of rotating the entire blade $\pm$ 20 degrees about its spindle axis. A positive rotation represents an increase in pitch.

The results are summarized in Table 3. Contour plots of the primary principal stresses are shown in Figures 33 to 38. A plot of change in pitch versus maximum stress is shown in Figure 39.

The results show a small decrease in stress with increasing pitch, accompanied by a substantial shifting of the point of maximum stress towards the trailing edge of the blade.

The second method employed to study the effects of varying pitch involved varying the pitch to diameter (P/D) ratio from 0.50 to 1.00. The P/D ratio for the existing blade falls in the middle of this range.

The results are summarized in Table 3. Stress contour plots are shown in Figures 40 to 45, and plots of P/D ratios versus maximum stress are given in Figure 46.

Again, the results show a small decrease in the maximum stress with increasing P/D ratios. However, now there is only a slight shifting of the point of maximum stress towards the trailing edge.

Blade Thickness

Two methods of changing the thickness of the existing blade were used to determine the significance of blade thickness on stresses. In the first method, the blade thickness was increased uniformly by 5 and 10 percent from the root to the tip. In the second method, the blade thickness was increased by 5 and 10 percent at the root with the increases tapering (linearily) to zero at the tip.

The results are summarized in Table 3. Stress contour plots, and plots of increase in blade thickness versus maximum stress are given in Figures 47 to 59.

The uniform increases in blade thickness had essentially no effect on the stress distribution on the blade but did result in a decrease in the maximum stress.

The linear increases in the blade thickness had the effect of reducing the maximum stress for all three loading cases, but also had an effect on the stress distribution. The stresses were increased near the tip relative to the root for all loading cases. Furthermore, the position of maximum stress was shifted from the root fillet to a point further up the blade (i.e. towards the tip) for load case L1-A.

Section Size

The blade section size was increased by increasing both chord length and maximum section thickness, while holding the chord length to thickness ratio constant. The increase in chord length and maximum section thickness, expressed as a percentage of the existing blade, was held constant from blade root to blade tip. Increases of 10 and 20 percent were considered. This particular form of parameter variation does not affect the blade radius but does result in increased blade area.

The results are summarized in Table 3. Stress contour plots are shown in Figures 60 to 65. Plots of increase in size versus maximum stress are shown in Figure 66.

Figure 66 shows a decrease in the maximum stress with increasing size for all three loading cases.

Blade Diameter

The blade diameter was increased to 5150 mm and 6180 mm from the existing 4120 mm. This represents a 25 percent and 50 percent increase in the blade diameter.

The results are summarized in Table 3. Stress contour plots are shown in Figures 67 to 72. Plots of blade diameter versus maximum stress are shown in Figure 73. Figure 74 shows the maximum stress versus the cutting depth for the existing blade and the two modified blades. Figure 75 shows the effects of increasing the blade diameter on the maximum stress for selected cutting depths.

Figure 74 shows that, for constant cutting depths, the maximum stress is increased as the blade diameter is increased. For small increases in diameter, the increase in stress is small; for large increases in diameter, the stresses are increased significantly.

Hub Diameter

In order to determine the effect of hub diameter on blade stresses, two runs were made. The first run was conducted with the hub diameter increased 10 percent, and the second run with a 10 percent decrease in the hub diameter.

The results are summarized in Table 3. Stress contour plots are shown in Figures 76 to 81. Maximum stress versus increase in hub diameter are shown in Figure 82.

Results show that an increase in the hub diameter of 10 percent produces a change in maximum stress ranging from zero percent for a small cutting depth (load case L1-A) to a decrease of about five percent for a large cutting depth (load case L3-A). For a 10 percent decrease in hub diameter, the change in maximum stress ranged from zero percent for the small cutting depth to an increase of about five percent for the large cutting depth.

Blade Diameter/Hub Diameter

In order to show the combined effect of changes in both blade and hub diameters, the following two runs were made: (i) a 50 percent increase in blade diameter accompanied by a 10 percent increase in hub diameter, and (ii) a 50 percent increase in blade diameter accompanied by a 10 percent decrease in hub diameter.

The results are summarized in Table 3, and stress contour plots are shown in Figures 83 to 88. Plots of blade diameter versus maximum stress for the different hub diameters are shown in Figure 73.

Summary

Changes in maximum stress due to 10 percent variation in the geometric parameters investigated are provided in Table 4.

The percent change in maximum stress versus percent change in geometric parameter (within the range of $\pm$ 10 percent) is shown in Figures 89 to 91. There diagrams are based on the assumption that change in maximum stress varies linearily with change in parameter, which is a reasonable approximation for demonstrating the effect of small variations in parameters (i.e. up to $\pm$ 10 percent).

## 4.2 Effect of Various Loading Formulations

Analyses were performed on the existing blade for non-uniform chordwise pressure distributions, i.e. load cases L1-B, L2-B, L3-B, L1-C, L2-C, and L3-C (see Figure 6). The results are summarized in Table 2. The stress contours are shown in Figures 92 to 97. Stress directions are shown in Figures 98 to 103.

For load cases of Type B, i.e. with the pressure acting on the leading edge area of the blade, the location of the maximum stress changed significantly with the cutting depth. For the deepest cut (load case L3-B), the maximum stress occurred at the top of the blade root fillet. This area of high stress remained as the cutting depth was decreased. However, a new area of stress concentration developed toward the blade tip. Furthermore, for the shallowest cut (load case L1-B), the value of stress in this area was found to be higher than the stress developed at the blade root.

For load cases of Type C, i.e. with the pressure acting on the trailing edge area of the blade, the stresses were generally concentrated along the trailing edge. The location of maximum stress shifted towards the tip with decreasing cutting depth. The value of maximum stress for load cases of Type C were found to be the highest of all three types of loading cases.

Figure 104 shows the variation of maximum stress with cutting depth for the three types of pressure distributions considered (i.e. Types A, B and C). It is seen that the difference in maximum stress between Types

A and B becomes less with increasing cutting depth, while the reverse is true for Types A and C. This suggests a possible adverse effect of blade skew on stress when the blade is subjected to trailing edge forces. It should be noted that the results shown in Figure 104 are based on constant thrust for a particular cutting depth. As indicated in Section 3, this was achieved by using a pressure of 7.36 MPa for pressure distribution Types B and C. Obviously, if a pressure of 1.83 MPa had been used throughout, blade stresses for pressure distribution Types B and C would be much less than those shown in Figure 104.

## 5. Discussion and Conclusion

The most sensitive geometric parameters affecting stress levels in the Pierre Radisson/Franklin blade were found to be blade diameter, blade thickness and section size. Variations in rake skew and pitch had little effect on stresses. However, the conclusions drawn from the sensitivity analysis are based on a simplified representation of propeller/ice interaction, i.e. a uniformly distributed pressure over the depth of the blade immersed in ice. This approach fails to take into account the complex relationship between skew, rake and pitch, and propeller/ice interaction forces. Consequently, it cannot be assumed that the true influence of rake, skew and pitch on blade stresses has been determined.

Stress levels in the CCGS Pierre Radisson/Franklin propeller operating in ice are largely dependent upon the cutting depth. The stress distribution and areas of critical stress depend on both the cutting depth and chordwise distribution of pressure due to the blade/ice interaction forces. When the chordwise pressure distribution is uniform, the maximum stress develops near the blade root, and the stress distribution is approximately symmetric about the mid-chord line; when the chordwise pressure is concentrated at the leading or trailing edge, the stress distribution is no longer symmetric, and for shallow cutting depths, the location of maximum stress shifts towards the blade tip. This indicates that the description of propeller/ice interaction forces is a very important consideration in the stress analysis of propellers. Furthermore, the complexity of stress patterns under the more sophisticated load descriptions emphasizes the need for using the finite element method.

TABLE 1

GEOMETRIC PARAMETERS CONSIDERED IN SENSITIVITY ANALYSIS

| Parameter | Nature of Variation | Comments |
|---|---|---|
| Skew | zero skew<br>twice existing skew | Blade radius, section sizes and depths of immersion same as existing blade. No significant change in loaded areas (for load cases L1, L2, and L3). |
| Rake | zero rake<br>twice existing rake | Blade radius, section sizes and depths of immersion same as existing blade. No significant change in loaded areas. |
| Pitch | P/D ratio = 0.5<br>P/D ratio = 1.0 | Blade radius, section sizes and depths of immersion same as existing blade. No significant change in loaded areas. |
| | - 20° rotation about spindle axis<br>+ 20° rotation about spindle axis | Blade radius, section sizes and depths of immersion same as existing blade. No significant change in loaded areas. |
| Thickness | 5% increase in thickness over entire area<br>10% increase in thickness over entire blade<br>5% increase in thickness at root, zero percent increase at tip and linear variation between<br>10% increase in thickness at root, zero percent increase at tip and linear variation between | Blade radius, chord lengths and depths of immersion same as existing blade. No change in loaded areas. |
| Section size (maintaining same t/c proportions) | 10% increase in chord and thickness<br>20% increase in chord and thickness | Blade radius and depths of immersion same as existing blade. Significant change in loaded areas. |
| Blade diameter | 25% increase in blade diameter<br>50% increase in blade diameter | Blade section size vs. fraction radius same as existing blade. Significant change in depths of immersion and loaded areas. |
| Hub diameter | 10% increase in hub diameter<br>10% decrease in hub diameter | Blade radius, section sizes and depths of immersion same as existing blade. No change in loaded areas. |
| Blade/hub diameter | 50% increase in blade diameter and 10% increase in hub diameter<br>50% increase in blade diameter and 10% decrease in hub diameter | Blade section size vs. fraction radius same as existing blade. Significant change in depths of immersion and loaded areas. |

TABLE 2

SUMMARY OF RESULTS FROM ANALYSIS OF EXISTING BLADE

| Blade Loading Case | Uniform Pressure of 1.83 MPa for Load Type A and 7.36 MPa for Load Types B and C | | | | | | | | Normalized for a Fz (Thrust) of 1 MNt. | |
|---|---|---|---|---|---|---|---|---|---|---|
| | Fx (MNt.) | Fy (MNt.) | Fz (MNt.) | Mx (Nt.mx10$^{-8}$) | My (Nt.mx10$^{-8}$) | Mz (Nt.mx10$^{-8}$) | Maximum Deflection (mm) | Maximum Stress (MPa) | Pressure (MPa) | Maximum Stress (MPa) |
| L1-A | -0.19 | 0.052 | -0.62 | -14.10 | -5.0 | 4.2 | -5.007 | -130 | 2.95 | 210 |
| L1-B | -0.18 | 0.100 | -0.62 | -16.0 | -10.6 | 5.3 | -2.722 | -162 | 11.87 | 261 |
| L1-C | -0.20 | 0.005 | -0.62 | -18.9 | -1.8 | 5.3 | -7.186 | -209 | 11.87 | 337 |
| L2-A | -0.52 | 0.129 | -1.54 | -27.1 | -9.4 | 9.2 | -8.011 | -259 | 1.19 | 168 |
| L2-B | -0.46 | 0.297 | -1.55 | -29.9 | -23.0 | 11.4 | -4.225 | -281 | 4.75 | 181 |
| L2-C | -0.55 | -0.042 | -1.55 | -36.6 | -0.3 | 11.7 | -12.35 | -368 | 4.75 | 237 |
| L3-A | -0.95 | 0.219 | -2.55 | -37.3 | -12.4 | 14.6 | -8.950 | -329 | 0.72 | 129 |
| L3-B | -0.87 | 0.572 | -2.55 | -40.7 | -34.4 | 17.8 | -4.649 | -347 | 2.89 | 136 |
| L3-C | -1.01 | -0.151 | -2.57 | -49.9 | 3.9 | 18.9 | -12.68 | -482 | 2.86 | 188 |

TABLE 3

SUMMARY OF RESULTS FROM SENSITIVITY ANALYSIS OF GEOMETRIC PARAMATERS

| Parameter | Nature of Variation | Blade Loading Case | Uniform Pressure of 1.83 MPa | | | | | | | | Normalized for Fz (Thrust) of 1 MNt. | |
|---|---|---|---|---|---|---|---|---|---|---|---|---|
| | | | Fx (MNt.) | Fy (MNt.) | Fz (MNt.) | Mx (Nt.mx10-8) | My (Nt.mx10-8) | Mz (Nt.mx10-8) | Maximum Deflection (mm) | Maximum Stress (MPa) | Pressure (MPa) | Maximum Stress (MPa) |
| Rake | Zero rake | L1-A | -0.16 | 0.050 | -0.62 | -13.8 | -4.3 | 4.2 | -4.93 | -134 | 2.95 | -216 |
| | | L2-A | -0.45 | 0.123 | -1.54 | -26.4 | -8.1 | 9.2 | -7.91 | -266 | 1.19 | -173 |
| | | L3-A | -0.85 | 0.196 | -2.55 | -36.4 | -10.4 | 14.6 | -8.84 | -336 | 0.72 | -132 |
| | Twice existing rake | L1-A | -0.22 | 0.159 | -.62 | -15.0 | -5.8 | 4.2 | -5.394 | -134 | 2.95 | -216 |
| | | L2-A | -0.59 | 0.386 | -1.54 | -28.8 | -11.1 | 9.2 | -8.567 | -250 | 1.19 | -162 |
| | | L3-A | -1.06 | 0.635 | -2.55 | -39.6 | -14.7 | 14.5 | -9.535 | -316 | 0.72 | -124 |
| Skew | Zero skew | L1-A | -0.17 | 0.108 | -0.62 | -14.7 | -0.5 | 4.2 | -4.625 | -122 | 2.95 | -197 |
| | | L2-A | -0.46 | 0.263 | -1.54 | -28.2 | -1.1 | 9.2 | -7.310 | -242 | 1.19 | -157 |
| | | L3-A | -0.87 | 0.434 | -2.55 | -38.6 | -1.7 | 14.6 | -8.122 | -306 | 0.72 | -120 |
| | Twice existing skew | L1-A | -0.20 | -0.005 | -0.62 | -12.1 | -9.1 | 4.2 | -5.983 | -142 | 2.95 | -229 |
| | | L2-A | -0.53 | -0.013 | -1.54 | -23.6 | -17.1 | 9.2 | -9.879 | -283 | 1.19 | -184 |
| | | L3-A | -0.99 | -0.011 | -2.55 | -33.1 | -22.4 | 14.5 | -11.230 | -377 | 0.72 | -148 |
| Pitch | Pitch/diameter ratio = 0.5 | L1-A | -0.14 | 0.069 | -0.63 | -14.4 | -4.8 | 2.9 | -5.306 | -136 | 2.90 | -216 |
| | | L2-A | -0.38 | 0.172 | -1.58 | -27.9 | -9.1 | 6.3 | -8.516 | -269 | 1.16 | -170 |
| | | L3-A | -0.69 | 0.287 | -2.64 | -38.7 | -11.9 | 10.1 | -9.524 | -339 | 0.69 | -128 |
| | Pitch/diameter ratio = 1.0 | L1-A | -0.24 | 0.035 | -0.60 | -14.0 | -5.2 | 5.2 | -5.045 | -125 | 3.05 | -208 |
| | | L2-A | -0.64 | 0.089 | -1.49 | -26.7 | -9.7 | 10.9 | -7.886 | -250 | 1.23 | -168 |
| | | L3-A | -1.18 | 0.156 | -2.45 | -36.1 | -12.7 | 17.3 | -8.433 | -320 | 0.75 | -131 |
| | - 20° rotation about spindle axis | L1-A | -0.39 | 0.36 | -0.52 | -12.0 | -5.7 | 9.0 | -4.665 | -133 | 3.52 | -256 |
| | | L2-A | -1.02 | 0.085 | -1.29 | -22.8 | -10.8 | 18.5 | -7.774 | -249 | 1.42 | -193 |
| | | L3-A | -1.78 | 0.140 | -2.09 | -30.8 | -14.2 | 27.5 | -8.906 | -321 | 0.88 | -154 |
| | + 20° rotation about spindle axis | L1-A | 0.04 | 0.058 | -0.64 | -14.5 | -4.2 | -1.1 | -5.197 | -136 | 2.86 | -213 |
| | | L2-A | 0.07 | 0.153 | -1.61 | -28.2 | -8.0 | -1.2 | -8.380 | -269 | 1.14 | -167 |
| | | L3-A | 0.04 | 0.267 | -2.70 | -39.5 | -10.4 | -0.1 | -9.403 | -339 | 0.68 | -126 |
| Blade Thickness | 5% increase over entire blade | L1-A | -0.19 | 0.052 | -0.62 | -14.1 | -5.0 | 4.2 | -4.419 | -119 | 2.95 | -192 |
| | | L2-A | -0.52 | 0.130 | -1.54 | -27.1 | -9.4 | 9.2 | -7.079 | -237 | 1.19 | -154 |
| | | L3-A | -0.95 | 0.219 | -2.55 | -37.3 | -12.4 | 14.6 | -7.919 | -301 | 0.72 | -118 |
| | 10% increase over entire blade | L1-A | -0.19 | 0.052 | -0.62 | -14.1 | -5.0 | 4.2 | -3.925 | -109 | 2.95 | -176 |
| | | L2-A | -0.52 | 0.130 | -1.54 | -27.1 | -9.4 | 9.2 | -6.297 | -218 | 1.19 | -142 |
| | | L3-A | -0.95 | 0.219 | -2.55 | -37.3 | -12.4 | 14.6 | -7.049 | -277 | 0.72 | -109 |

TABLE 3 (Continued)

SUMMARY OF RESULTS FROM SENSITIVITY ANALYSIS OF GEOMETRIC PARAMATERS

| Parameter | Nature of Variation | Blade Loading Case | Uniform Pressure of 1.83 MPa | | | | | | | | Normalized for a Fz (Thrust) of 1 MNt. | |
|---|---|---|---|---|---|---|---|---|---|---|---|---|
| | | | Fx (MNt.) | Fy (MNt.) | Fz (MNt.) | Mx (Nt.mx10$^{-8}$) | My (Nt.mx10$^{-8}$) | Mz (Nt.mx10$^{-8}$) | Maximum Deflection (mm) | Maximum Stress (MPa) | Pressure (MPa) | Maximum Stress (MPa) |
| Blade Thickness | + 5% at root 0% at tip, linear variation between | L1-A | -0.19 | 0.052 | -0.62 | -14.1 | -5.0 | 4.2 | -4.641 | -119 | 2.95 | -192 |
| | | L2-A | -0.52 | 0.130 | -1.54 | -27.1 | -9.4 | 9.2 | -7.381 | -237 | 1.19 | -154 |
| | | L3-A | -0.95 | 0.219 | -2.55 | -37.3 | -12.4 | 14.6 | -8.229 | -302 | 0.72 | -118 |
| | + 10% at root 0% at tip, linear variation between | L1-A | -0.19 | 0.052 | -0.62 | -14.1 | -5.0 | 4.2 | -4.315 | -115 | 2.95 | -186 |
| | | L2-A | -0.52 | 0.130 | -1.54 | -27.1 | -9.4 | 9.2 | -6.822 | -218 | 1.19 | -142 |
| | | L3-A | -0.95 | 0.219 | -2.55 | -37.3 | -12.4 | 14.6 | -7.592 | -278 | 0.72 | -109 |
| Section Size (Holding thickness/ chord ratio constant) | 10% increase in chord and thickness | L1-A | -0.21 | 0.057 | -0.68 | -15.4 | -5.5 | 4.6 | -3.910 | -112 | 2.69 | -165 |
| | | L2-A | -0.57 | 0.142 | -1.70 | -29.5 | -10.3 | 10.1 | -6.203 | -220 | 1.08 | -129 |
| | | L3-A | -1.04 | 0.238 | -2.81 | -40.4 | -13.5 | 15.9 | -6.907 | -279 | 0.65 | -99 |
| | 20% increase in chord and thickness | L1-A | -0.23 | 0.063 | -0.74 | -16.7 | -6.0 | 5.1 | -3.125 | -97.3 | 2.47 | -132 |
| | | L2-A | -0.62 | 0.154 | -1.86 | -31.9 | -11.2 | 11.0 | -4.924 | -191 | 0.98 | -103 |
| | | L3-A | -1.12 | 0.257 | -3.07 | -43.5 | -14.7 | 17.4 | -5.465 | -240 | 0.78 | -78 |
| Blade Diameter | 25% increase in blade diameter | L1-A | -0.23 | 0.054 | -0.77 | -22.4 | -6.3 | 6.6 | -13.06 | -197 | 2.38 | -256 |
| | | L2-A | -0.63 | 0.135 | -1.93 | -43.3 | -11.9 | 14.4 | -22.08 | -417 | 0.95 | -216 |
| | | L3-A | -1.17 | 0.227 | -3.19 | -60.0 | -15.6 | 22.7 | -25.74 | -567 | 0.57 | -178 |
| | 50% increase in blade diameter | L1-A | -0.27 | 0.055 | -0.93 | -32.6 | -7.5 | 9.5 | -28.54 | -282.0 | 1.97 | -303 |
| | | L2-A | -0.75 | 0.137 | -2.32 | -63.2 | -14.3 | 20.7 | -49.85 | -613.0 | 0.79 | -264 |
| | | L3-A | -1.40 | 0.232 | -3.83 | -87.8 | -18.8 | 32.8 | -59.72 | -864 | 0.48 | -226 |
| Hub Diameter | 10% increase in hub diameter | L1-A | -0.19 | 0.052 | -0.62 | -14.1 | -5.0 | 4.2 | -4.681 | -130 | 2.95 | -210 |
| | | L2-A | -0.52 | 0.130 | -1.57 | -27.1 | -9.4 | 9.2 | -7.337 | -253 | 1.17 | -161 |
| | | L3-A | -0.95 | 0.218 | -2.55 | -37.3 | -12.4 | 14.6 | -8.068 | -313 | 0.72 | -127 |
| | 10% decrease in hub diameter | L1-A | -0.19 | 0.052 | -0.62 | -14.1 | -5.0 | 4.2 | -5.333 | -129 | 2.95 | -208 |
| | | L2-A | -0.52 | 0.130 | -1.54 | -27.1 | -9.4 | 9.2 | -8.697 | -264 | 1.19 | -171 |
| | | L3-A | -0.95 | 0.219 | -2.55 | -37.3 | -12.4 | 14.6 | -9.873 | -345 | 0.72 | -135 |
| Combined Blade and Hub Diameter | + 50% blade diam. - 10% hub diam. | L1-A | -0.27 | 0.055 | -0.93 | -32.6 | -7.5 | 9.5 | -27.40 | -280 | 197 | 301 |
| | | L2-A | -0.75 | 0.137 | -2.32 | -63.2 | -14.3 | 20.7 | -47.37 | -603 | 79 | 260 |
| | | L3-A | 1.40 | 0.232 | -3.83 | -87.8 | -18.8 | 32.8 | -56.19 | -839 | 48 | 220 |
| | + 50% blade diam. - 10% hub diam. | L1-A | -0.27 | 0.055 | -0.93 | -32.6 | -7.5 | 9.5 | -29.72 | -285 | 197 | 306 |
| | | L2-A | -0.75 | 0.137 | -2.32 | -63.2 | -14.3 | 20.7 | -52.43 | -625 | 79 | 269 |
| | | L3-A | -1.40 | 0.232 | -3.83 | -87.8 | -18.8 | 32.8 | -63.42 | -890 | 48 | 232 |

TABLE 4

CHANGE IN MAXIMUM STRESS (MPa) DUE TO 10% VARIATION IN PARAMETERS

| Paramter | Cutting Depth (m) (Pressure = 1.83 MPa) | | |
|---|---|---|---|
| | 0.34 | 0.67 | 1.00 |
| Rake | +0 | -2 | -3 |
| Skew | +3 | +5 | +8 |
| Rotation about Spindle Axis | 0 | -2 | -2 |
| P/D Ratio | -1 | -2 | -2 |
| Thickness | -20 | -40 | -53 |
| Thickness and Chord | -18 | -35 | -45 |
| Blade Diameter | +11 | +30 | +53 |
| Hub Diameter | 0 | -5 | -15 |

NOTE: + indicates that an increase in the parameter results in an increase in stress.

- indicates that an increase in the parameter results in decrease in stress.

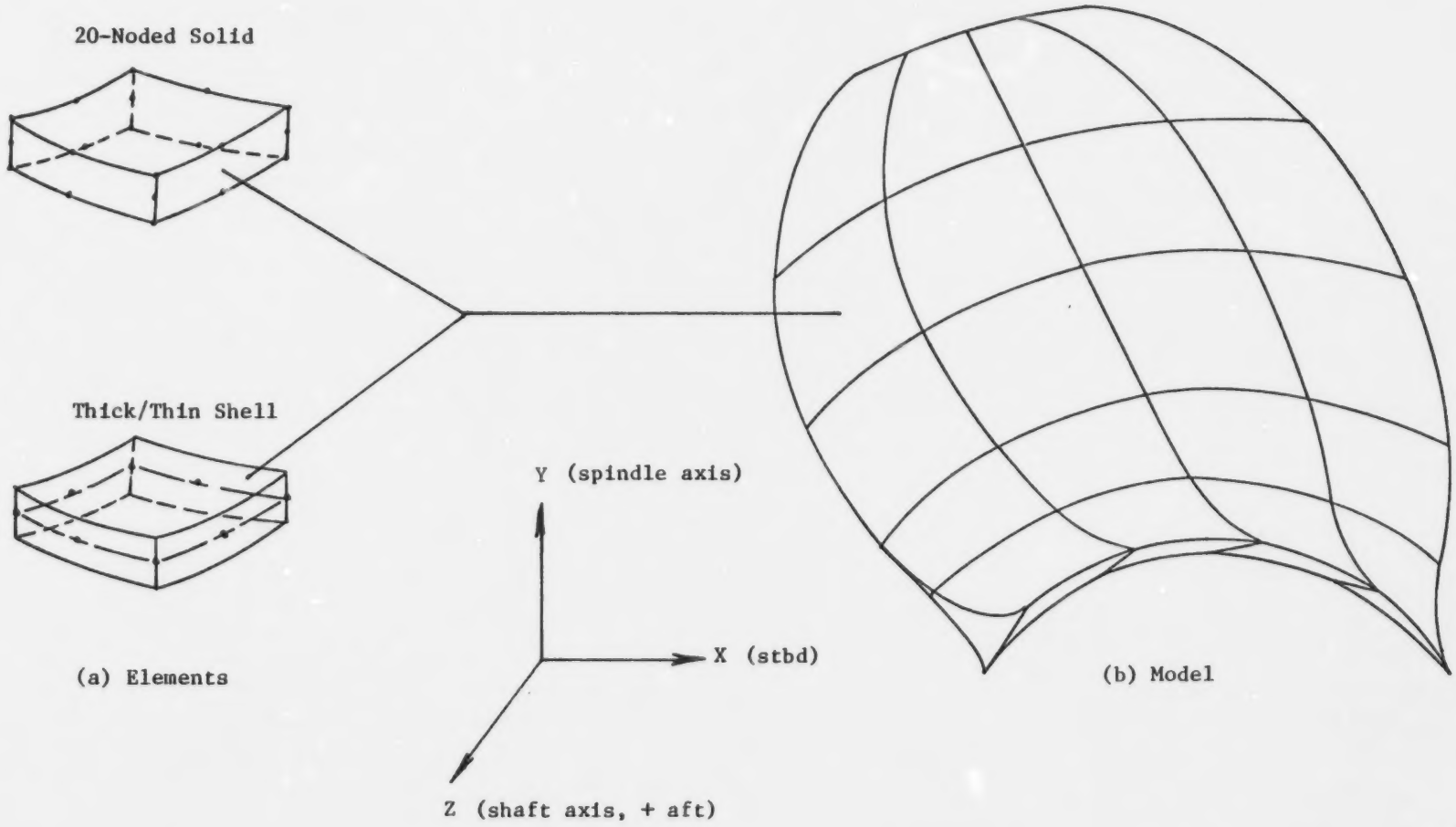


Figure 1: Finite Element Idealization

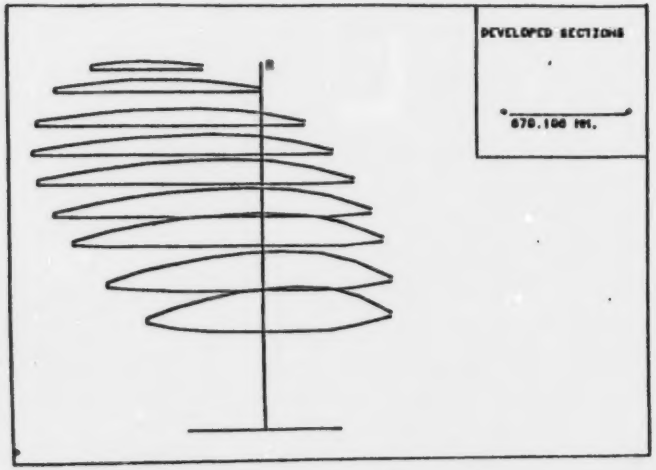


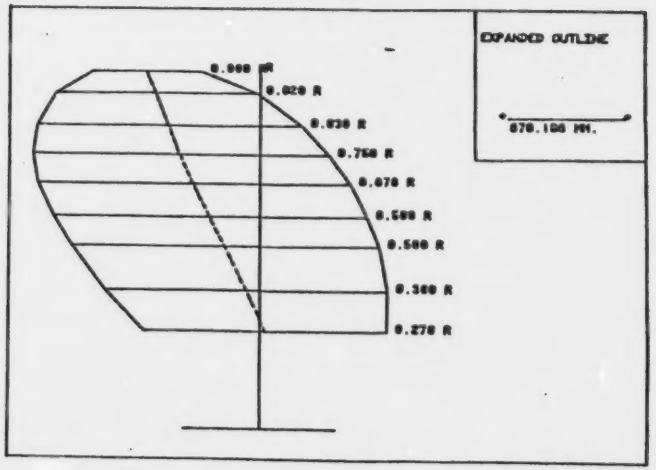


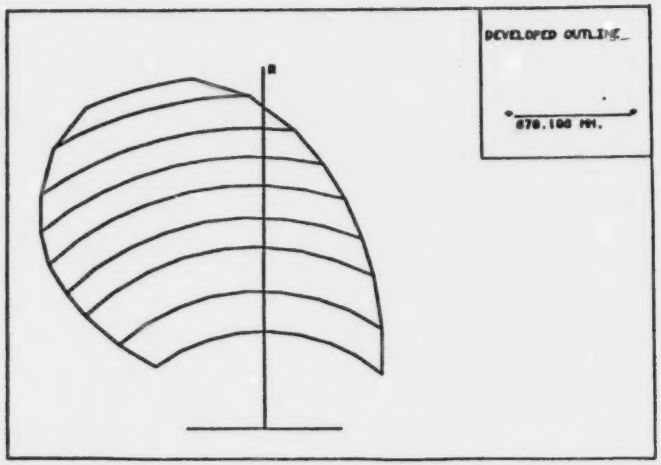


Figure 2: Computer Plots of Blade Geometry

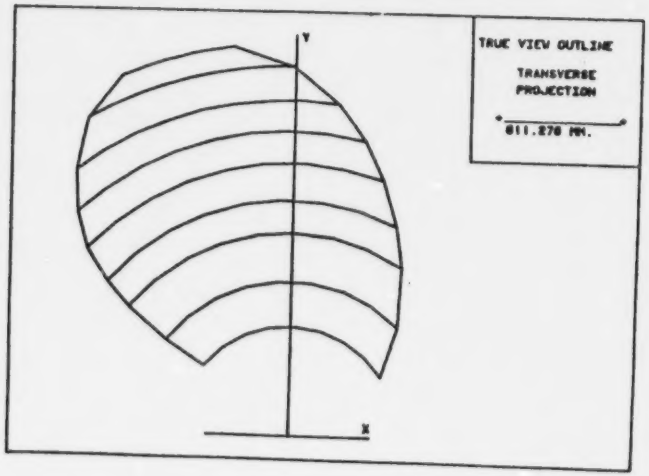


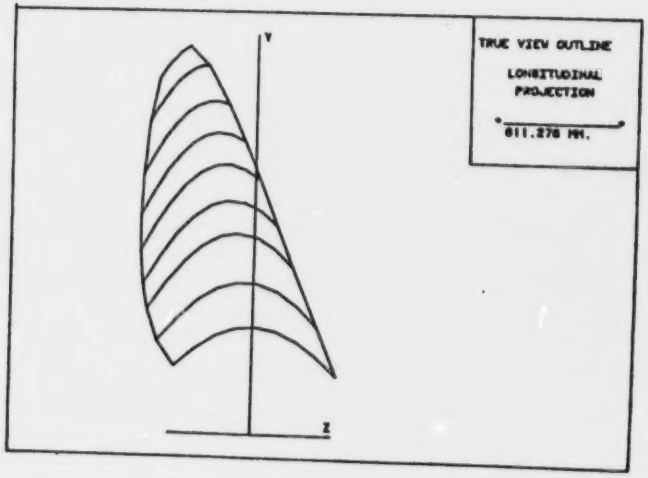


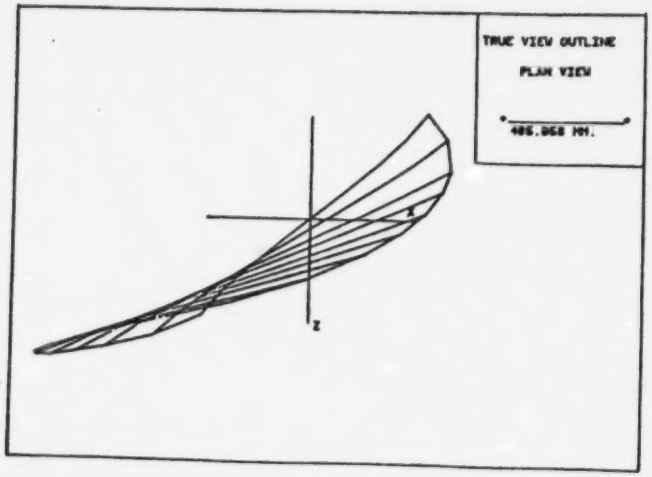


Figure 2 (Continued): Computer Plots of Blade Geometry

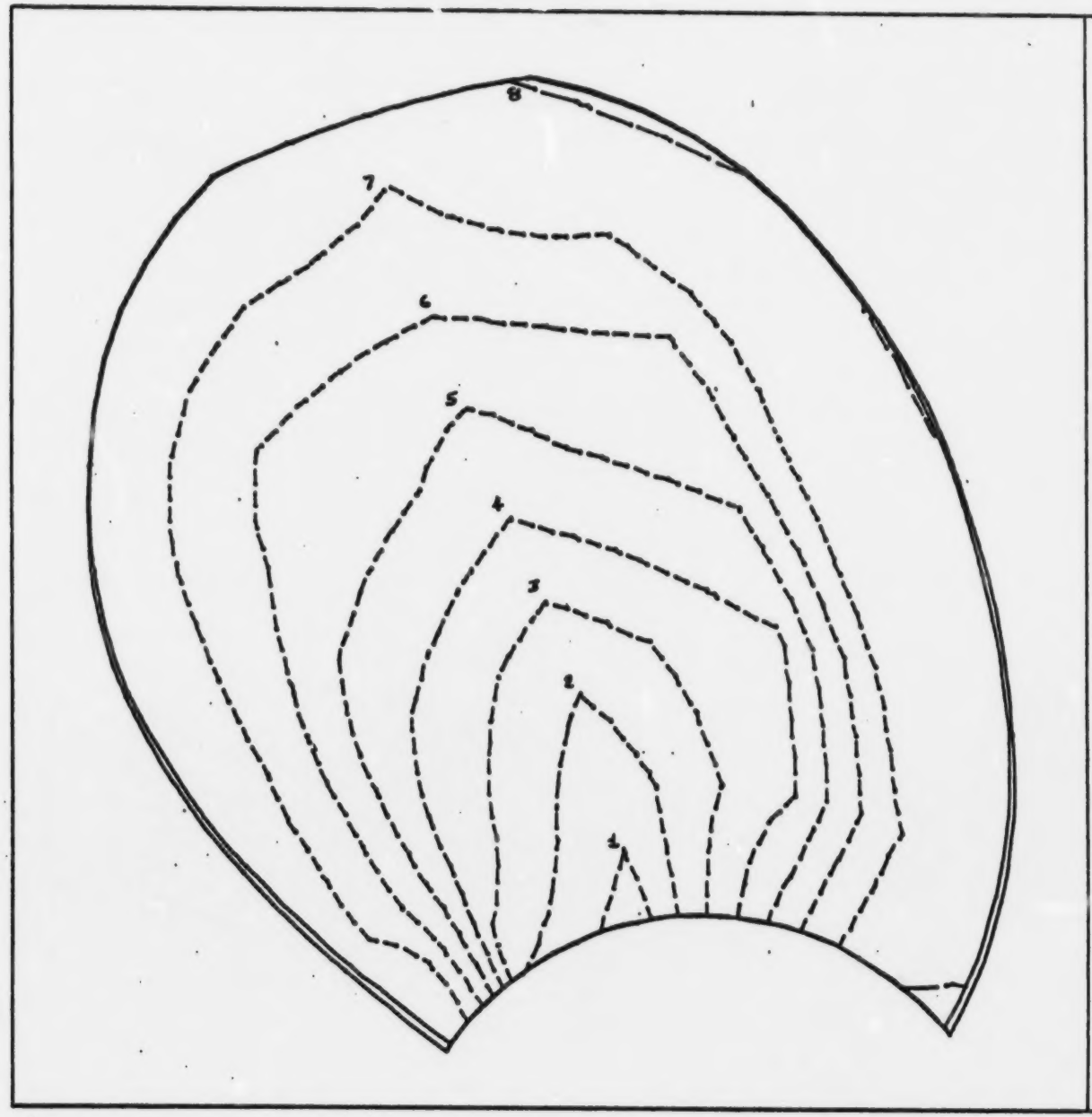


PRINCIPAL
STRESS

STRESS LEVELS

| CODE | STRESS |
|---|---|
| 1 | -350. |
| 2 | -300. |
| 3 | -250. |
| 4 | -200. |
| 5 | -150. |
| 6 | -100 |
| 7 | -50. |
| 8 | 0. |

505.882 MM.

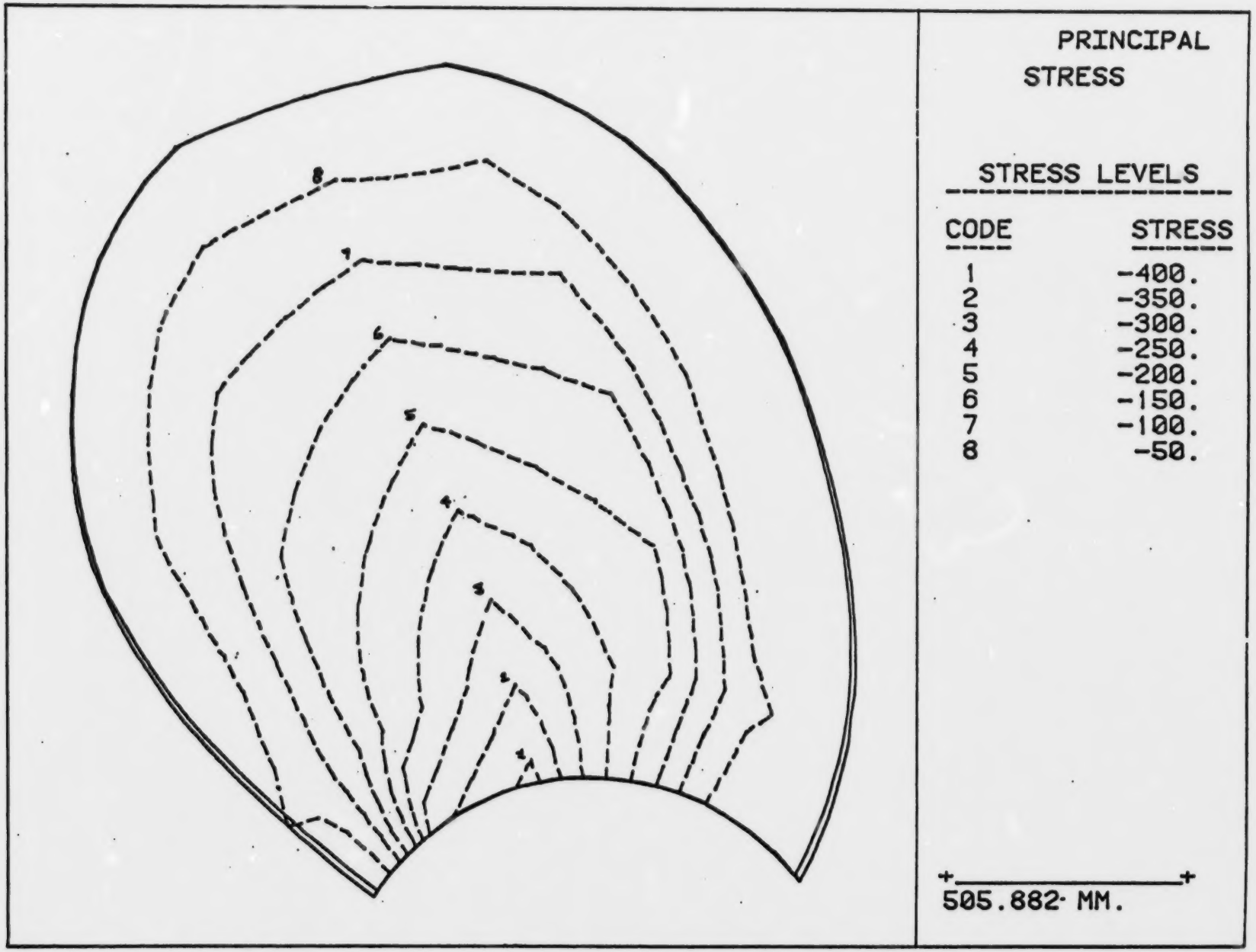


Figure 4: Finite Element Analysis using Thick/Thin Shell Elements

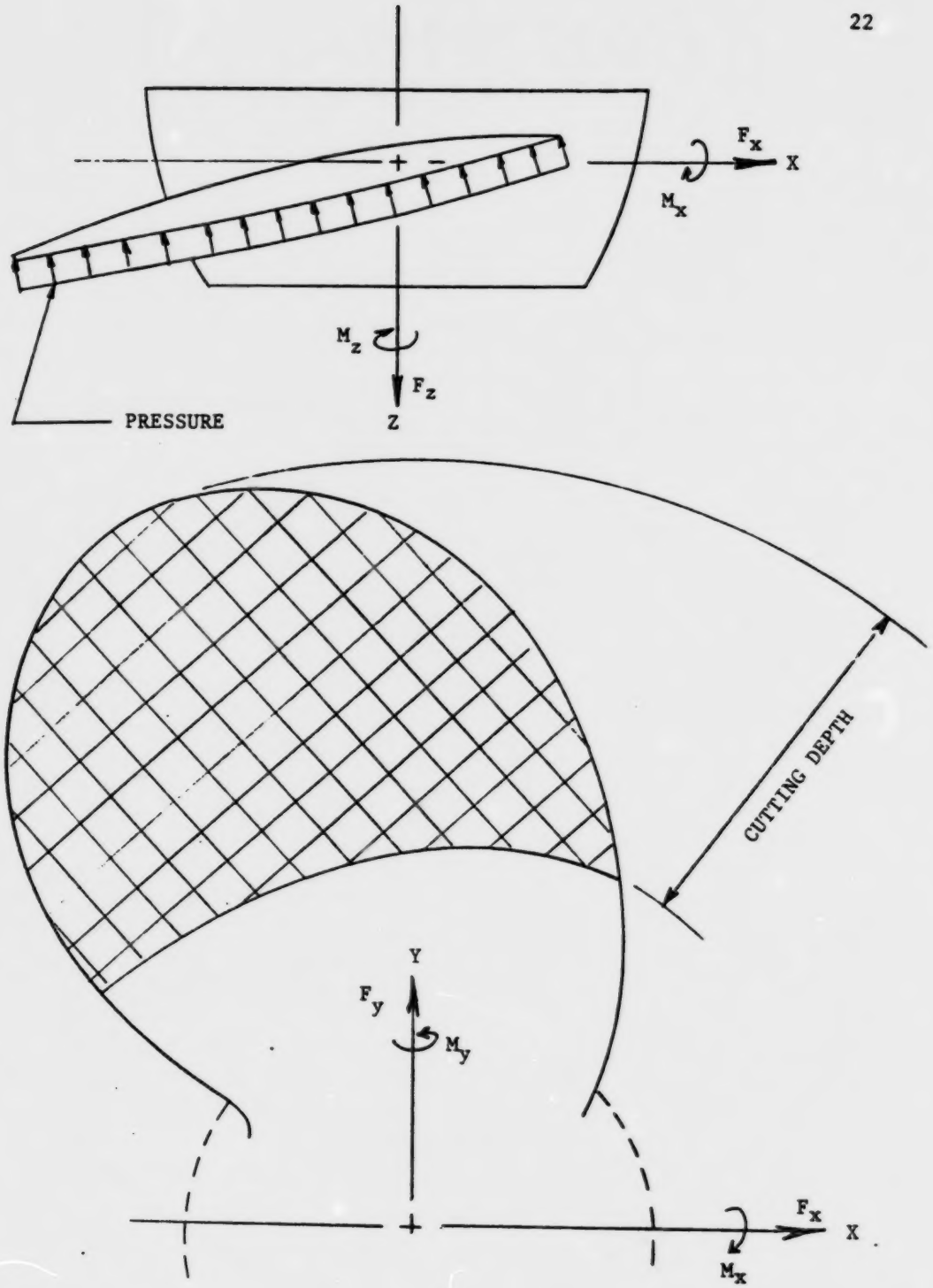


Figure 5: Blade Loading

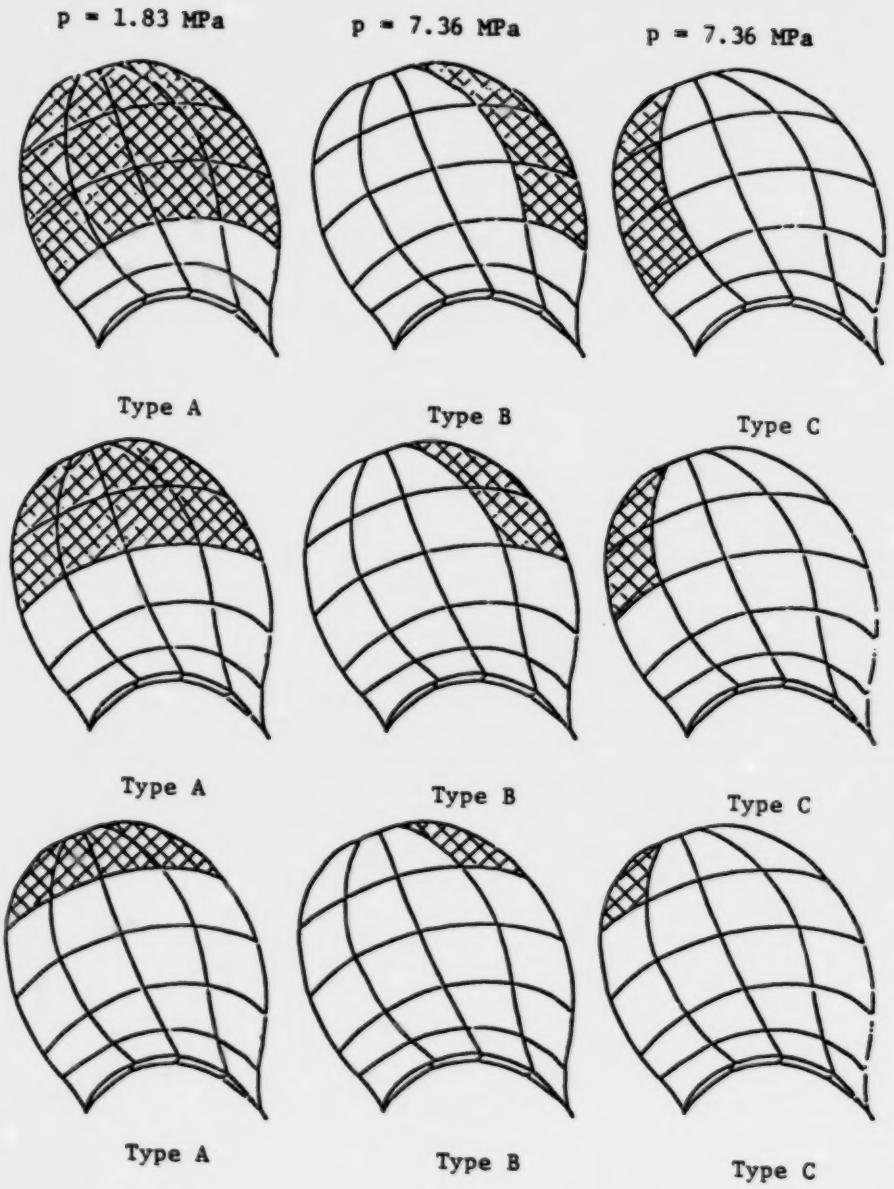


Figure 6: Types of Pressure Distribution Considered

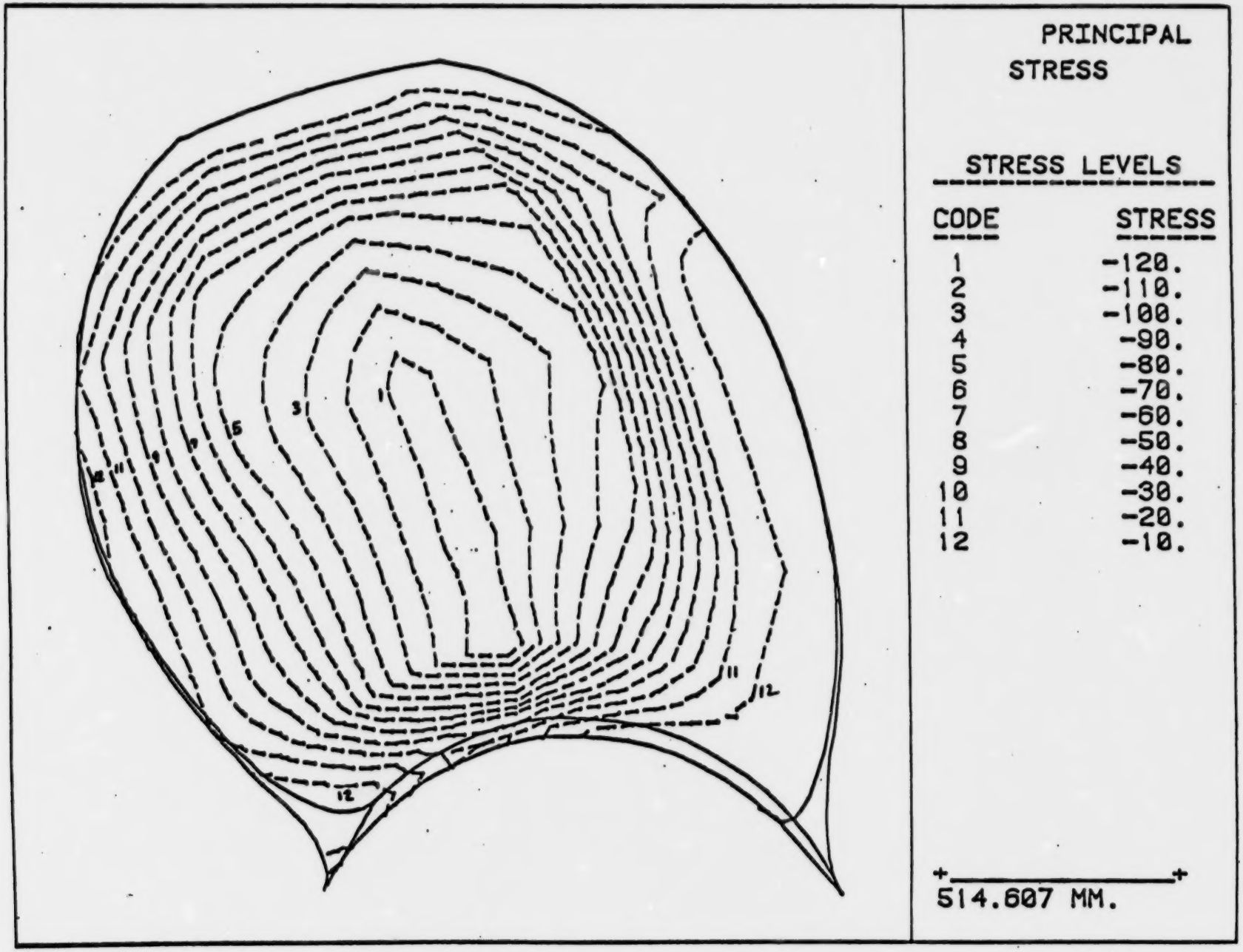
PRINCIPAL
STRESS
STRESS LEVELS
CODE STRESS
1 -120.
2 -110.
3 -100.
4 -90.
5 -80.
6 -70.
7 -60.
8 -50.
9 -40.
10 -30.
11 -20.
12 -10.
514.607 MM.

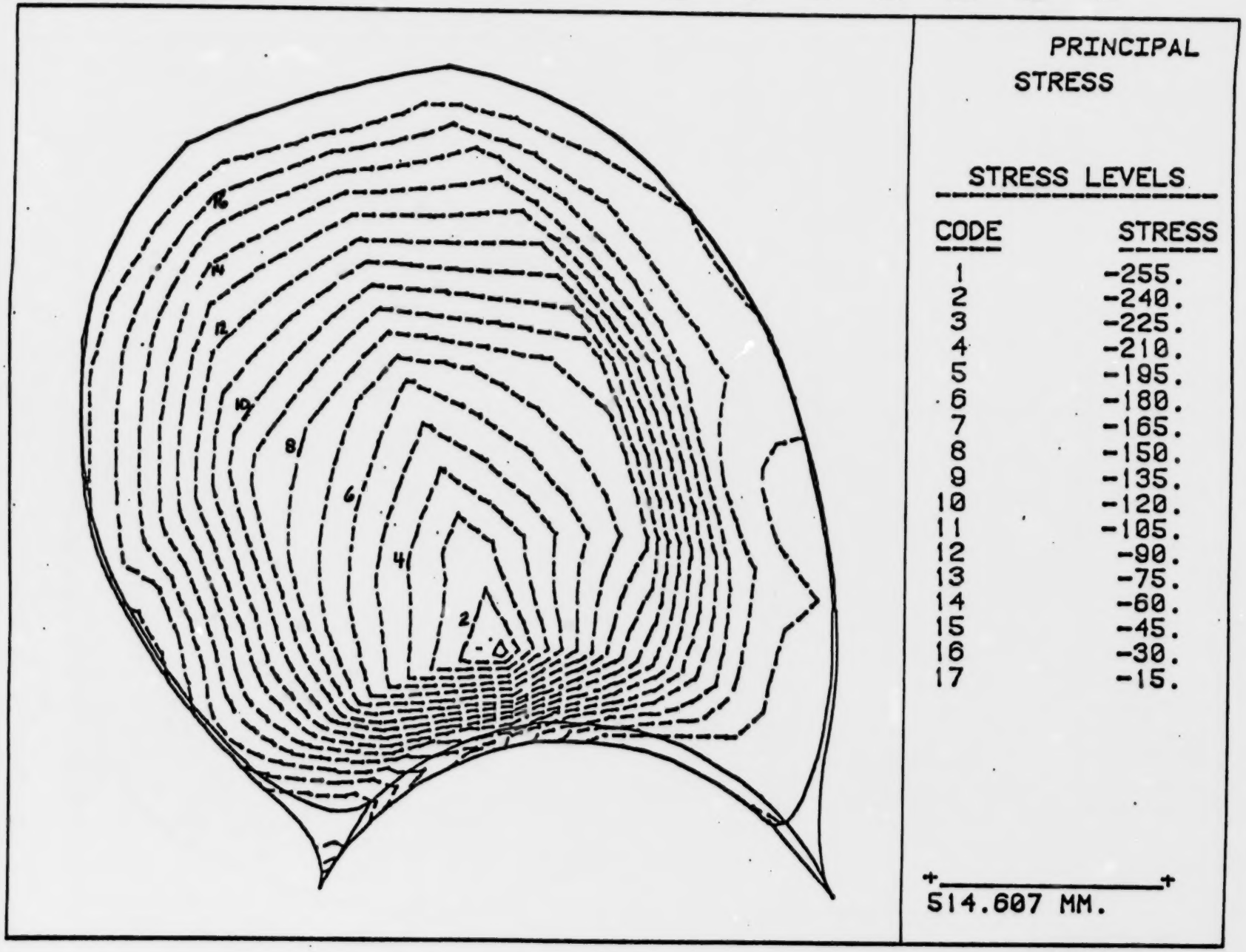


Figure 8: Existing Blade - Load Case L2-A

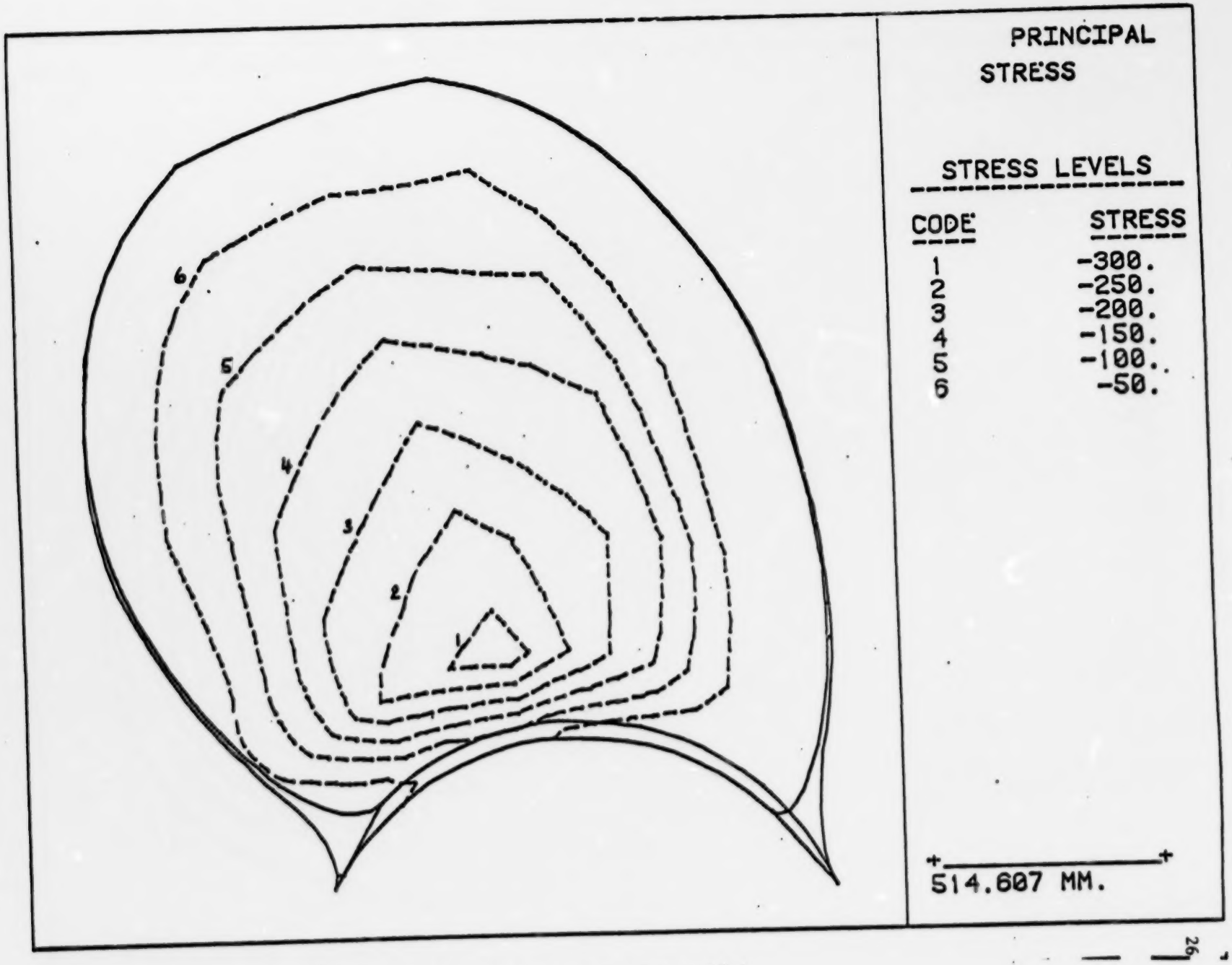


Figure 8. Existing blade - land C--- L3-1

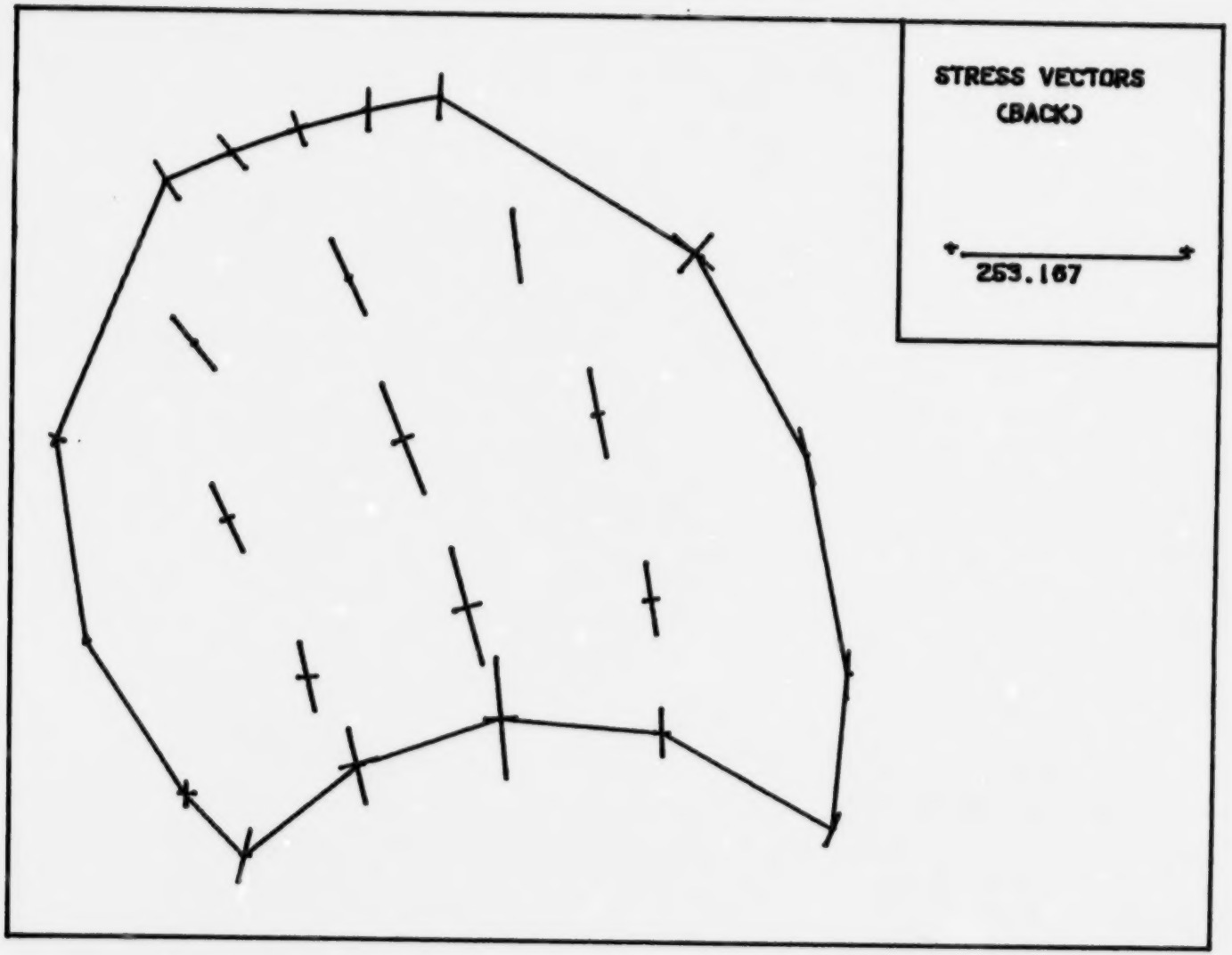


Figure 10: Principal Stress Directions for Load Case L1-A (Existing Blade)

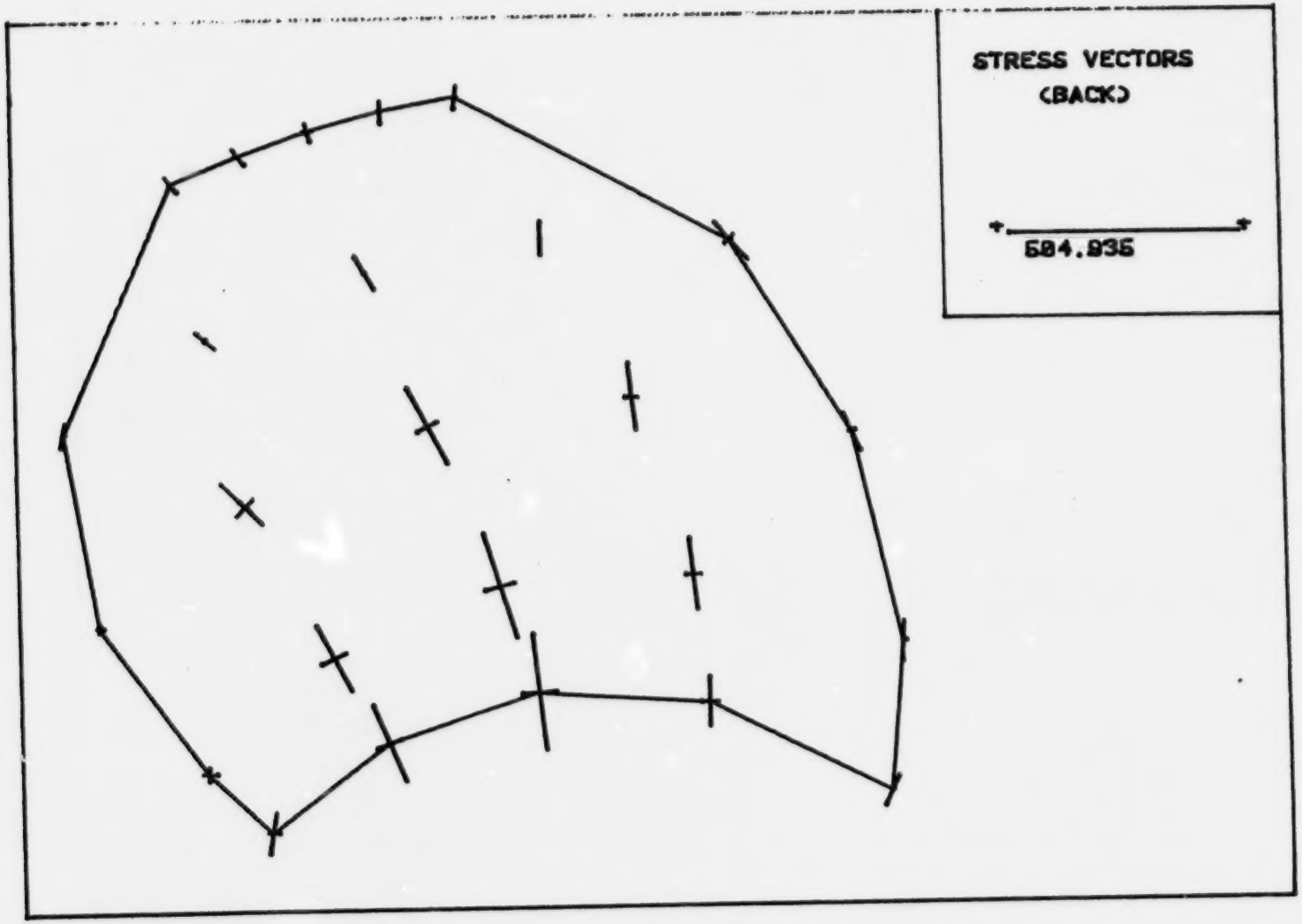


Figure 11: Principal Stress Directions for Load Case L2-A (Existing Blade)

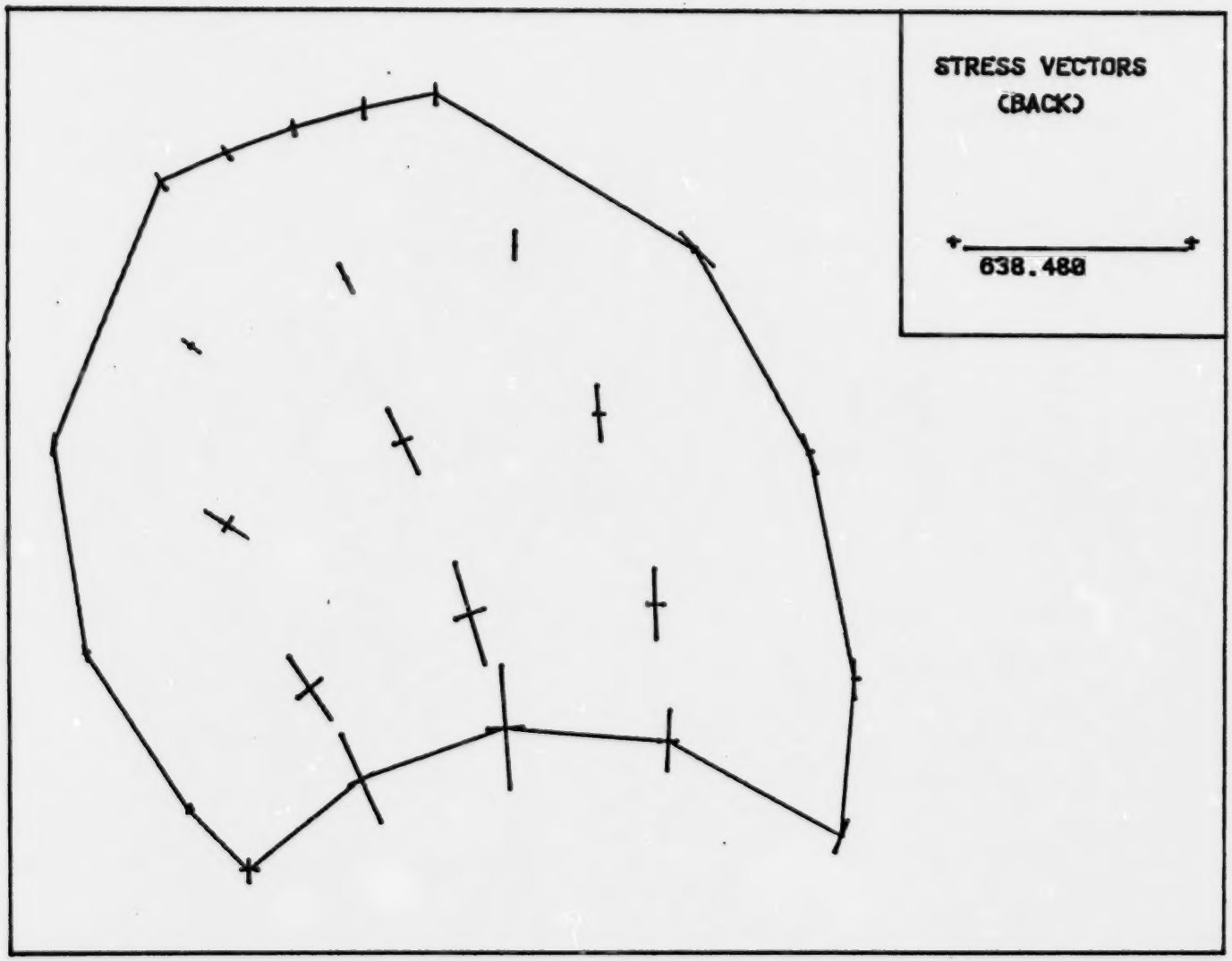


Figure 12: Principal Stress Directions for Load Case L3-A (Existing Blade)

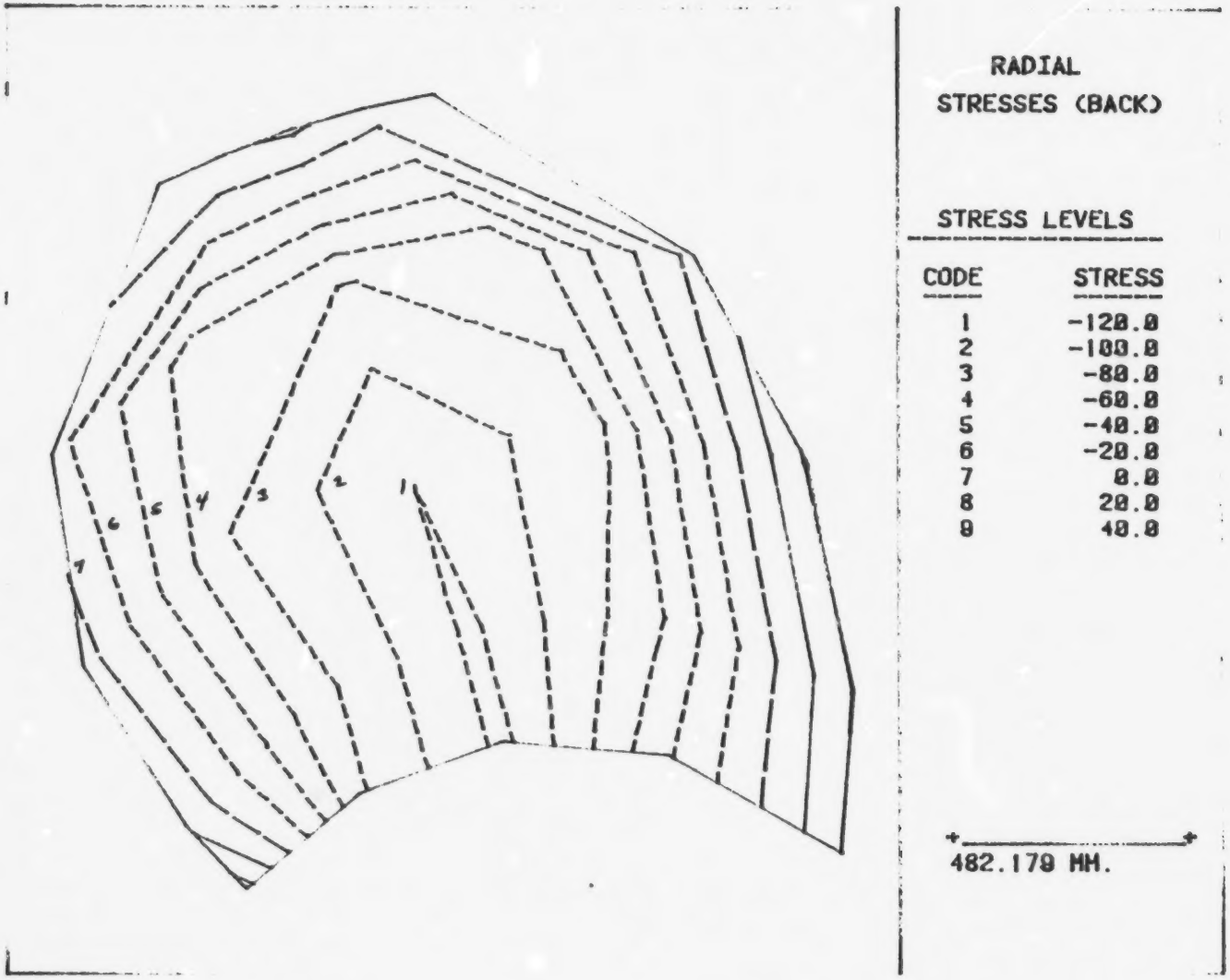


Figure 13: Existing Blade - Load Case L1-A

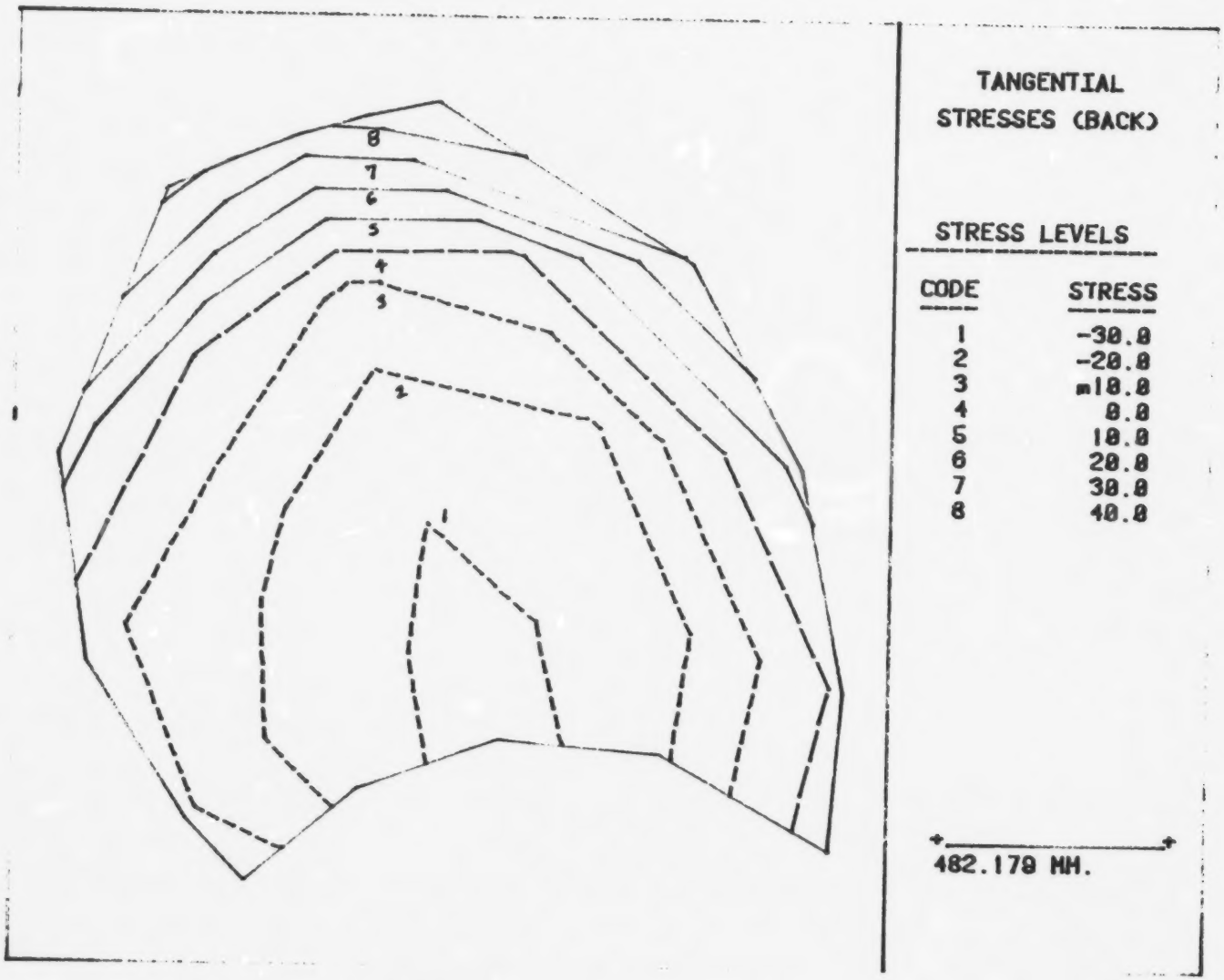


Figure 14: Existing Blade - Load Case L1-A

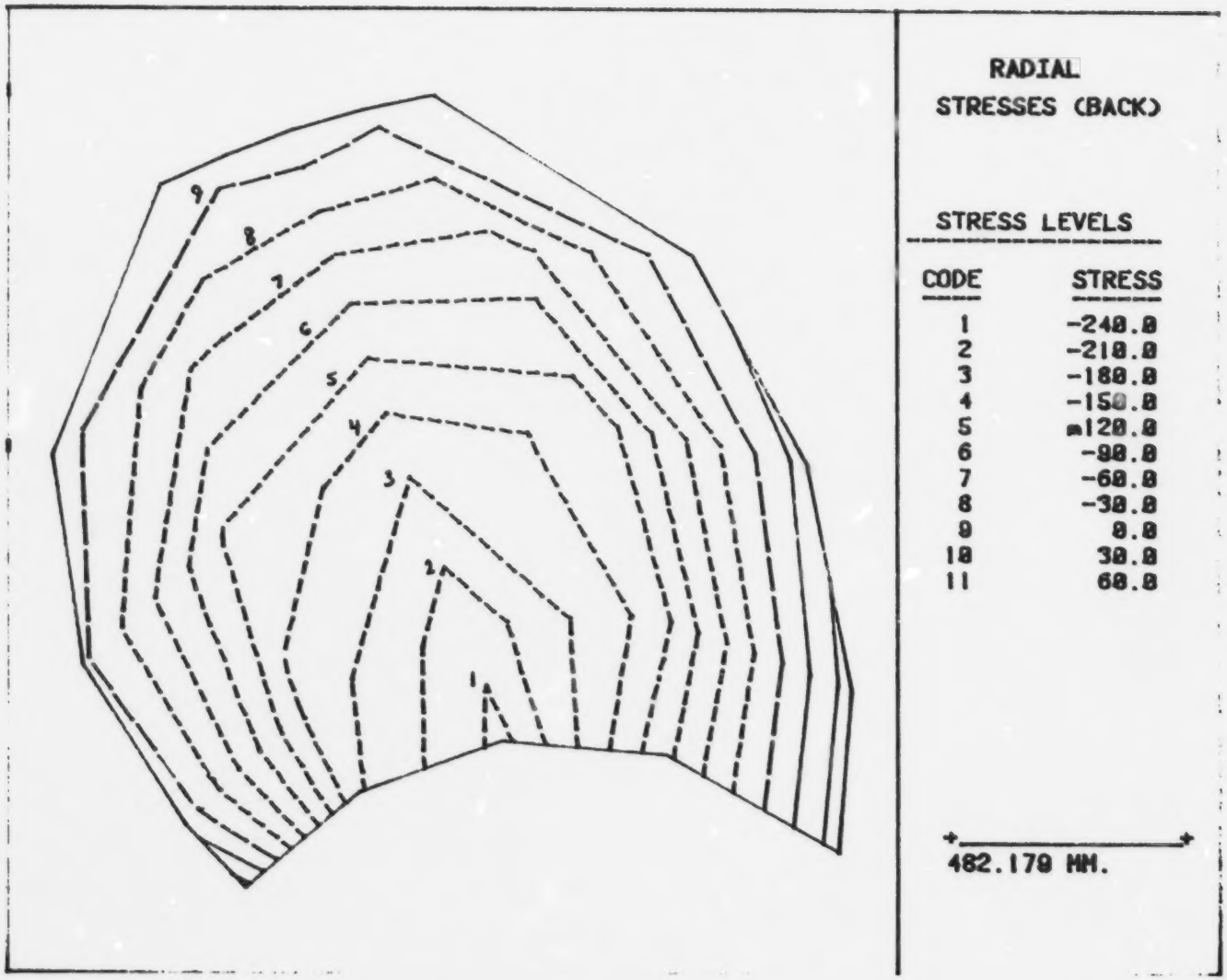


Figure 15: Existing Blade - Load Case L2-A

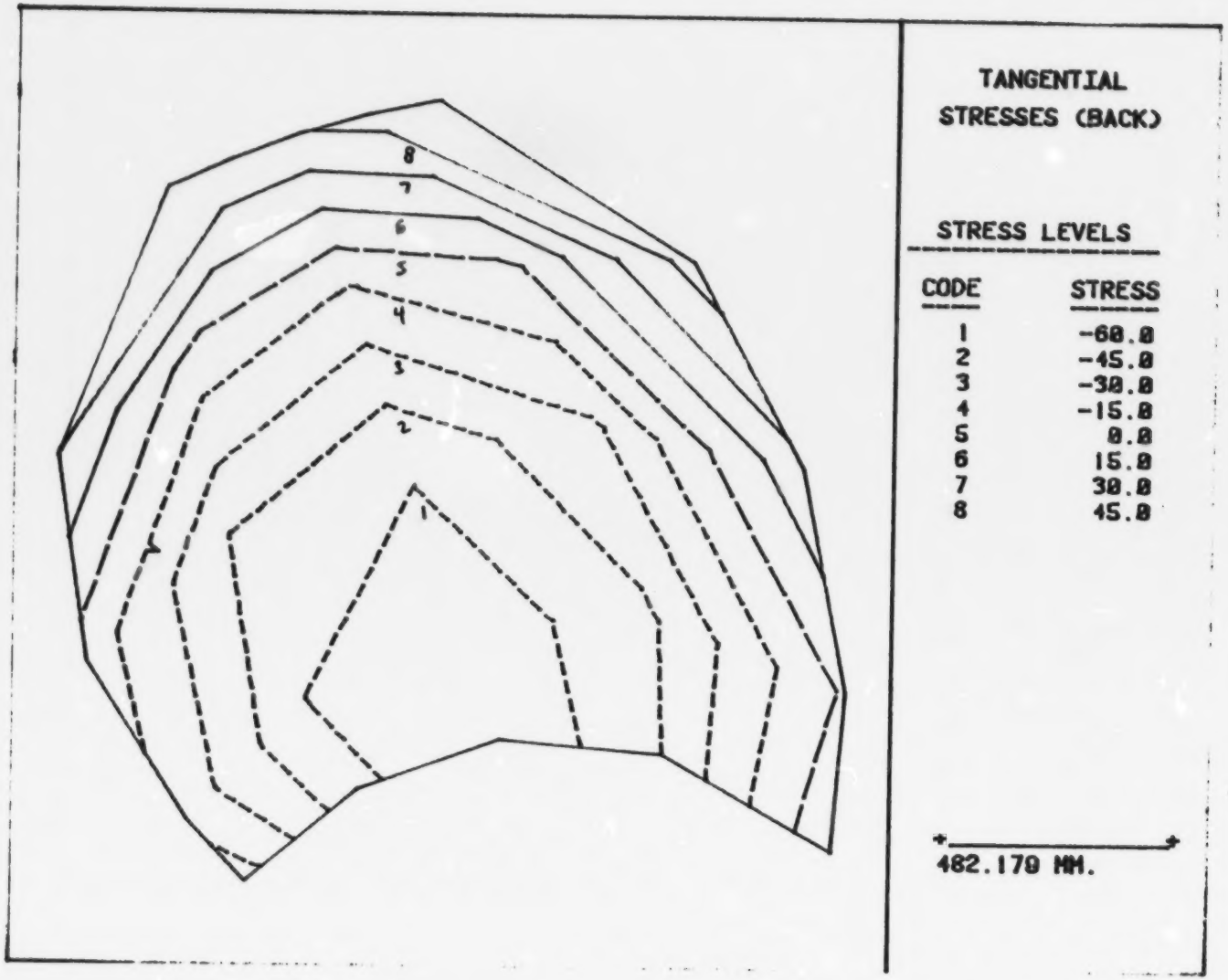


Figure 16: Existing Blade - Load Case L2-A

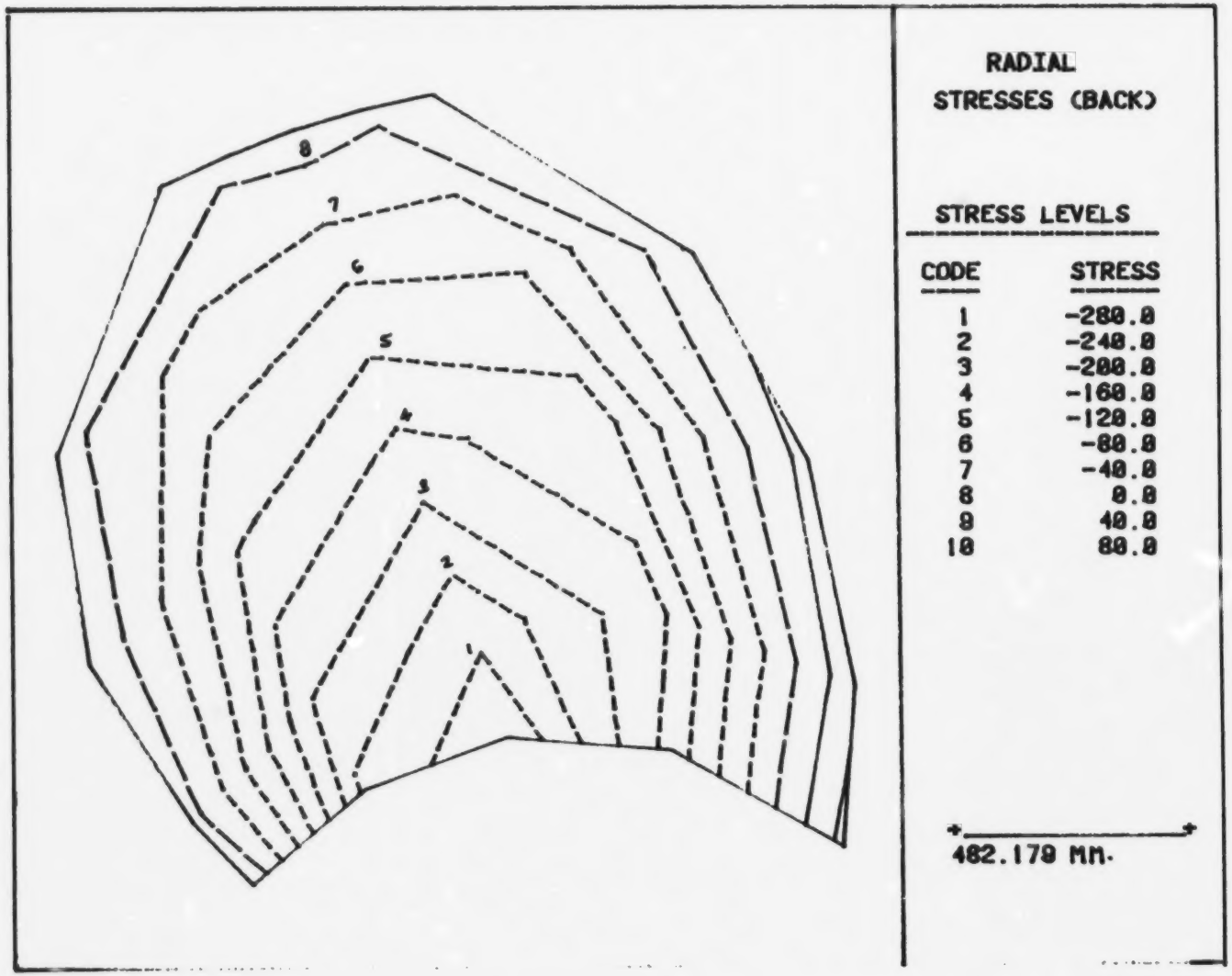


Figure 17: Existing Blade - Load Case L.-A

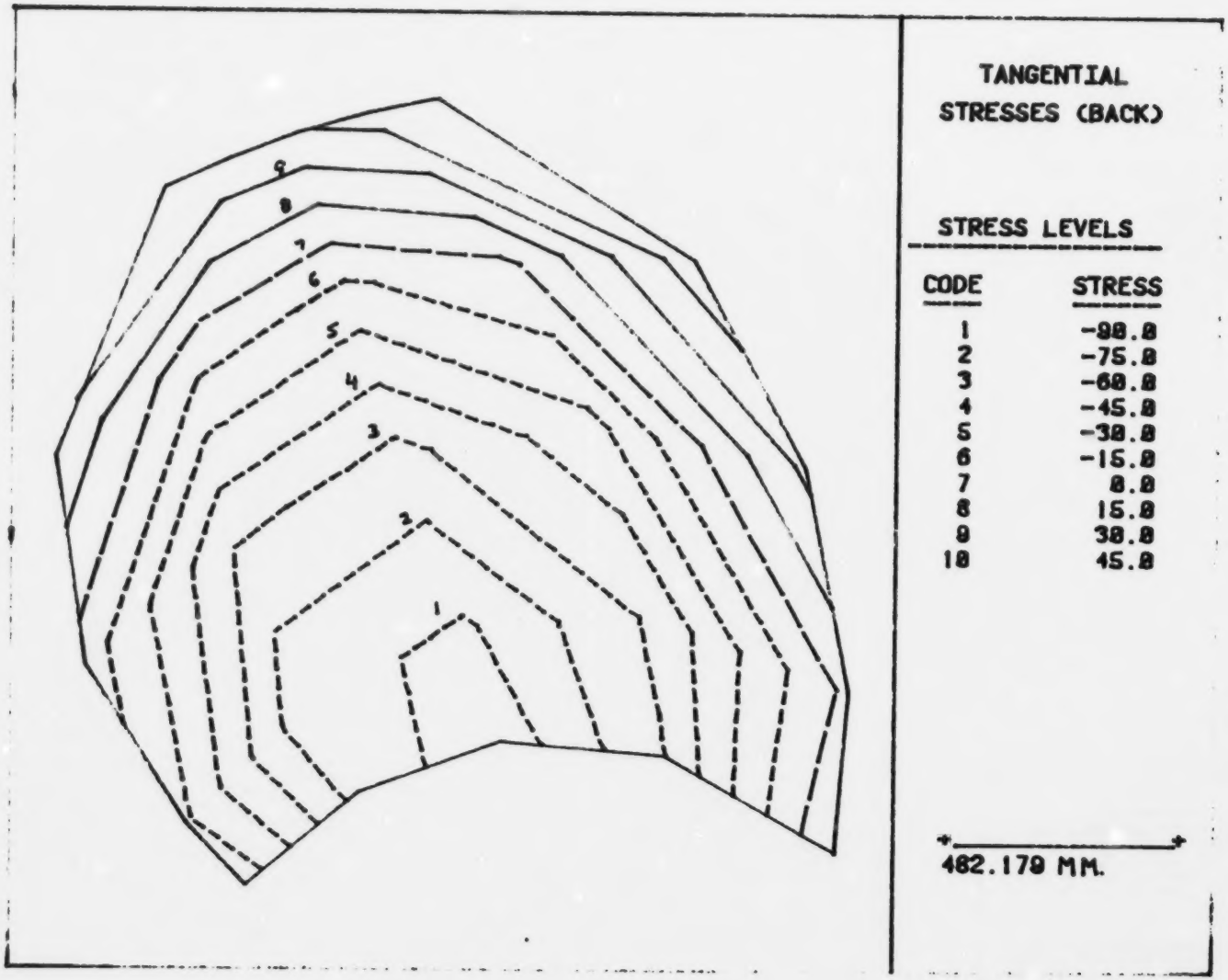


Figure 18: Existing Blade - Load Case L3-A

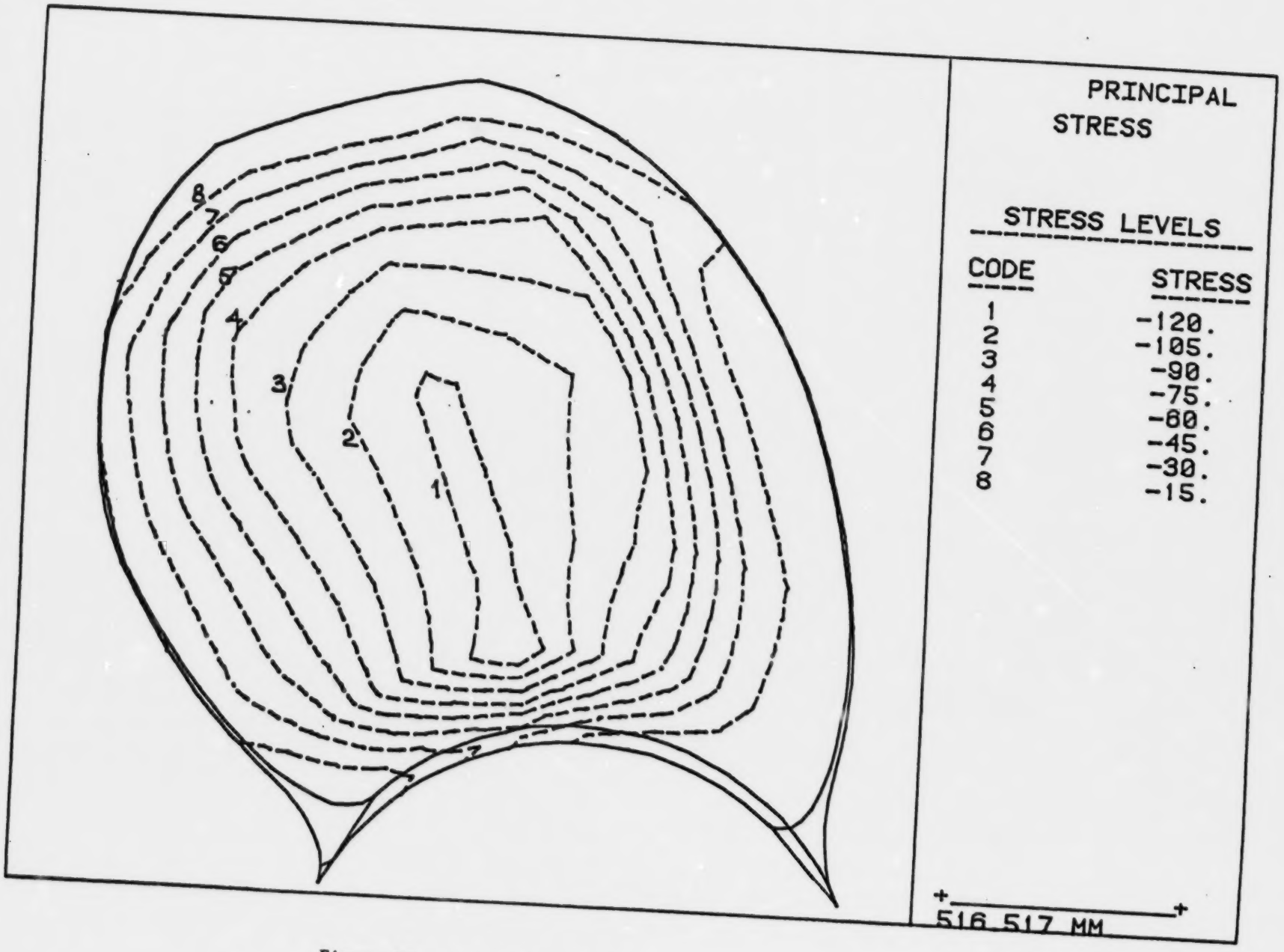


Figure 19: Zero Rake - Load Case L1-A

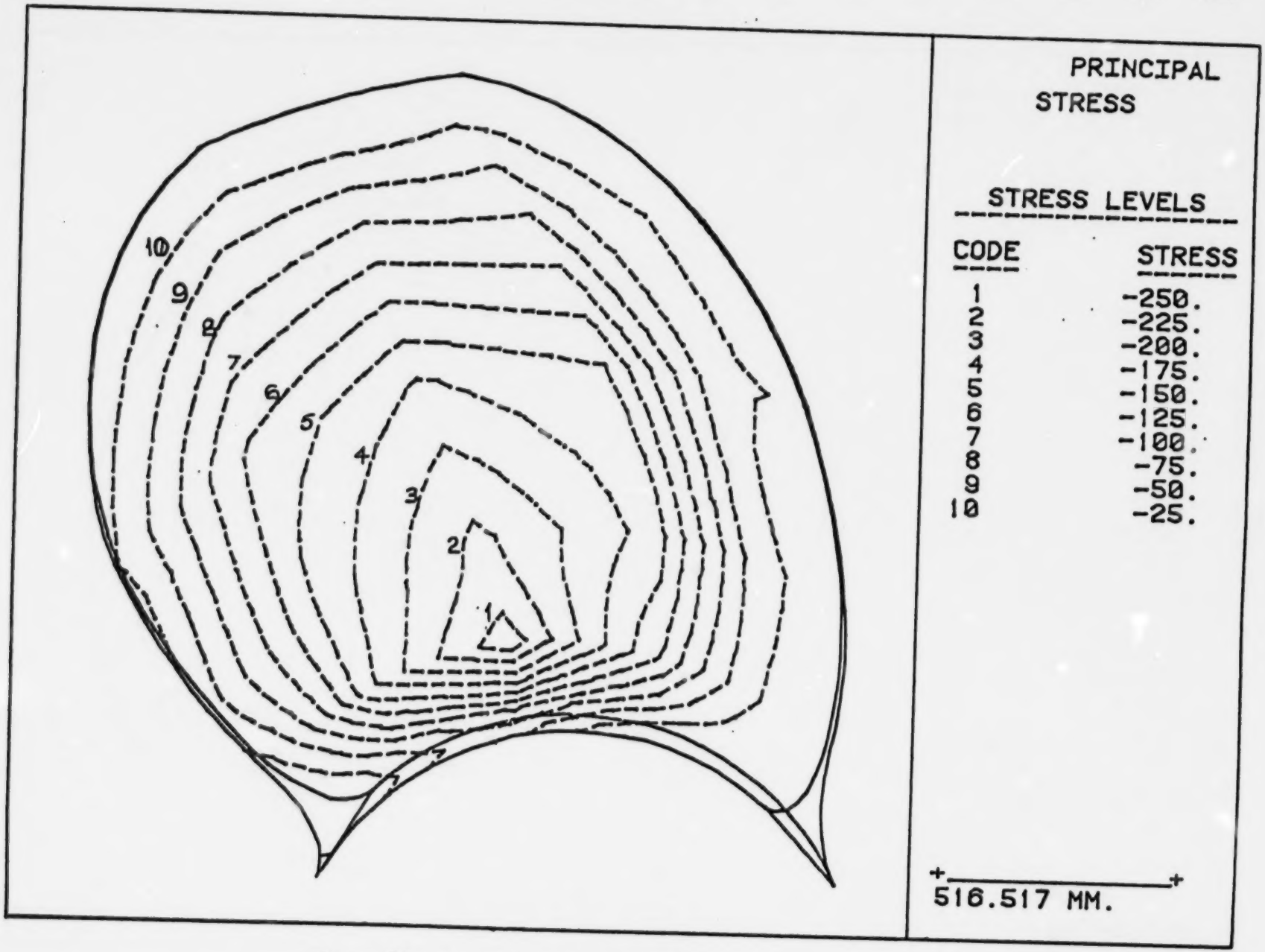


Figure 20: Zero Rake - Load Case L2-A

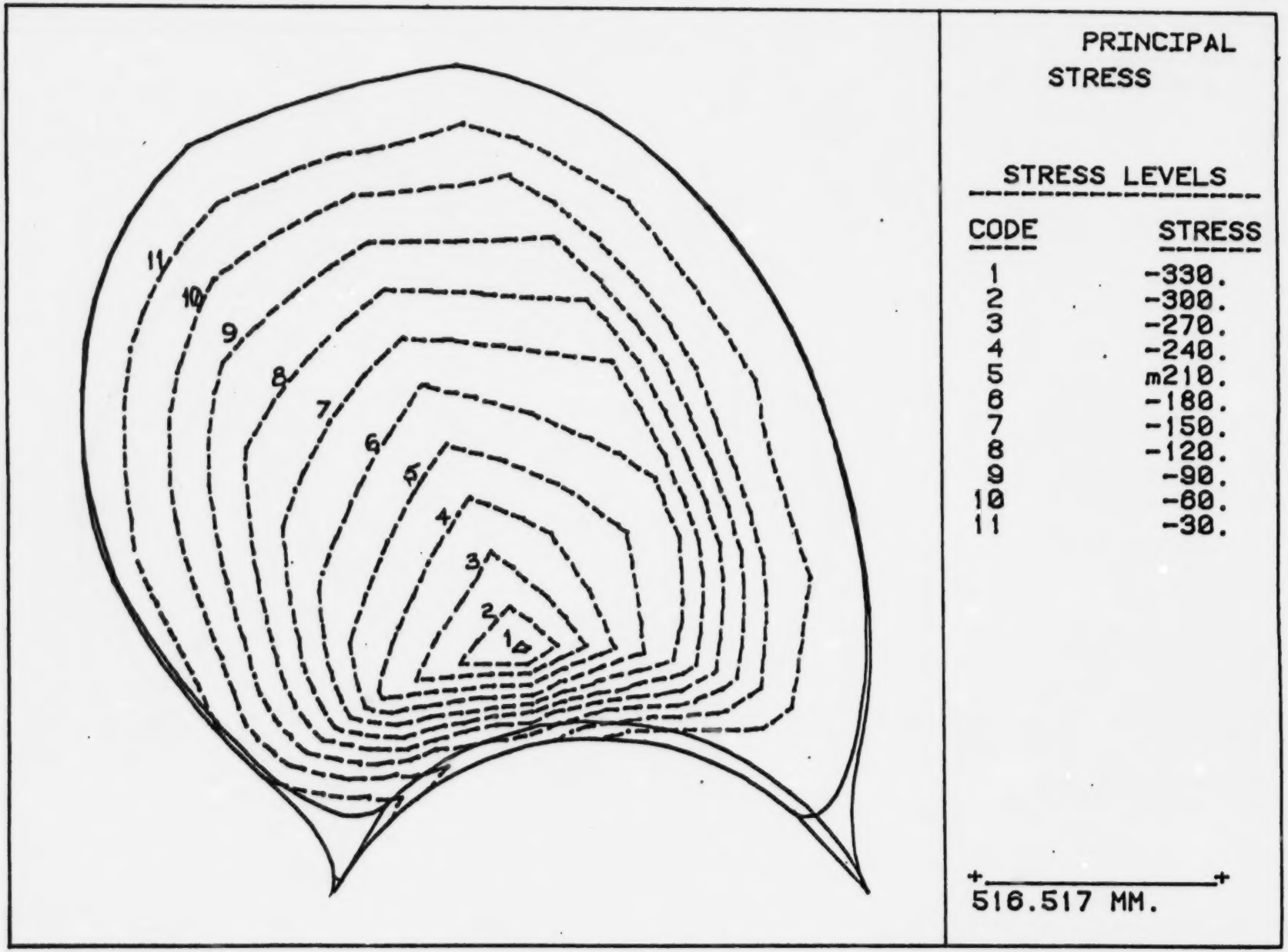


Figure 21: Zero Rake - Load Case I.3-A

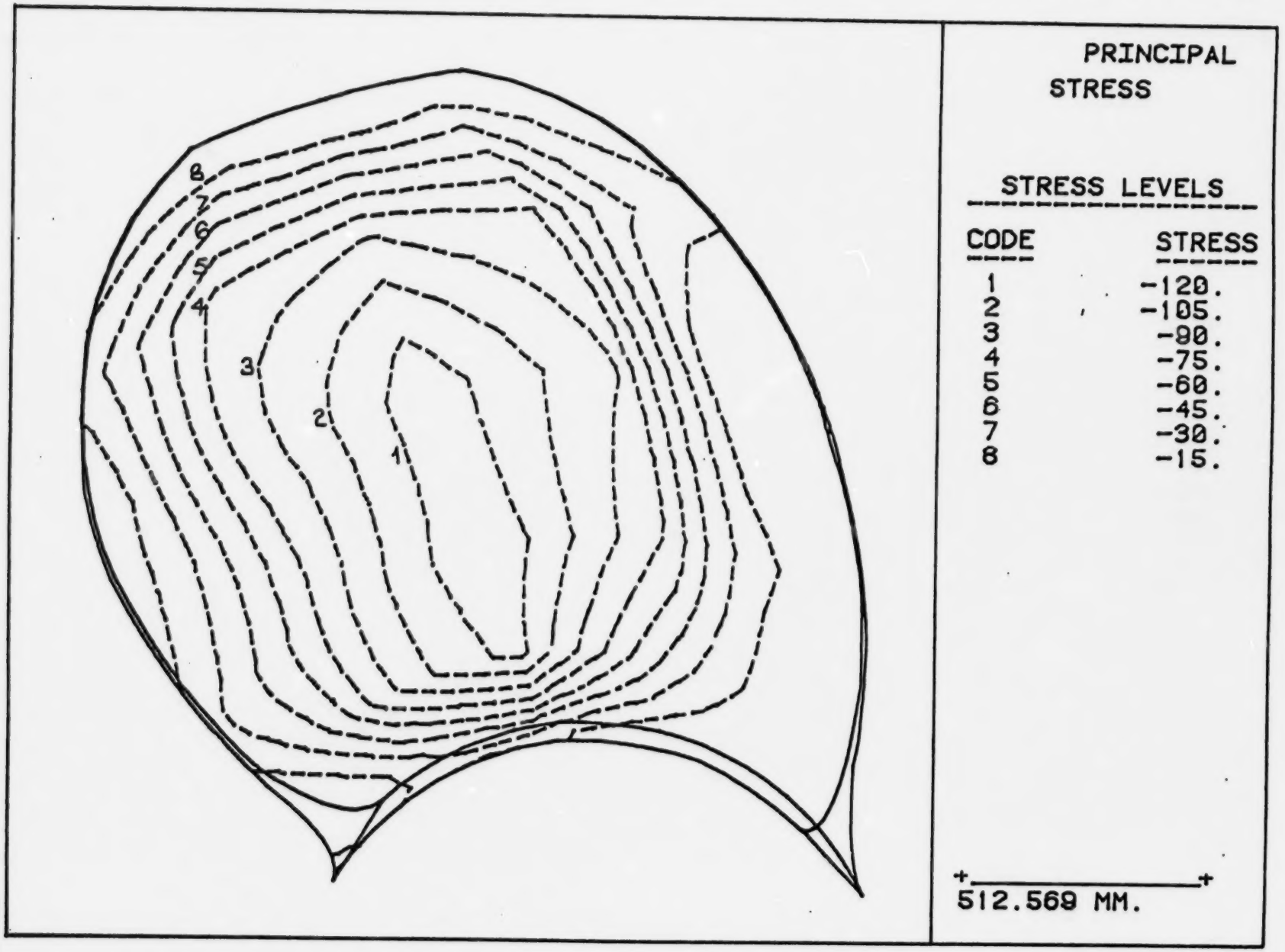


Figure 22: 100% Increase in Rake - Load Case L1-A

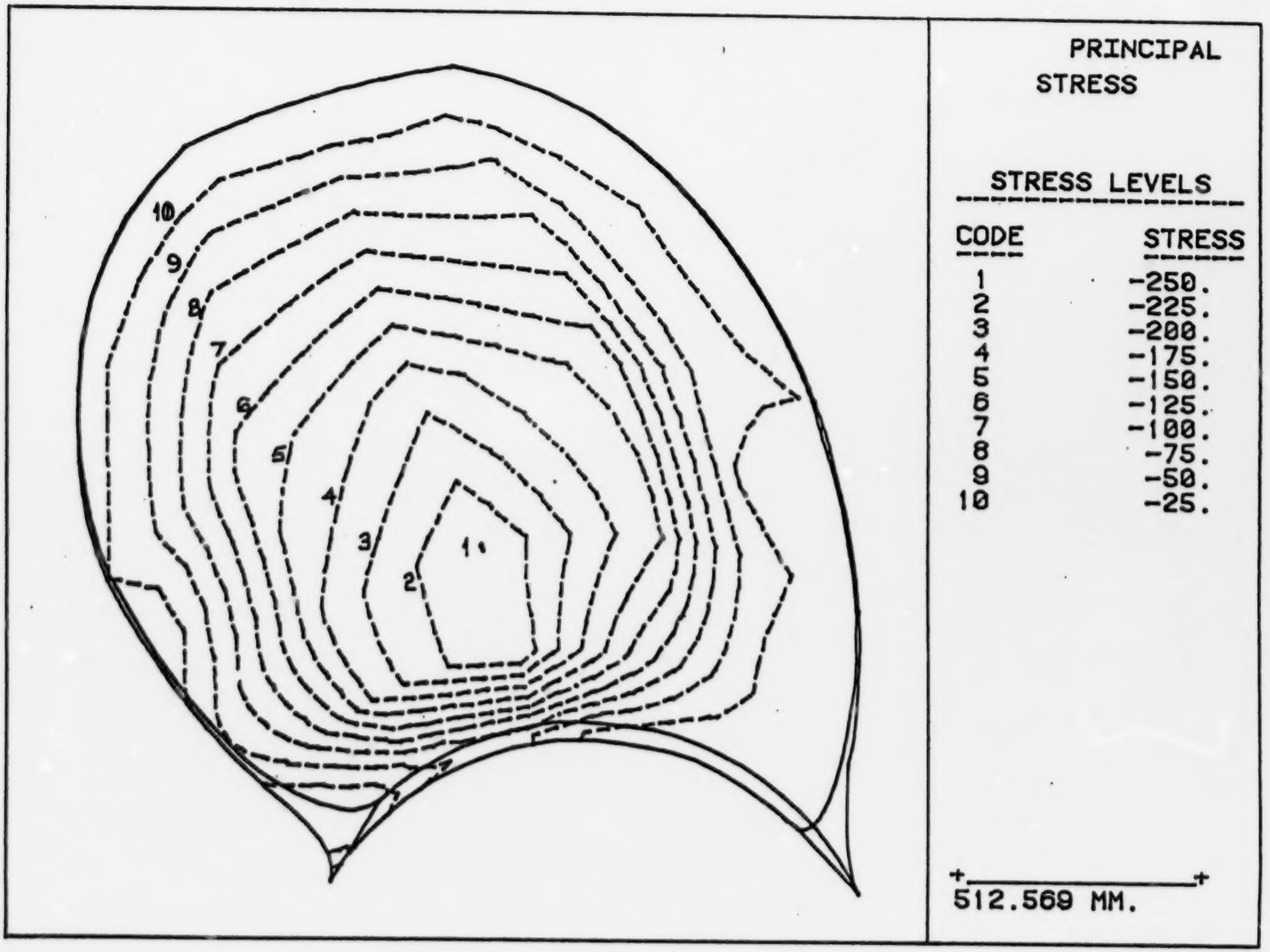


Figure 23: 100% Increase in Rake - Load Case L2-A

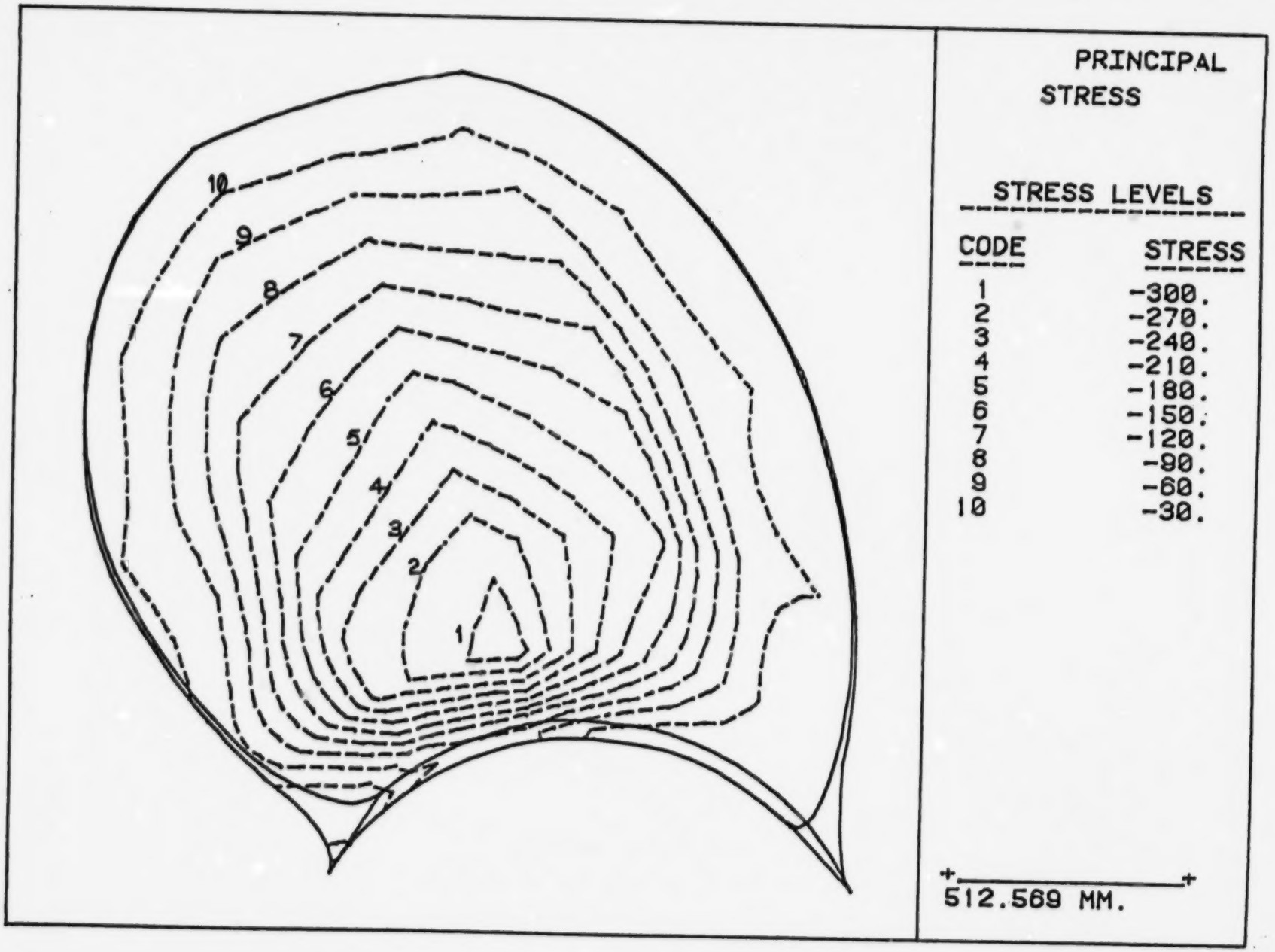


Figure 24: 100% Increase in Rake - Load Case L3-A

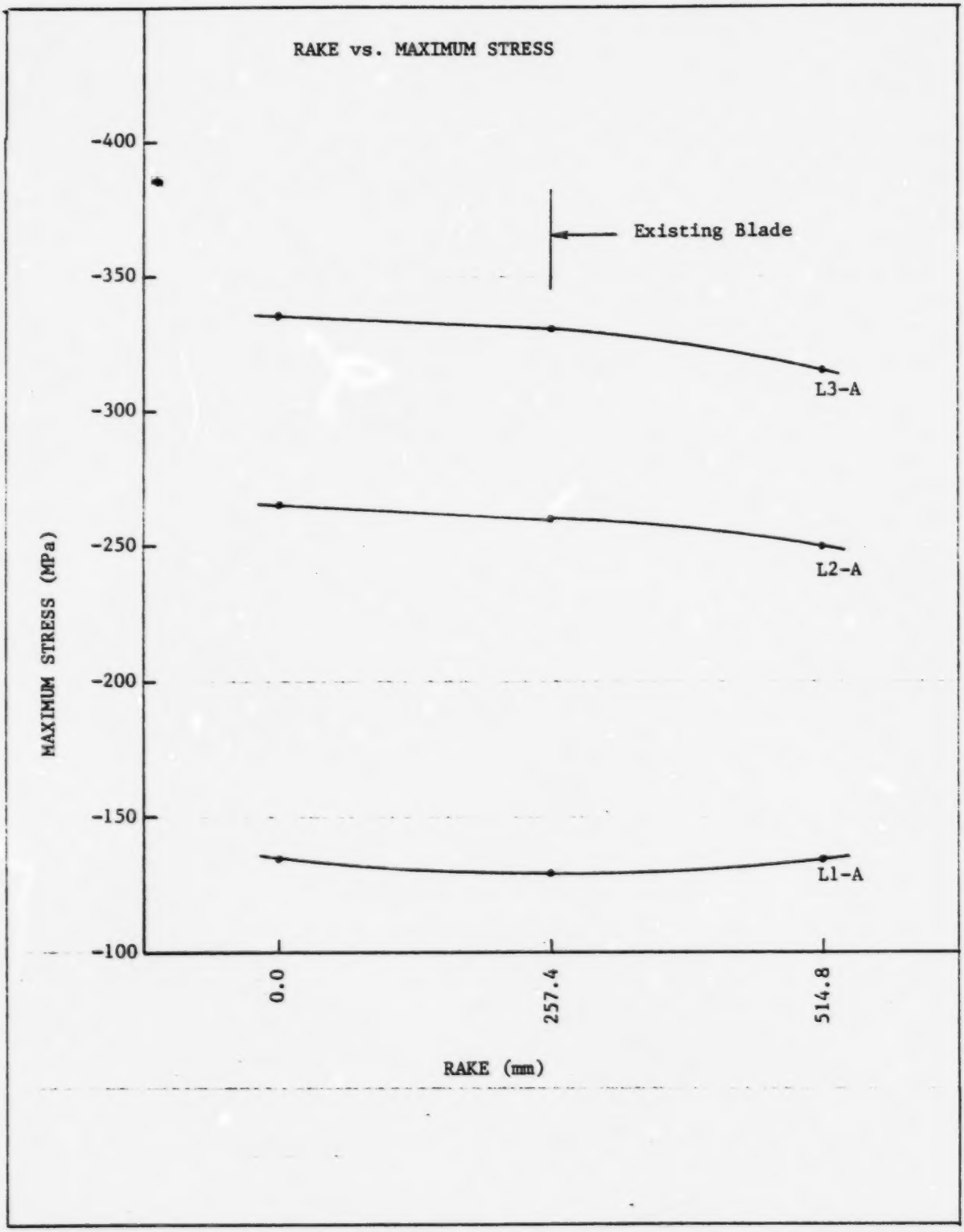


Figure 25: Effect of Rake on Maximum Stress

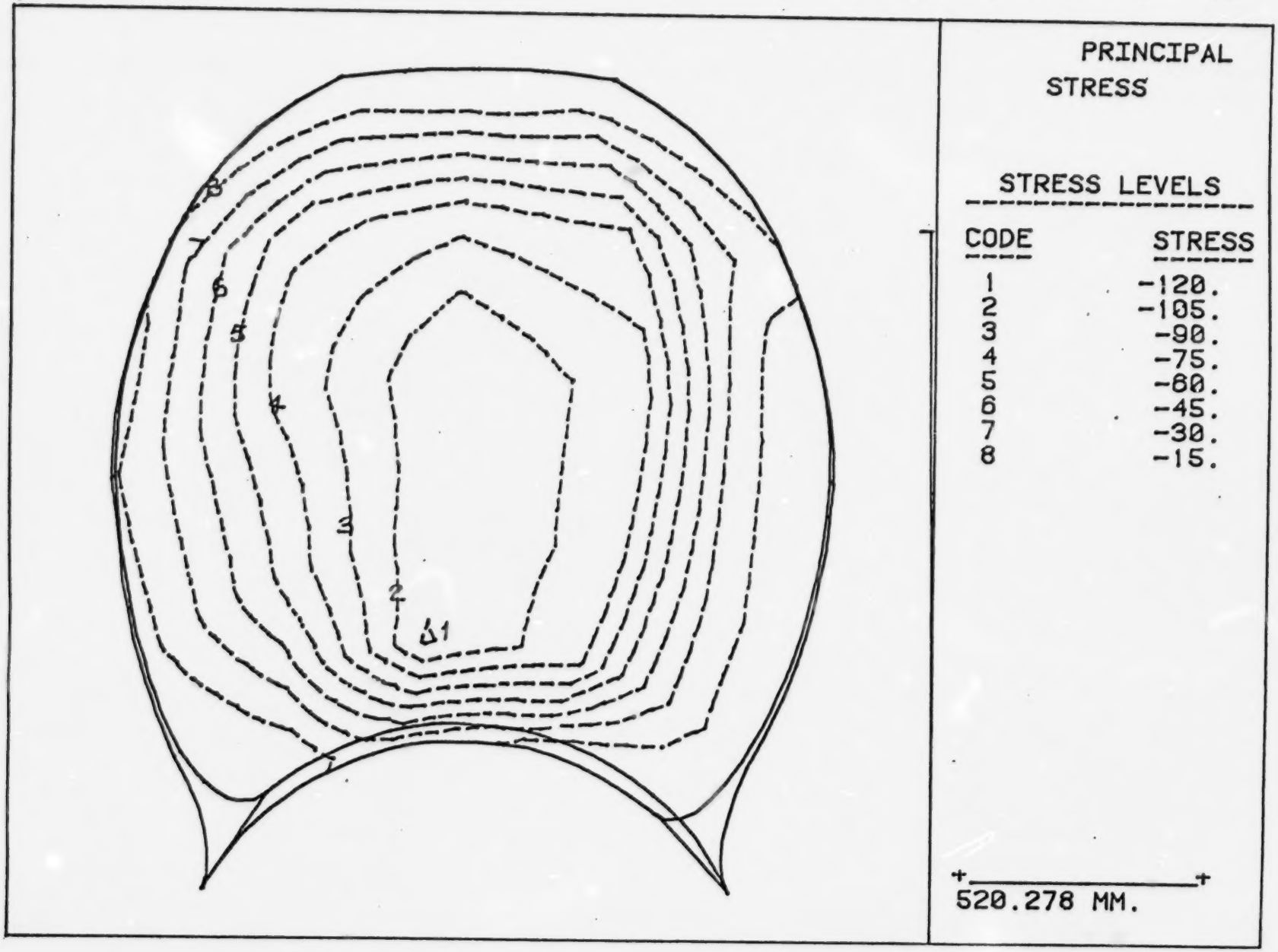


Figure 26: Zero Skew - Load Case L1-A

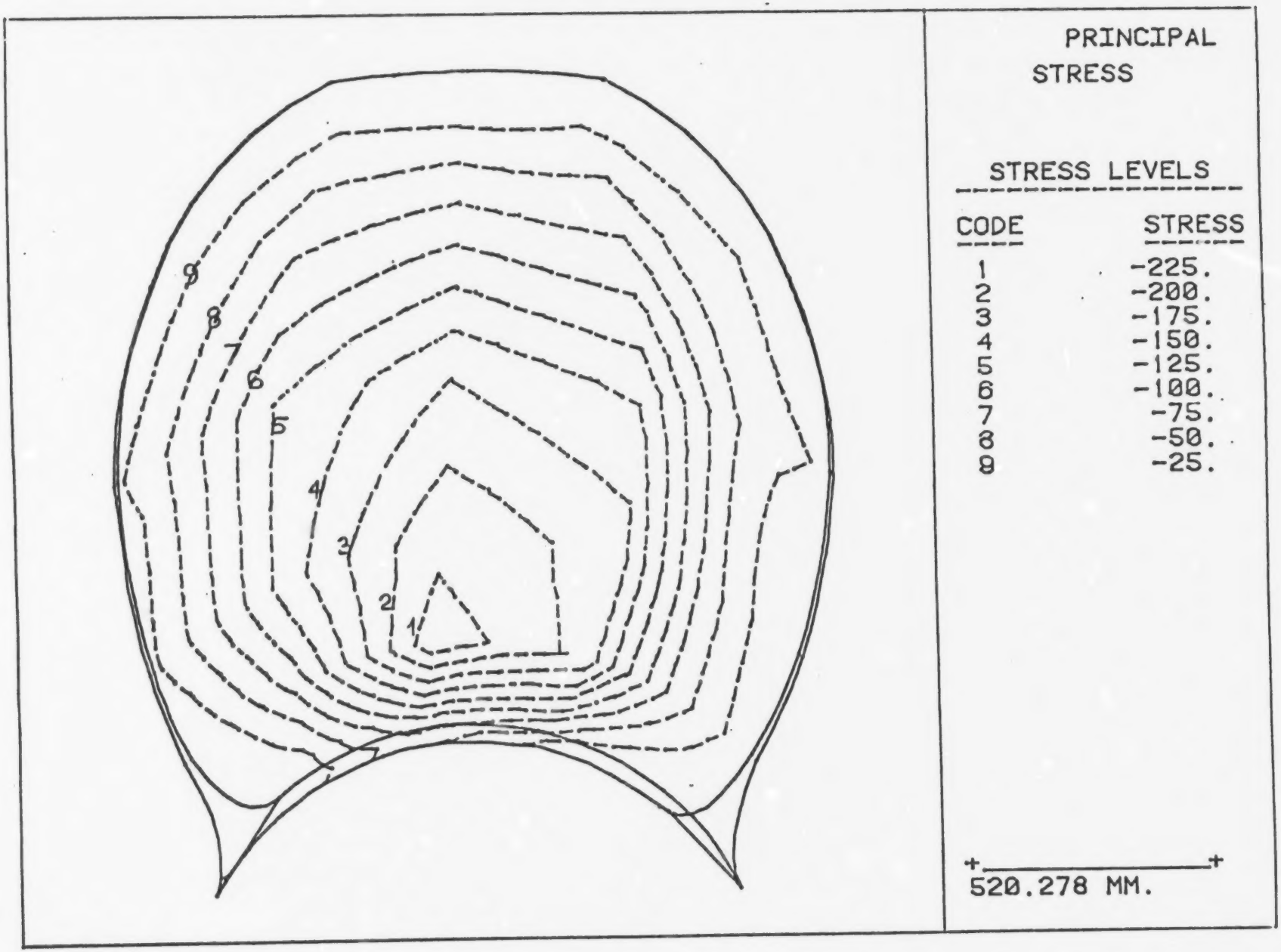


Figure 27: Zero Skew - Load Case L2-A

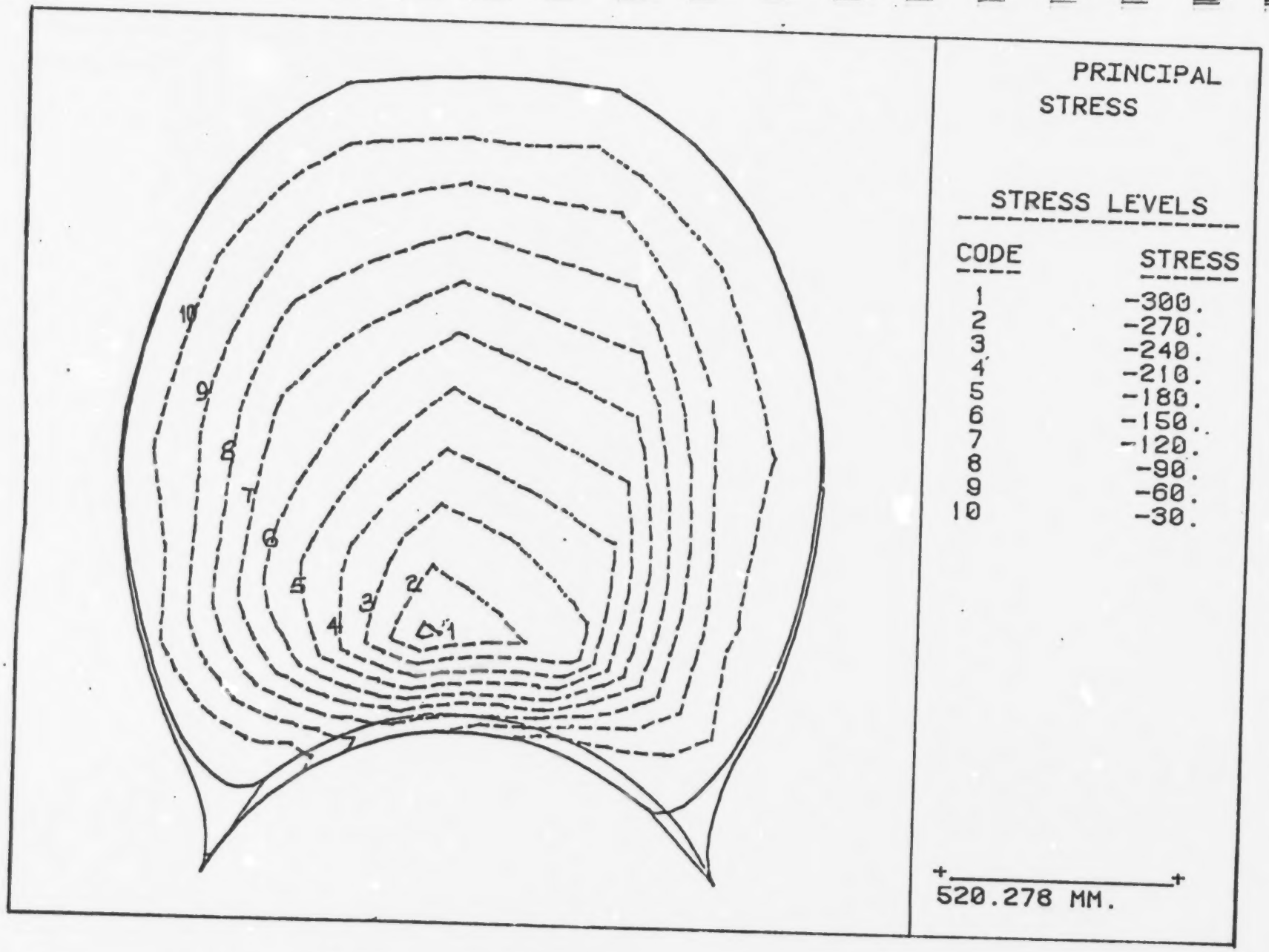


Figure 28: Zero Skew - Load Case L3-A

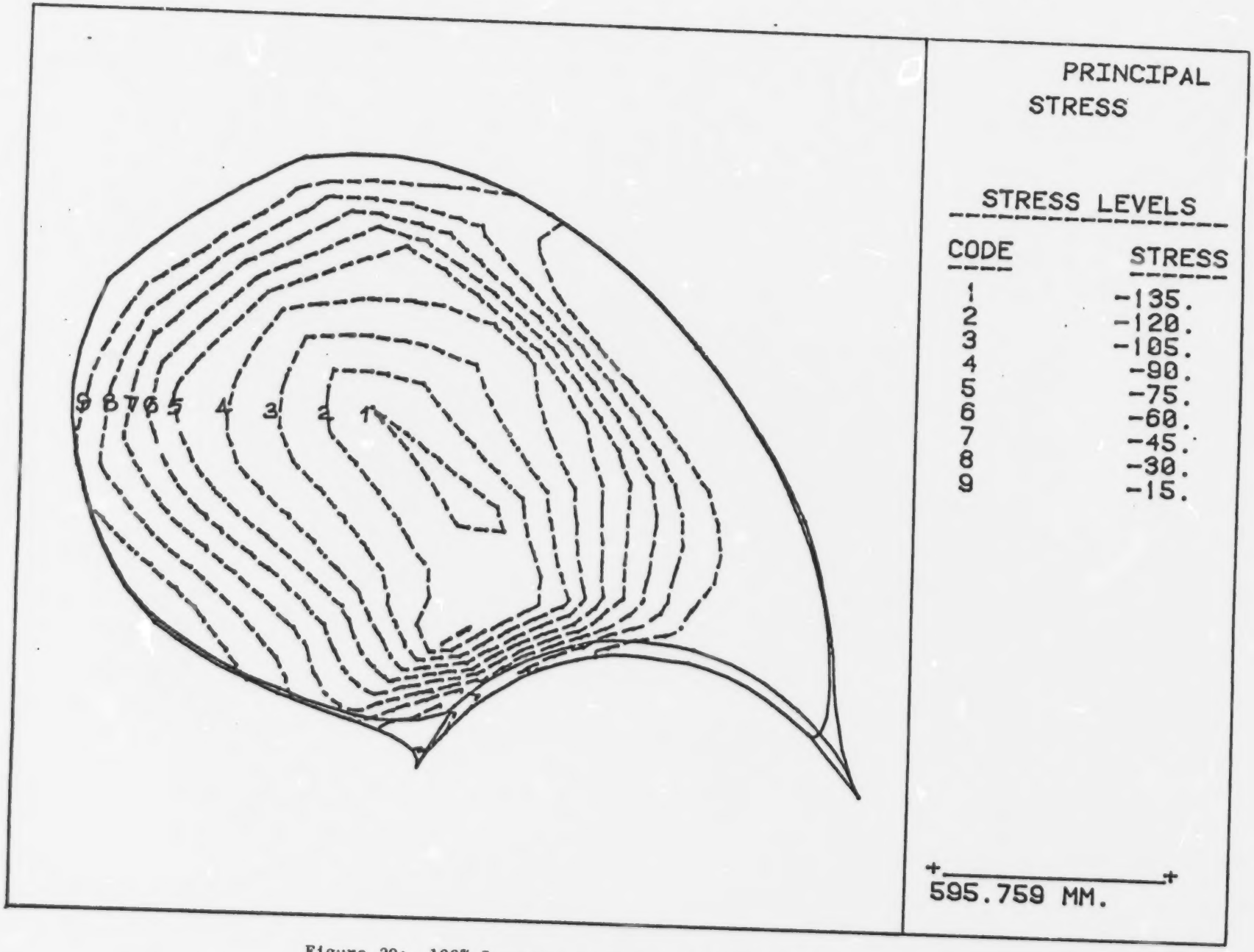


Figure 29: 100% Increase in Skew - Load Case L1-A

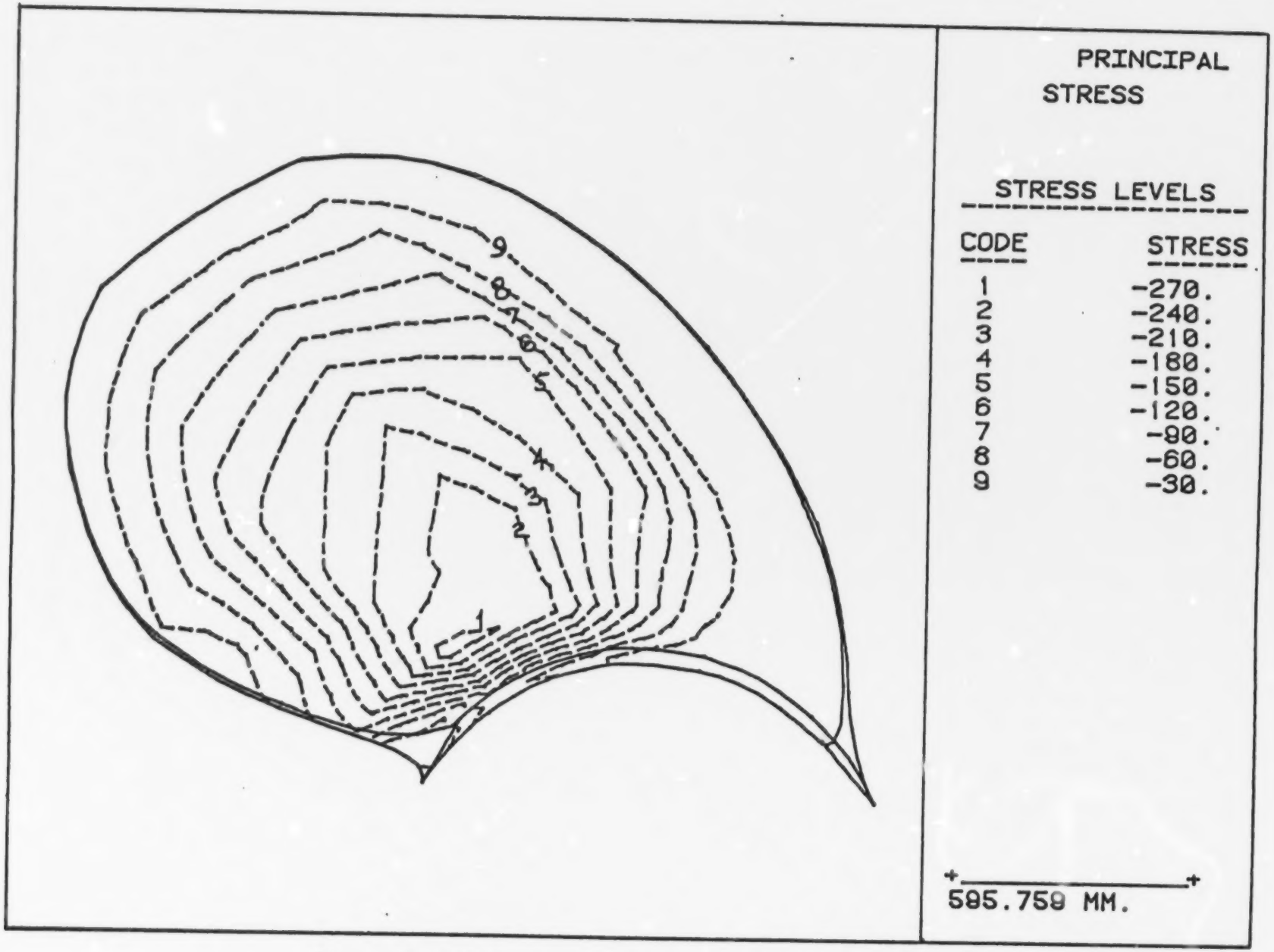


Figure 30: 100% Increase in Skew - Load Case L2-A

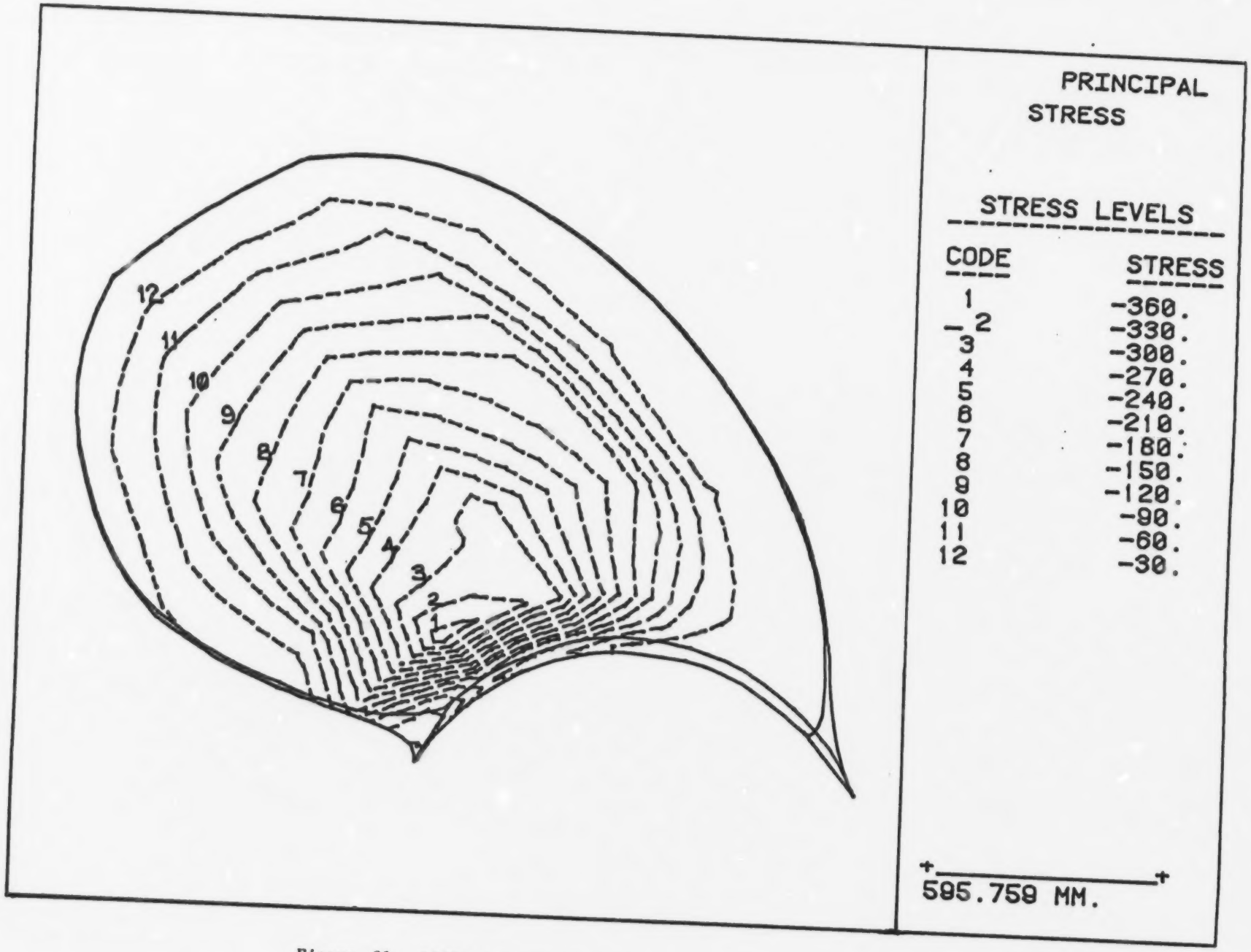


Figure 31: 100% Increase in Skew - Load Case L3-A

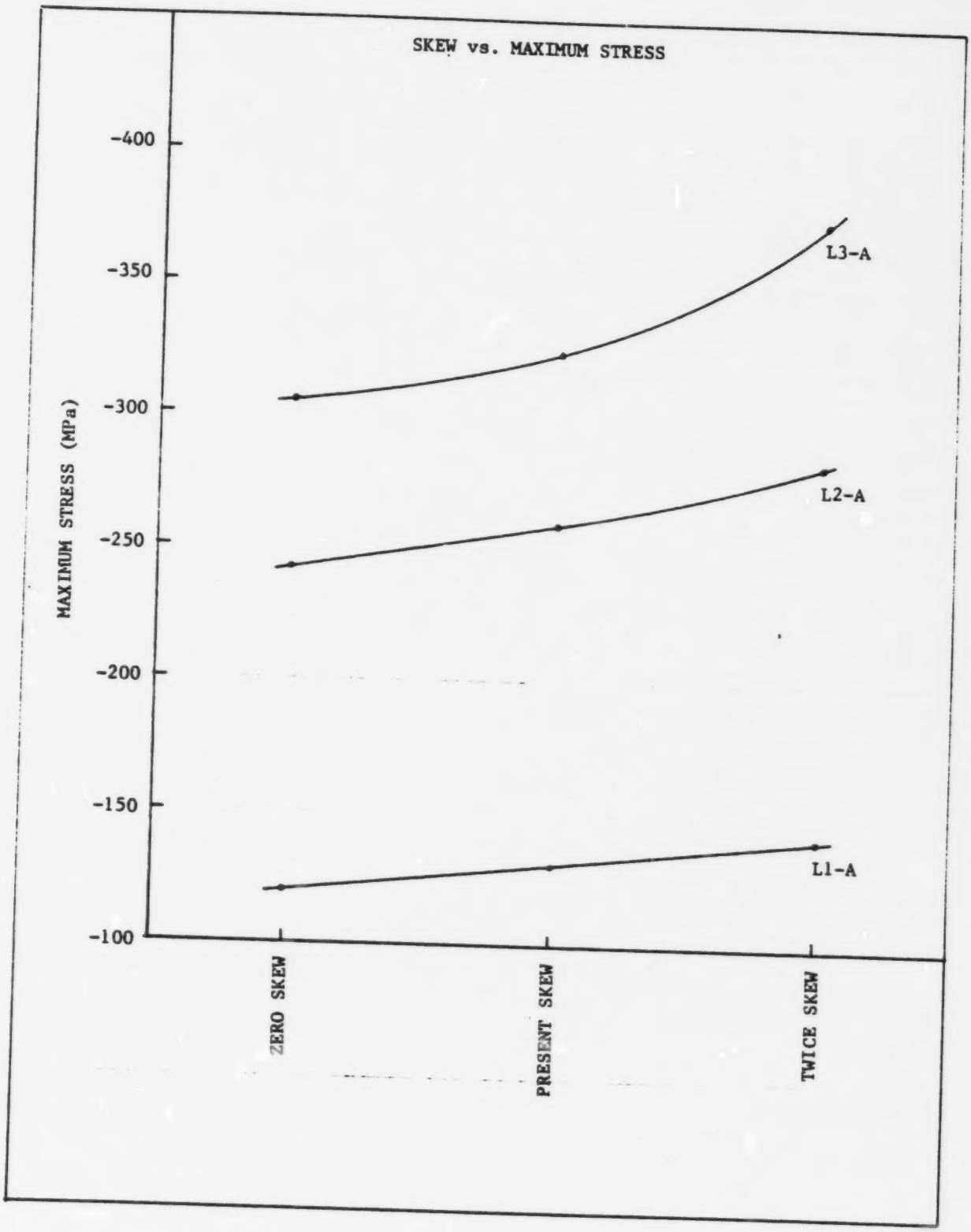


Figure 32: Effect of Skew on Maximum Stress

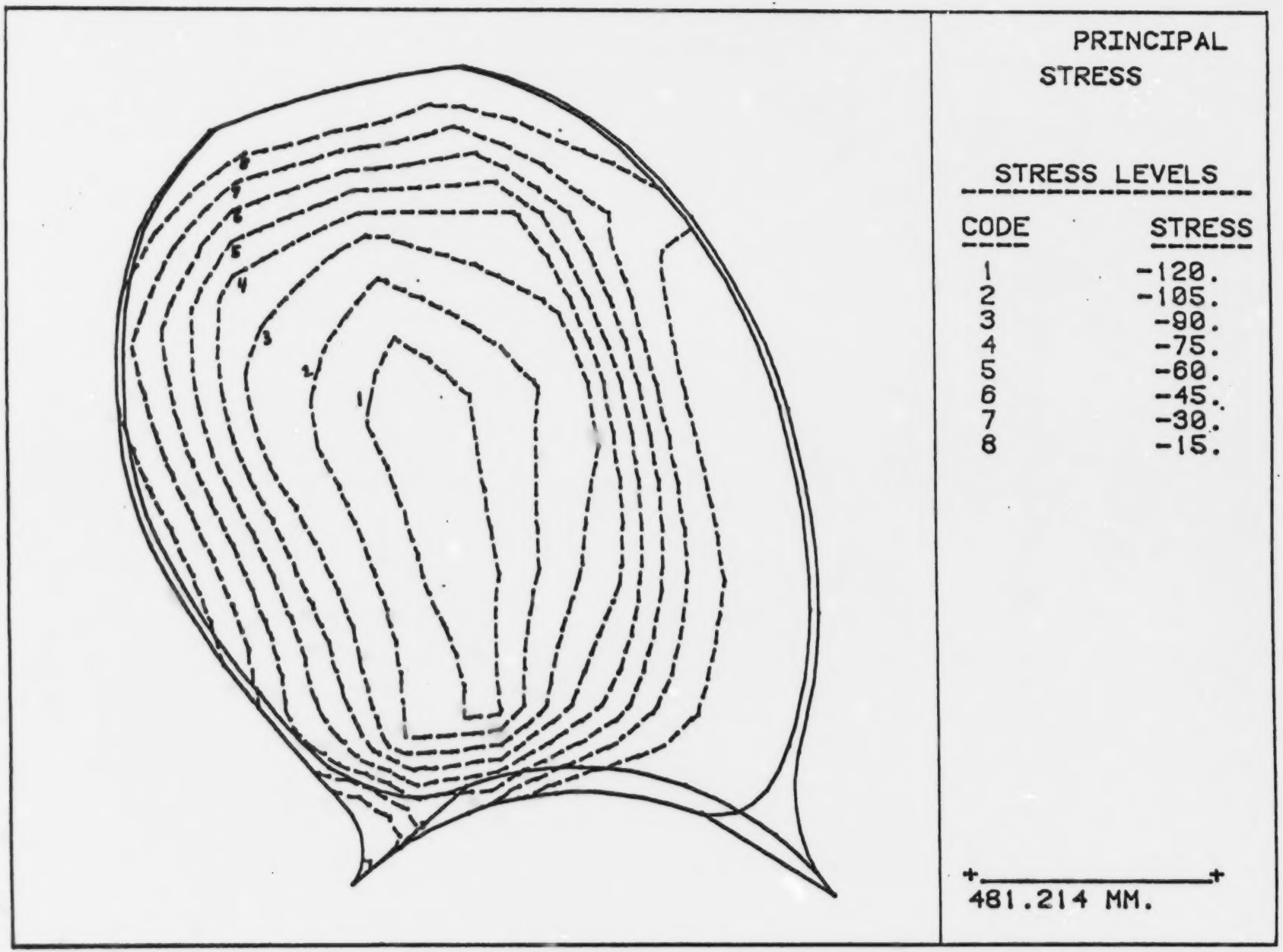


Figure 33: 20° Rotation about Spindle Axis (Increase in Pitch) - Load Case L1-A

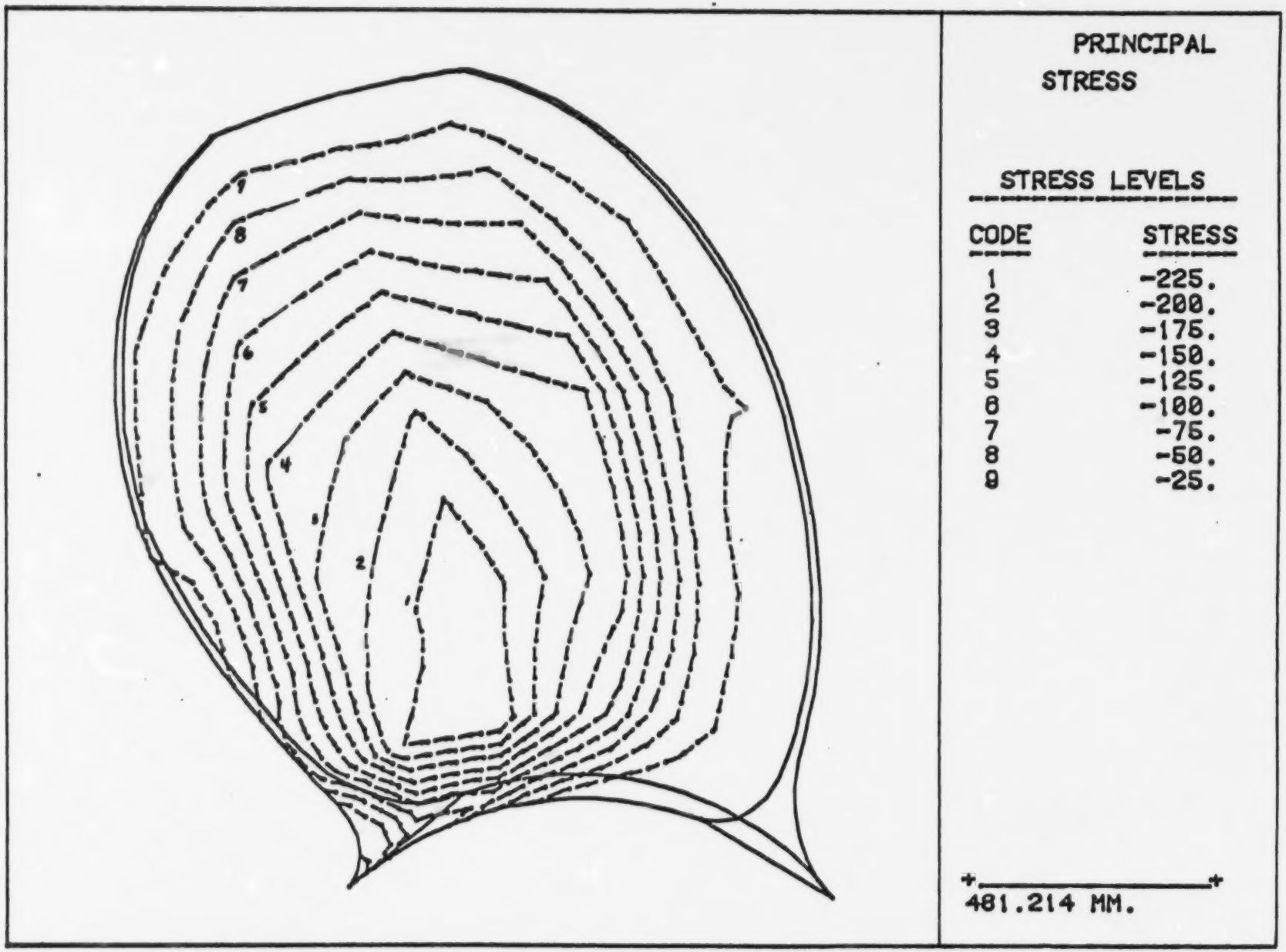


Figure 34: 20° Rotation about Spindle Axis (Increase in Pitch) - Load Case L2-A

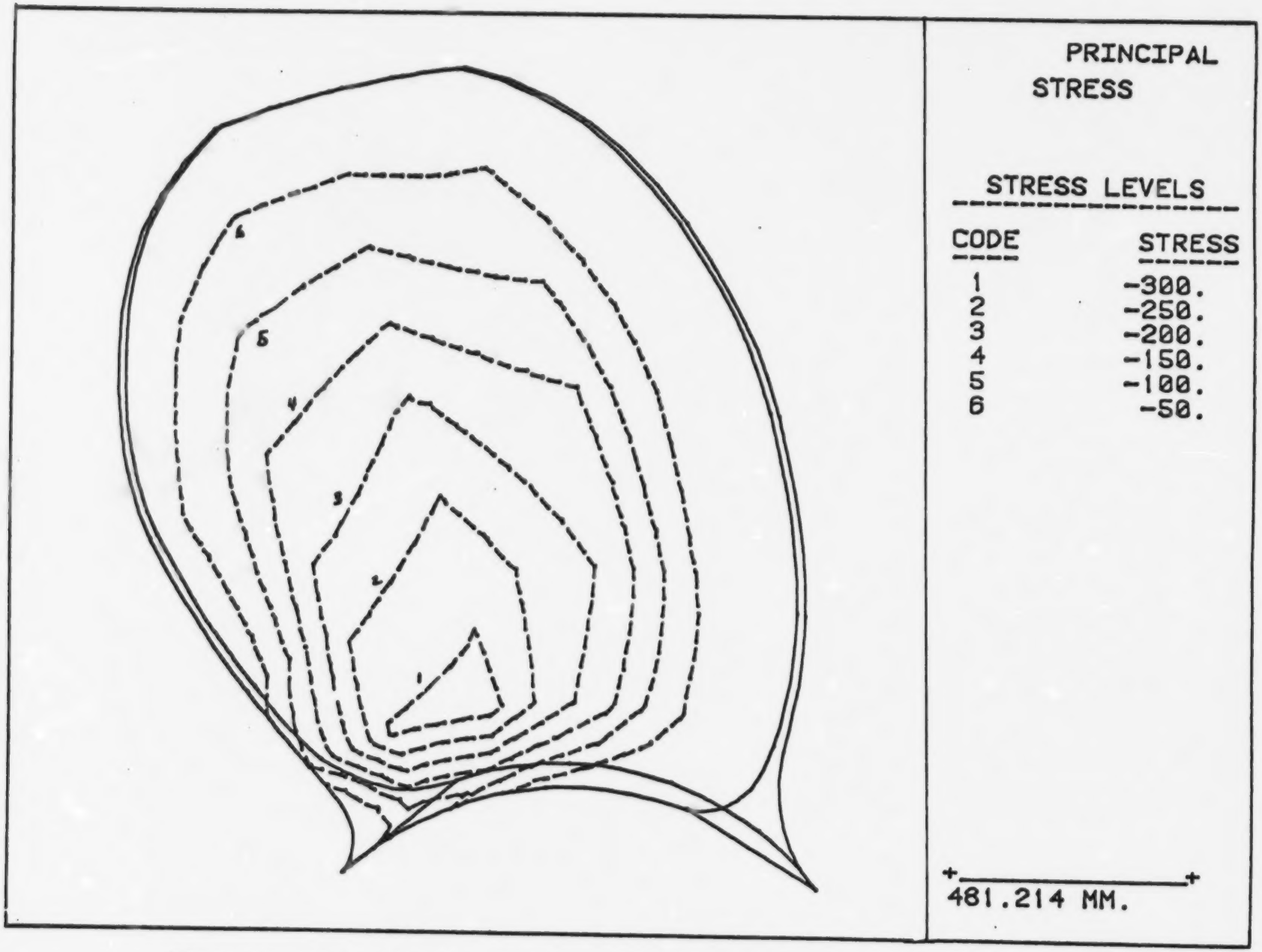


Figure 35: 20° Rotation about Spindle Axis (Increase in Pitch) - Load Case L3-A

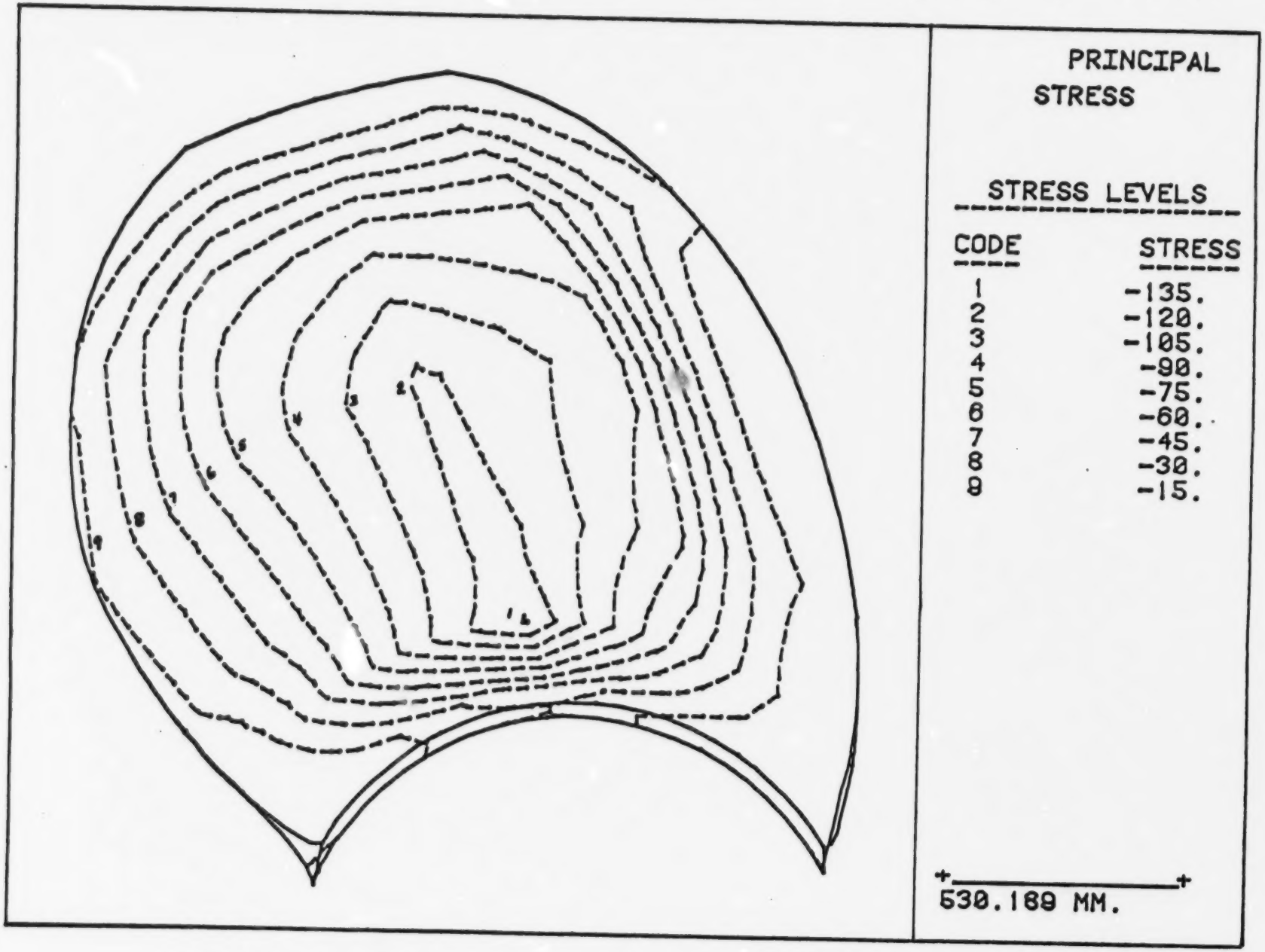


Figure 36: -20° Rotation about Spindle Axis (Decrease in Pitch) - Load Case L1-A

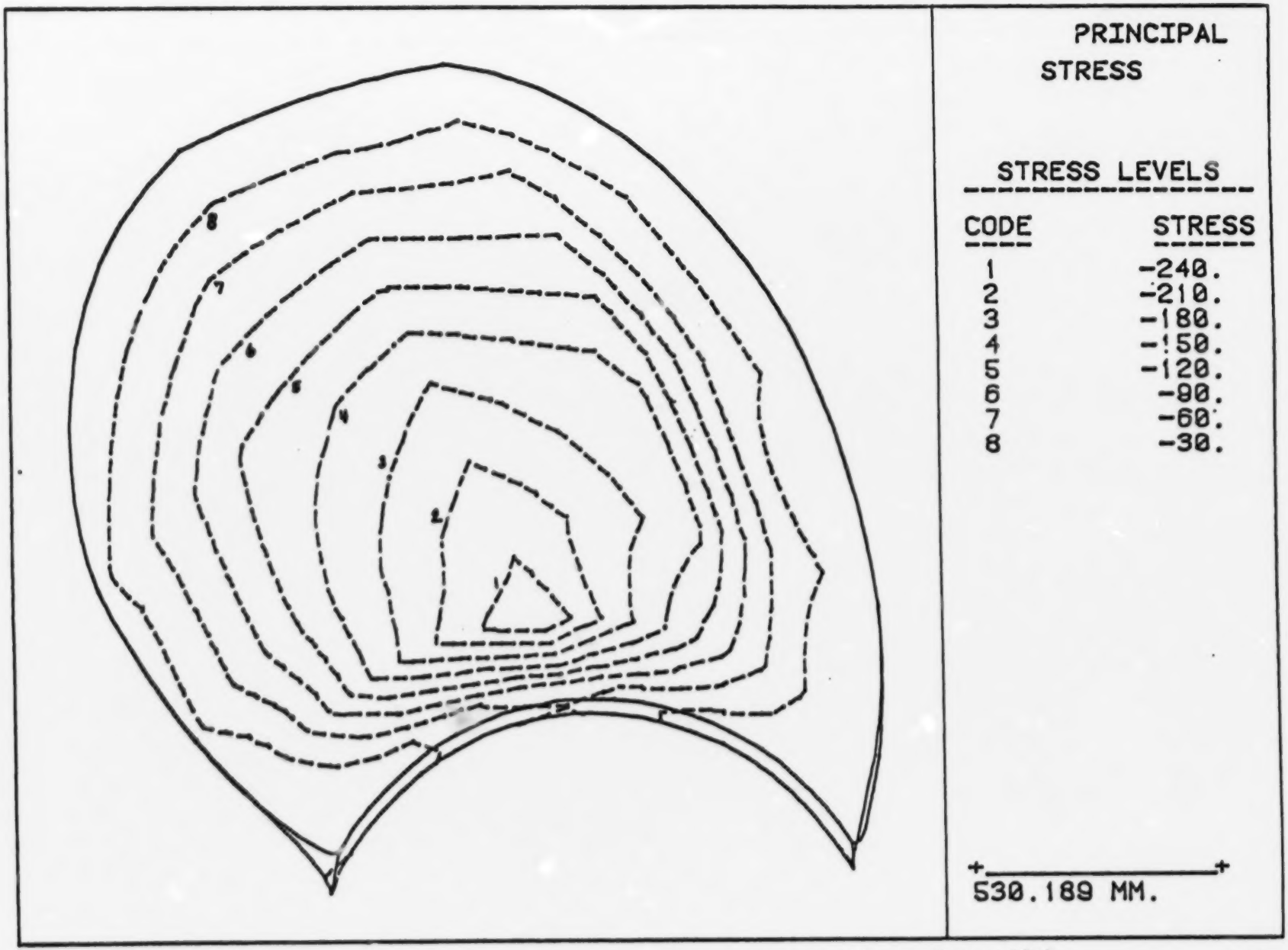


Figure 37: -20° Rotation about Spindle Axis (Decrease in Pitch) - Load Case L2-A

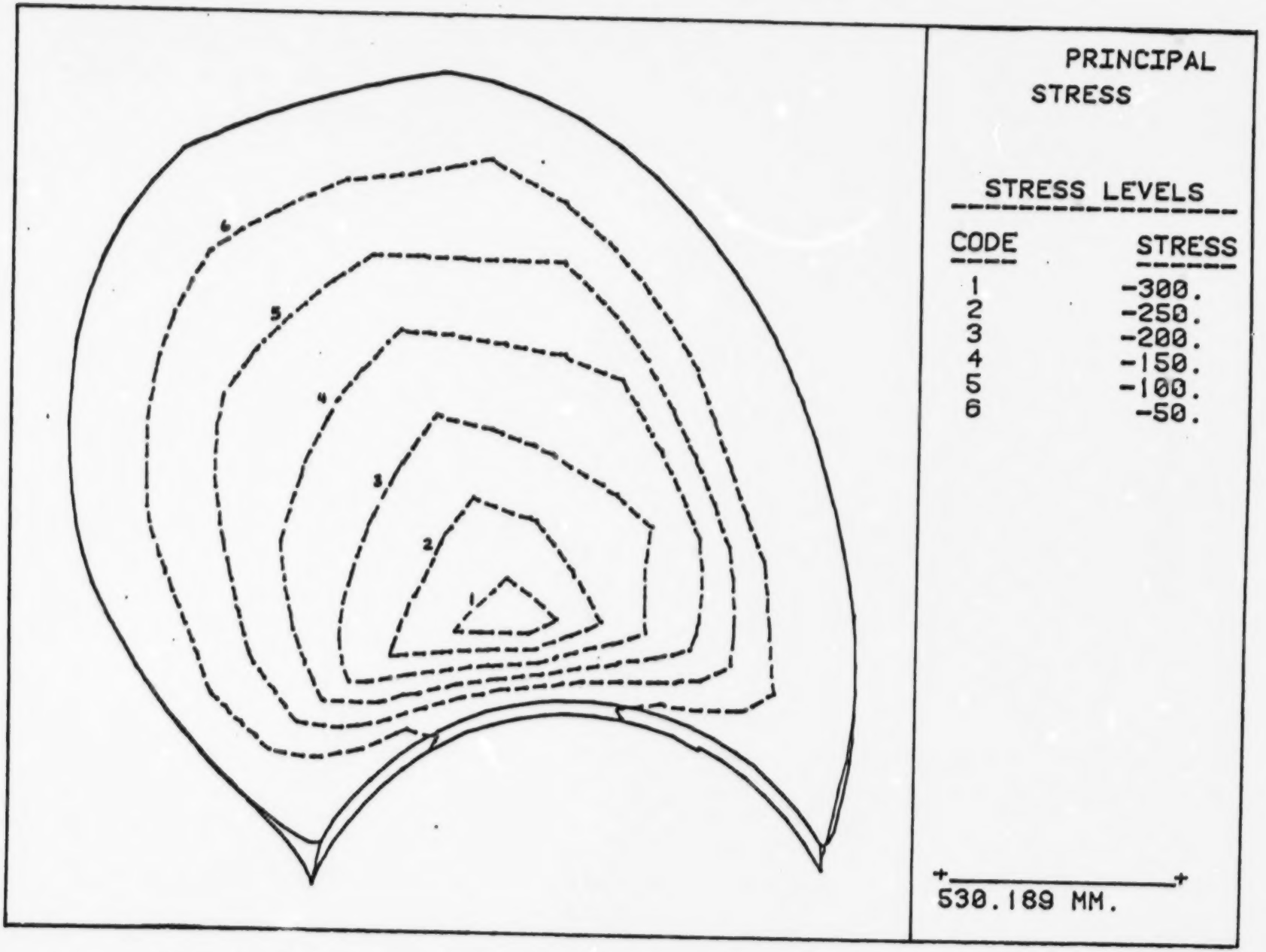


Figure 38 -20° Rotation about Spindle Axis (Decrease in Pitch) - Load Case L3-A

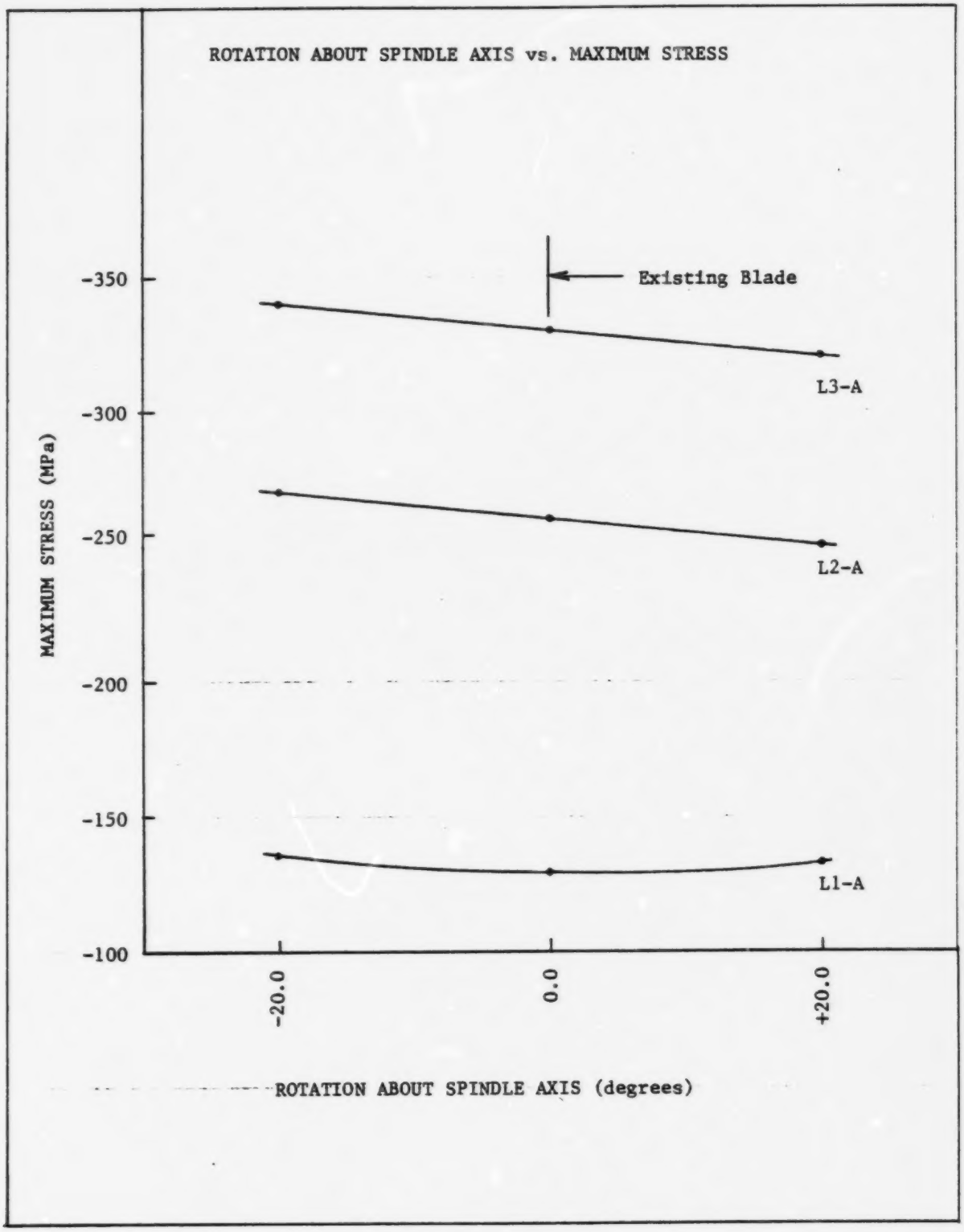


Figure 39: Effect of Rotation About Spindle Axis on
on Maximum Stress

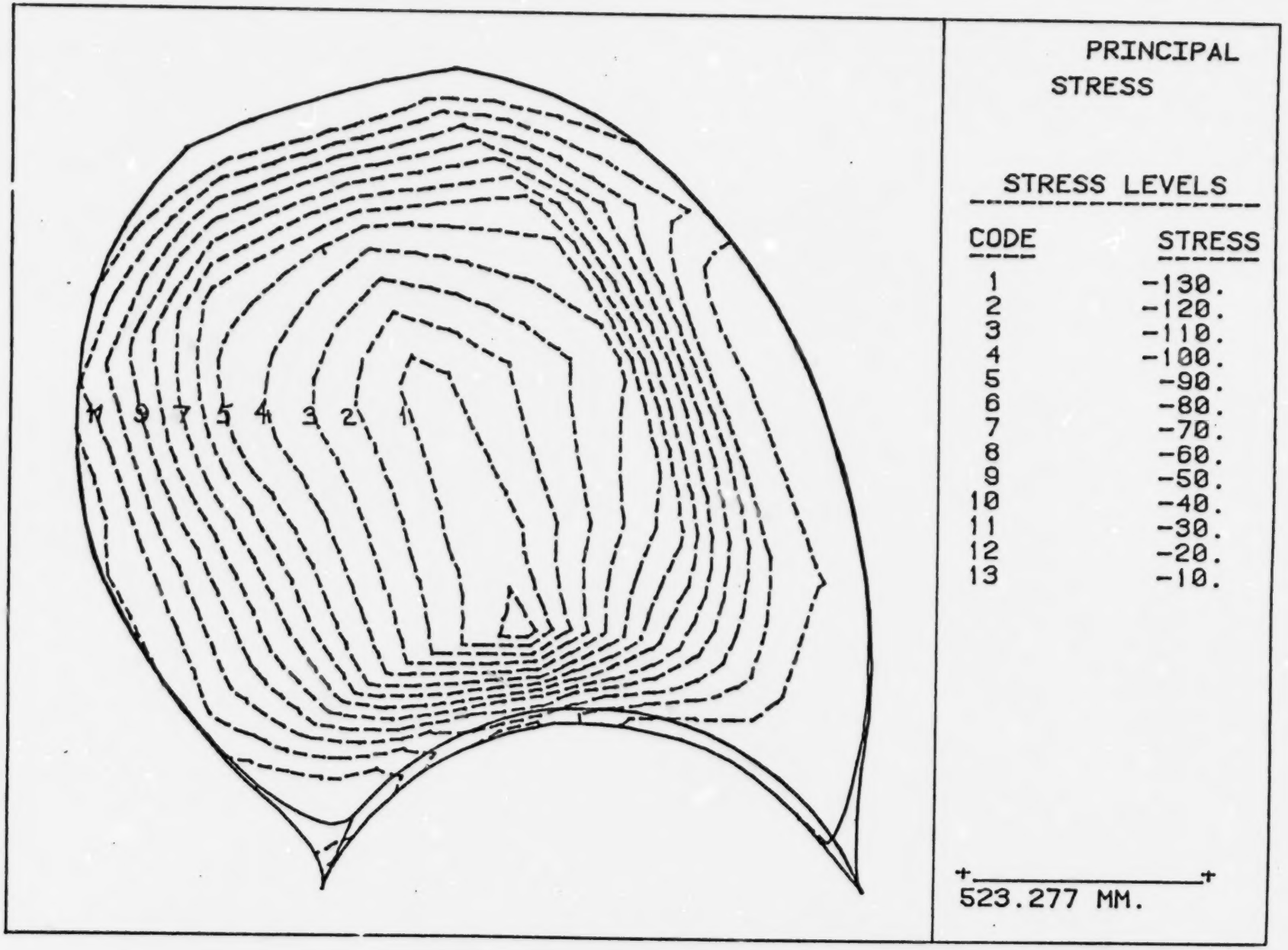


Figure 40: Pitch/Diameter Ratio = 0.50 - Load Case L1-A

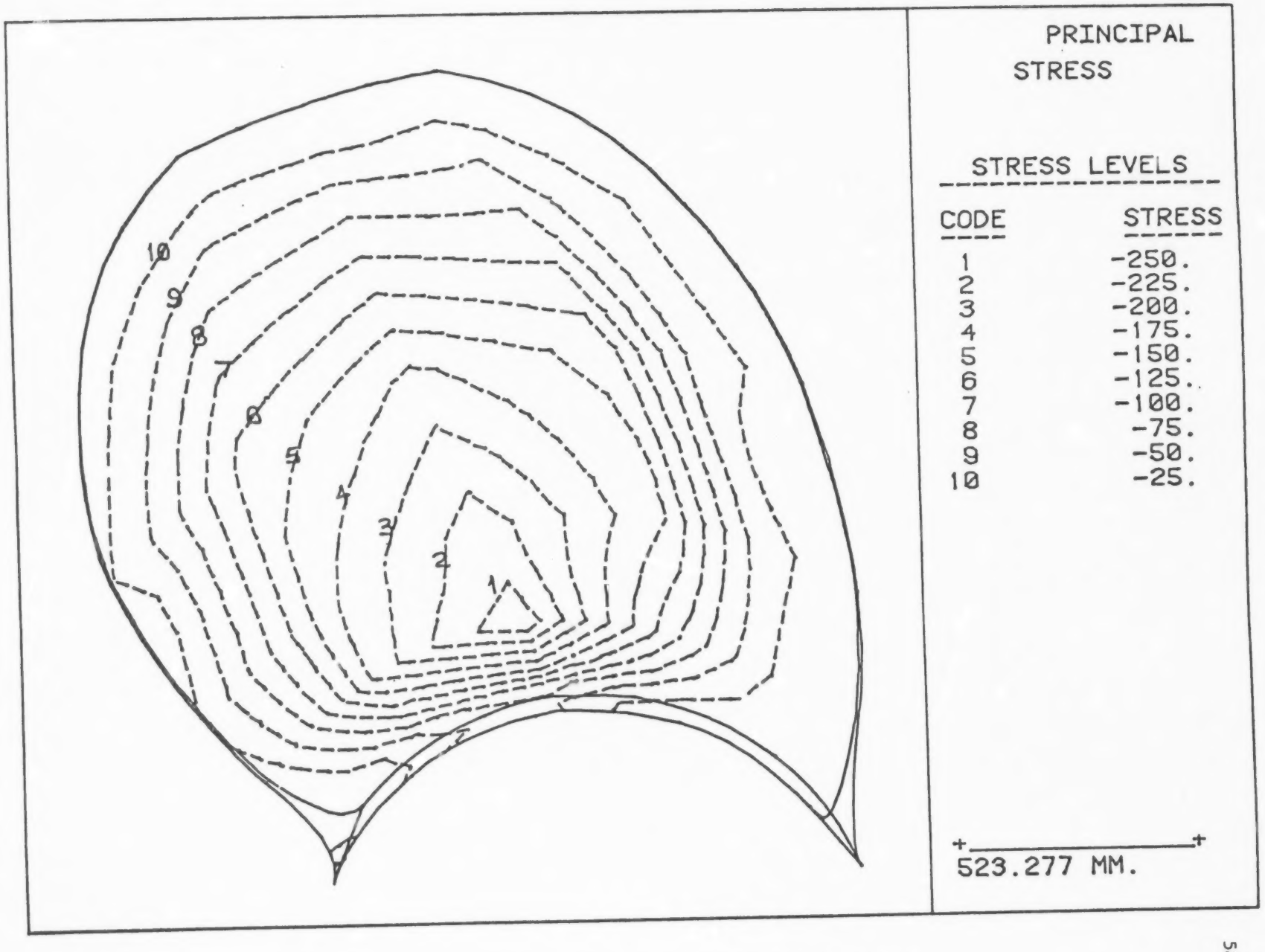


Figure 41: Pitch/Diameter Ratio = 0.50 - Load Case L2-A

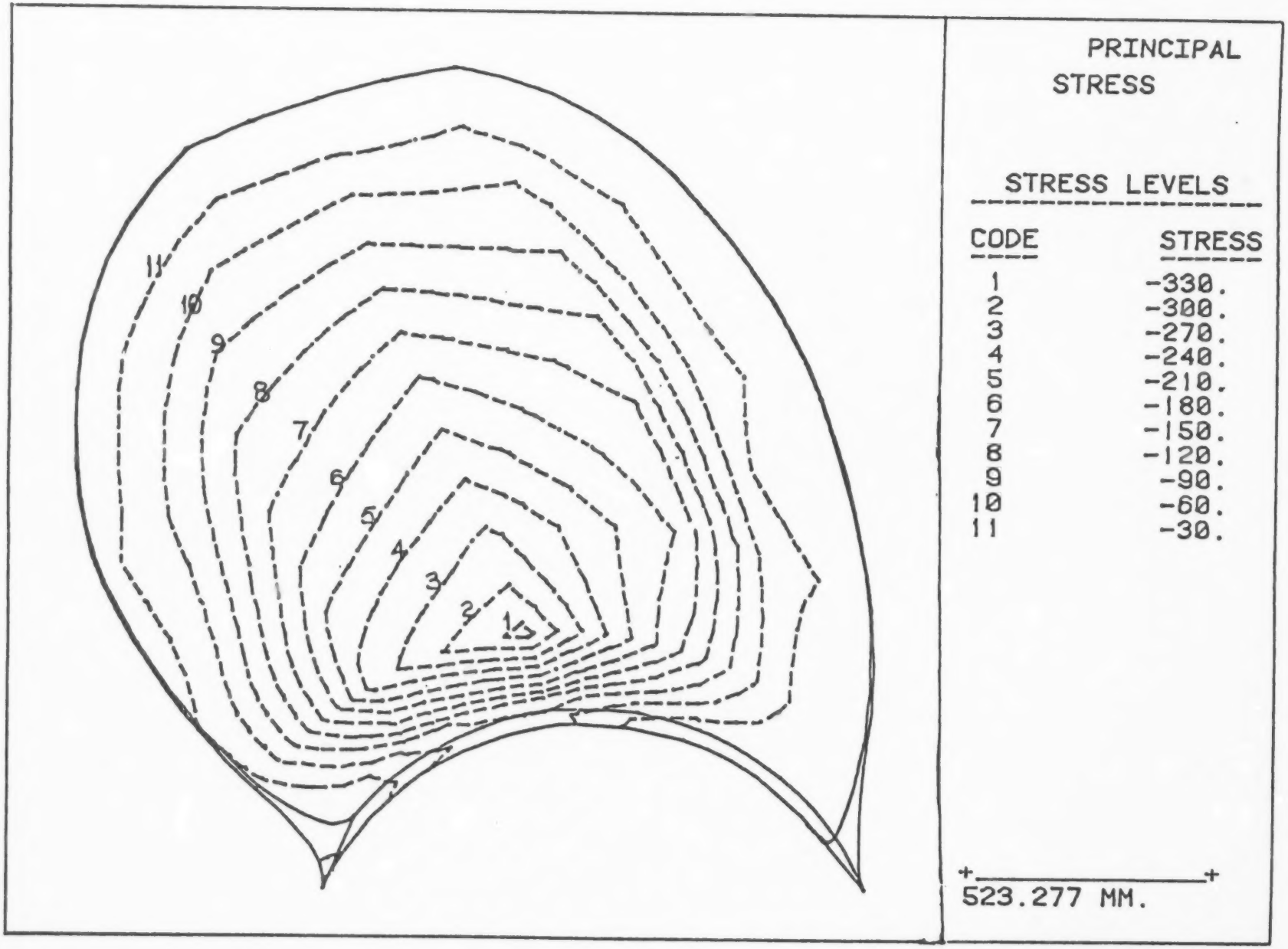


Figure 42: Pitch/Diameter Ratio = 0.50 - Load Case L3-A

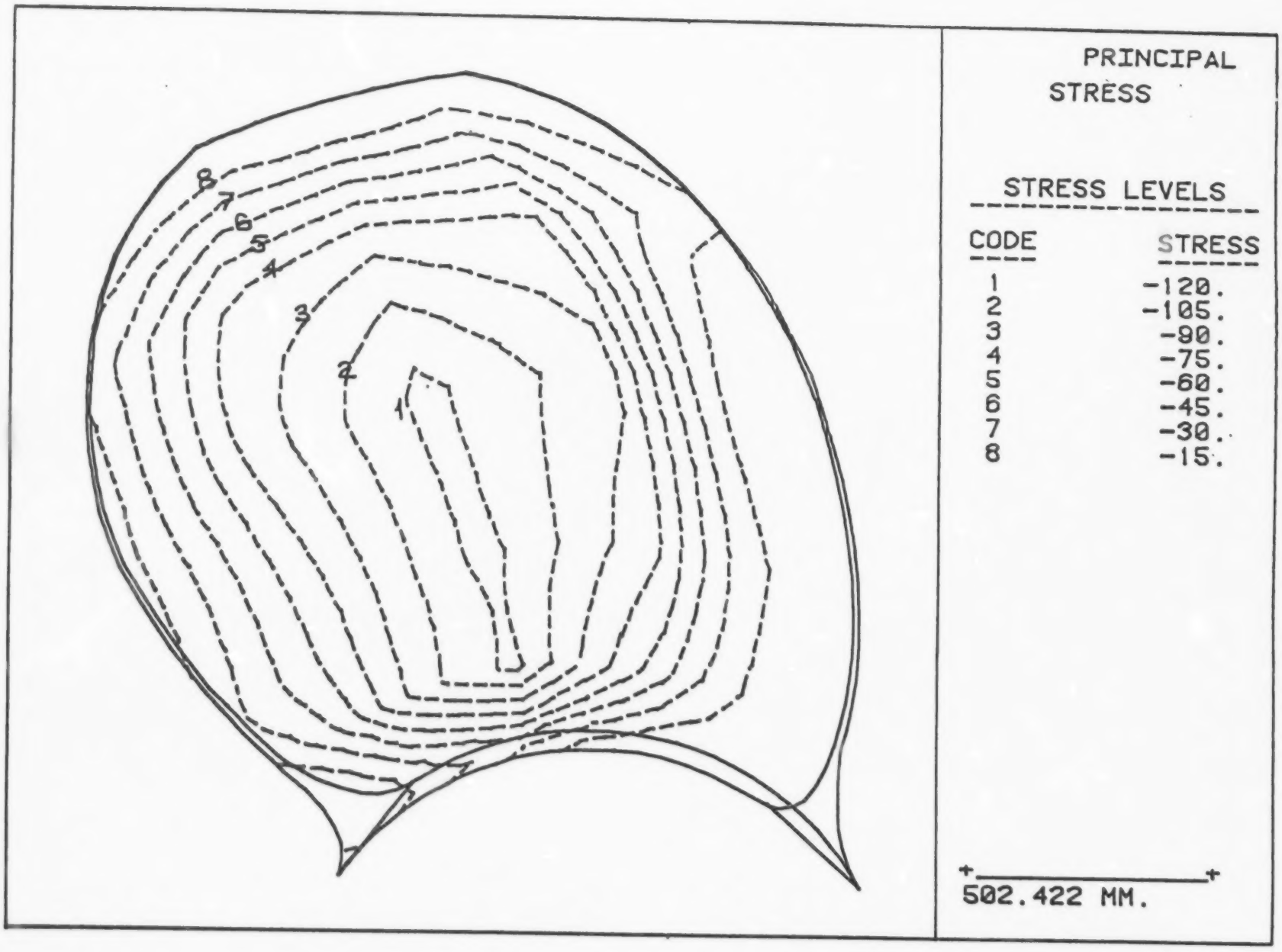


Figure 43: Pitch/Diameter Ratio = 1.00 - Load Case L1-A

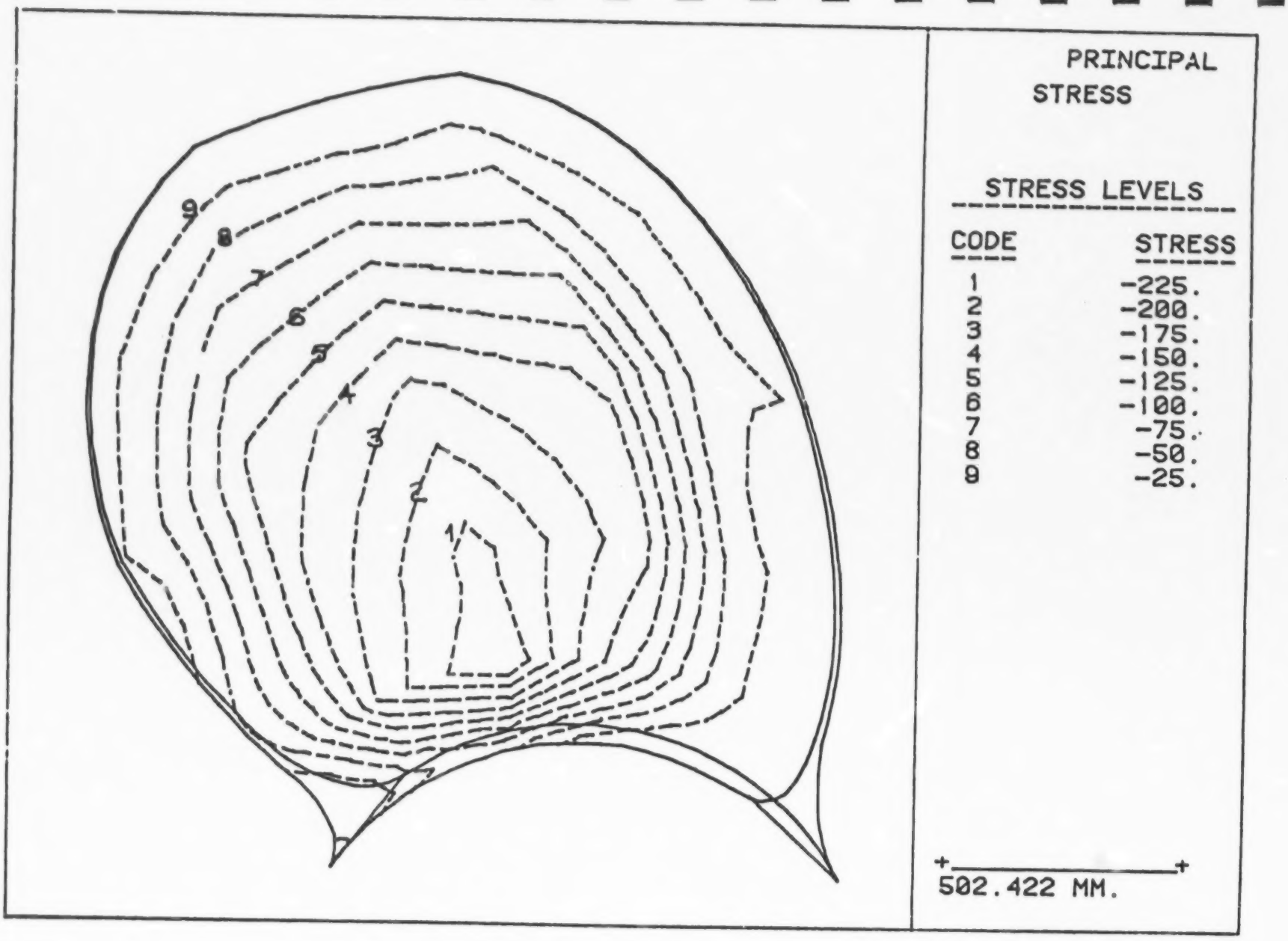


Figure 44: Pitch/Diameter Ratio = 1.00 - L2-A

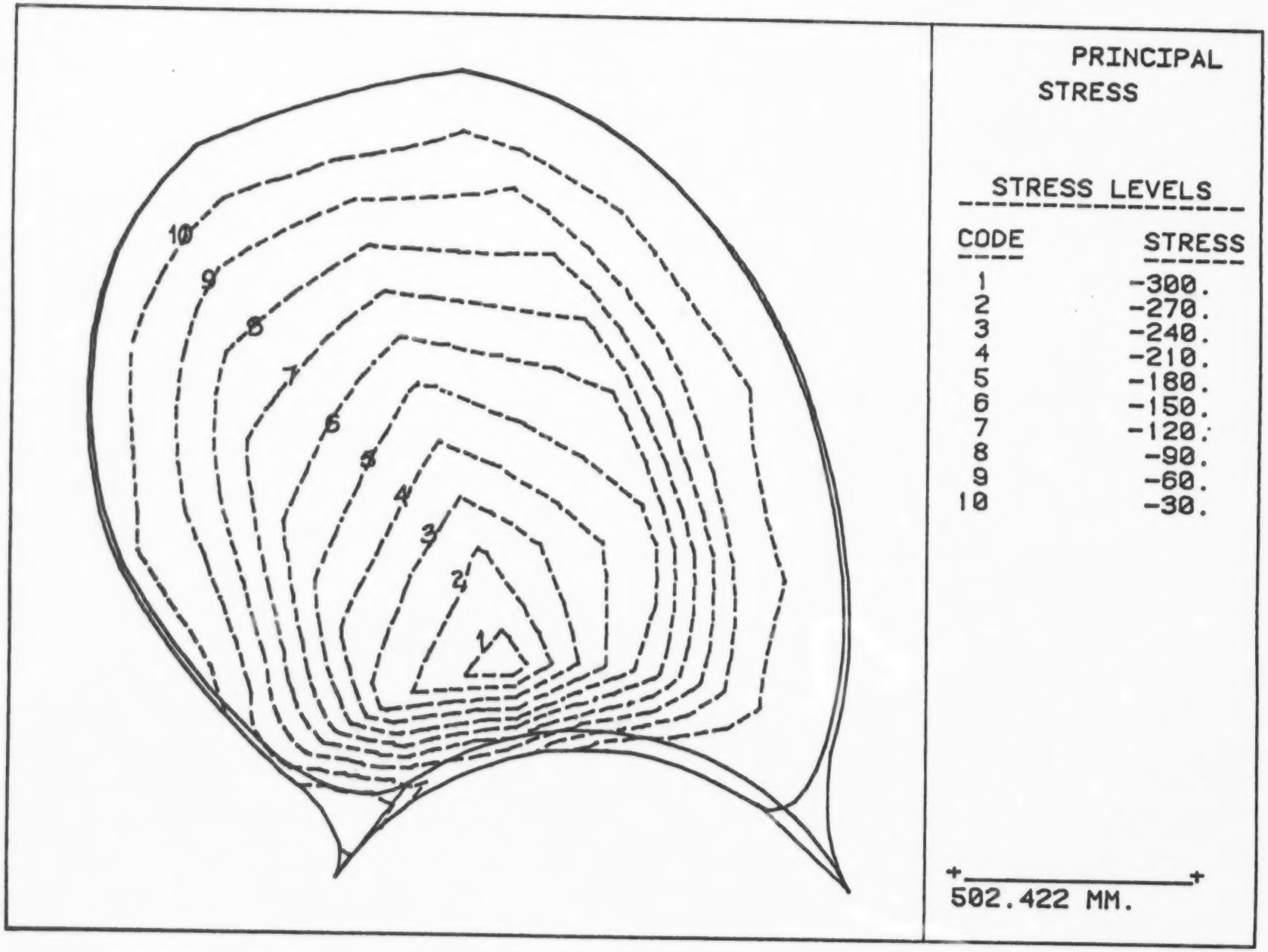


Figure 45: Pitch/Diameter Ratio = 1.00 - Load Case L3-A

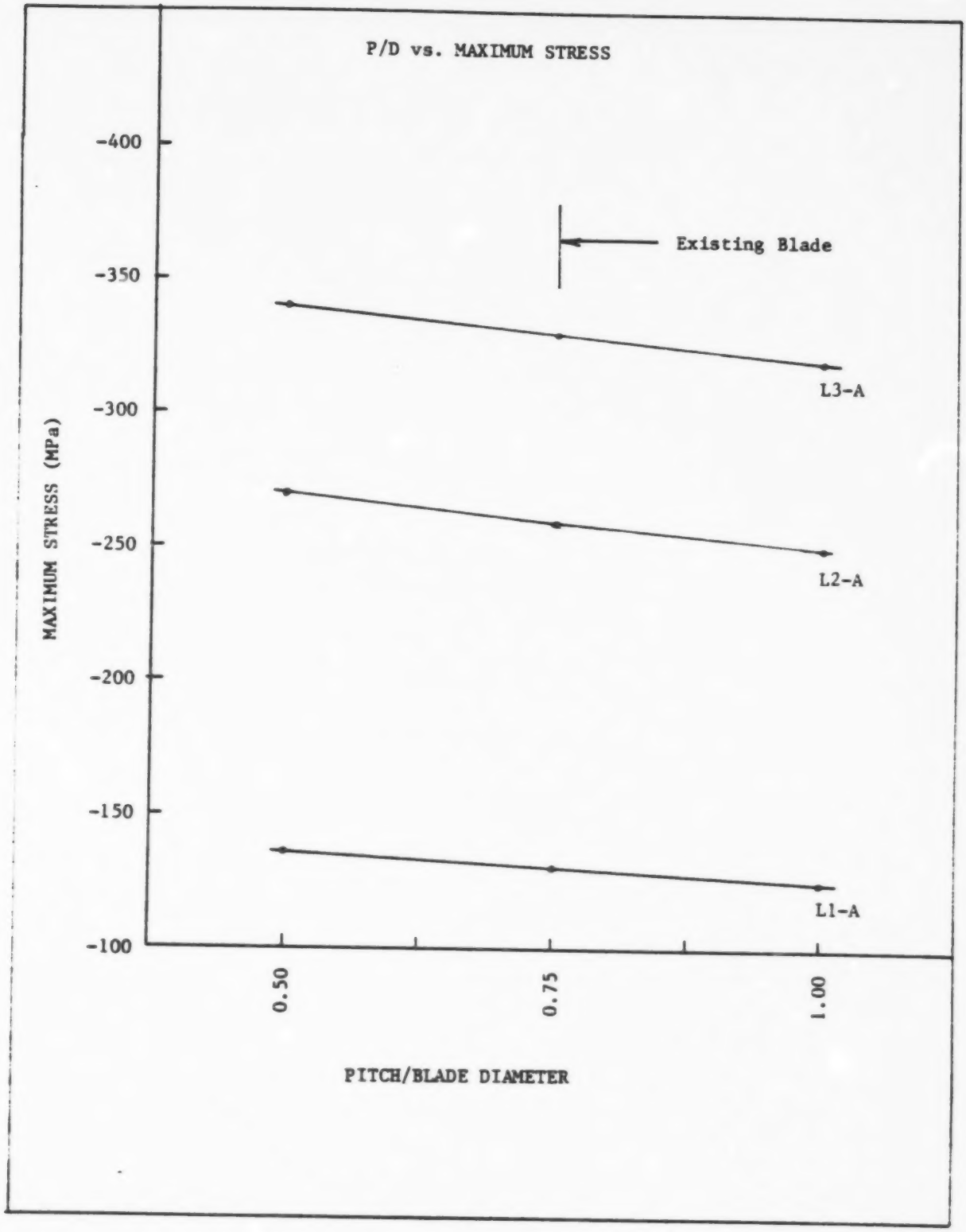


Figure 46: Effect of P/D Ratio on Maximum Stress

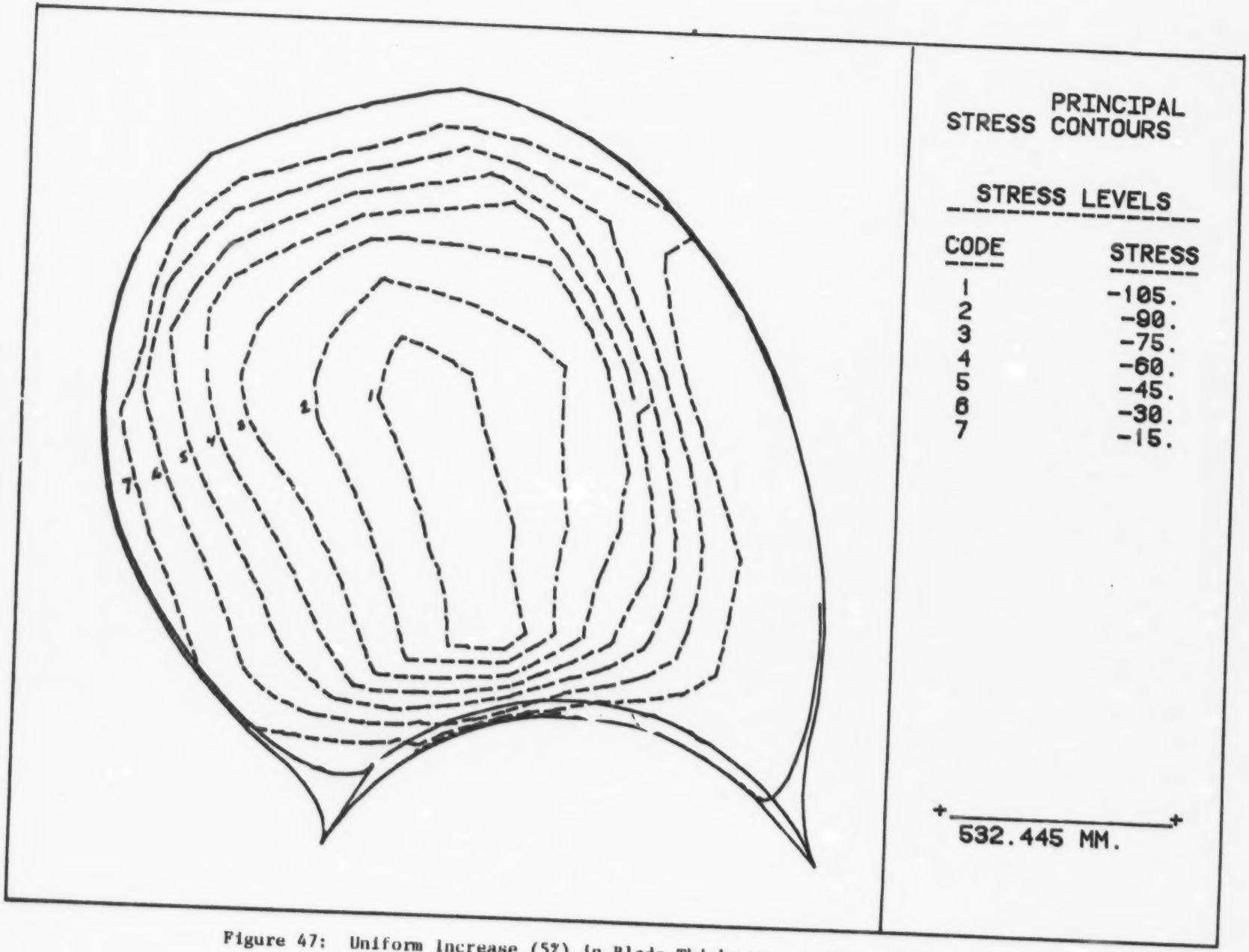


Figure 47: Uniform Increase (5%) in Blade Thickness - Load Case L1-A

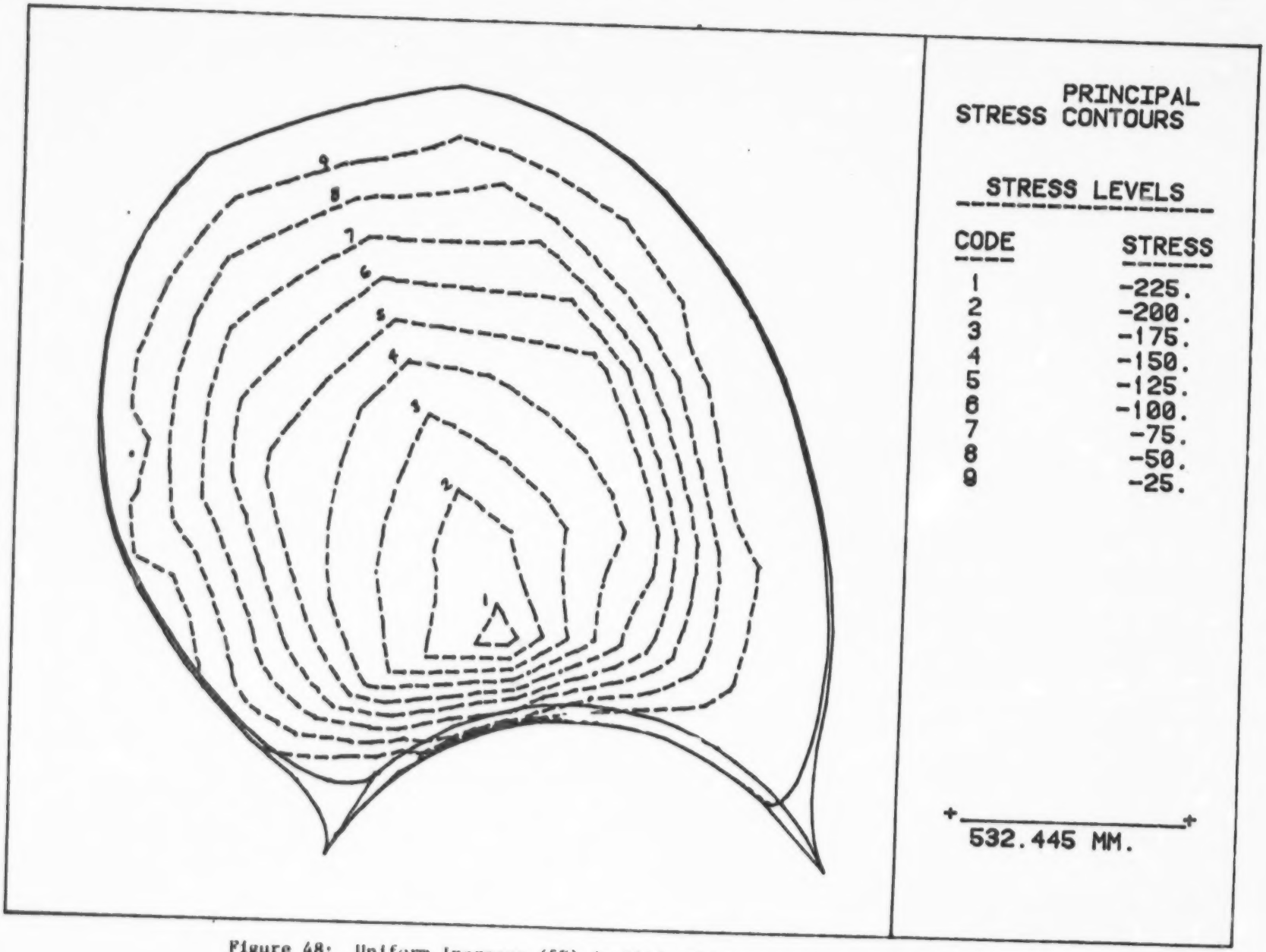


Figure 48: Uniform Increase (5%) in Blade Thickness - Load Case L2-A

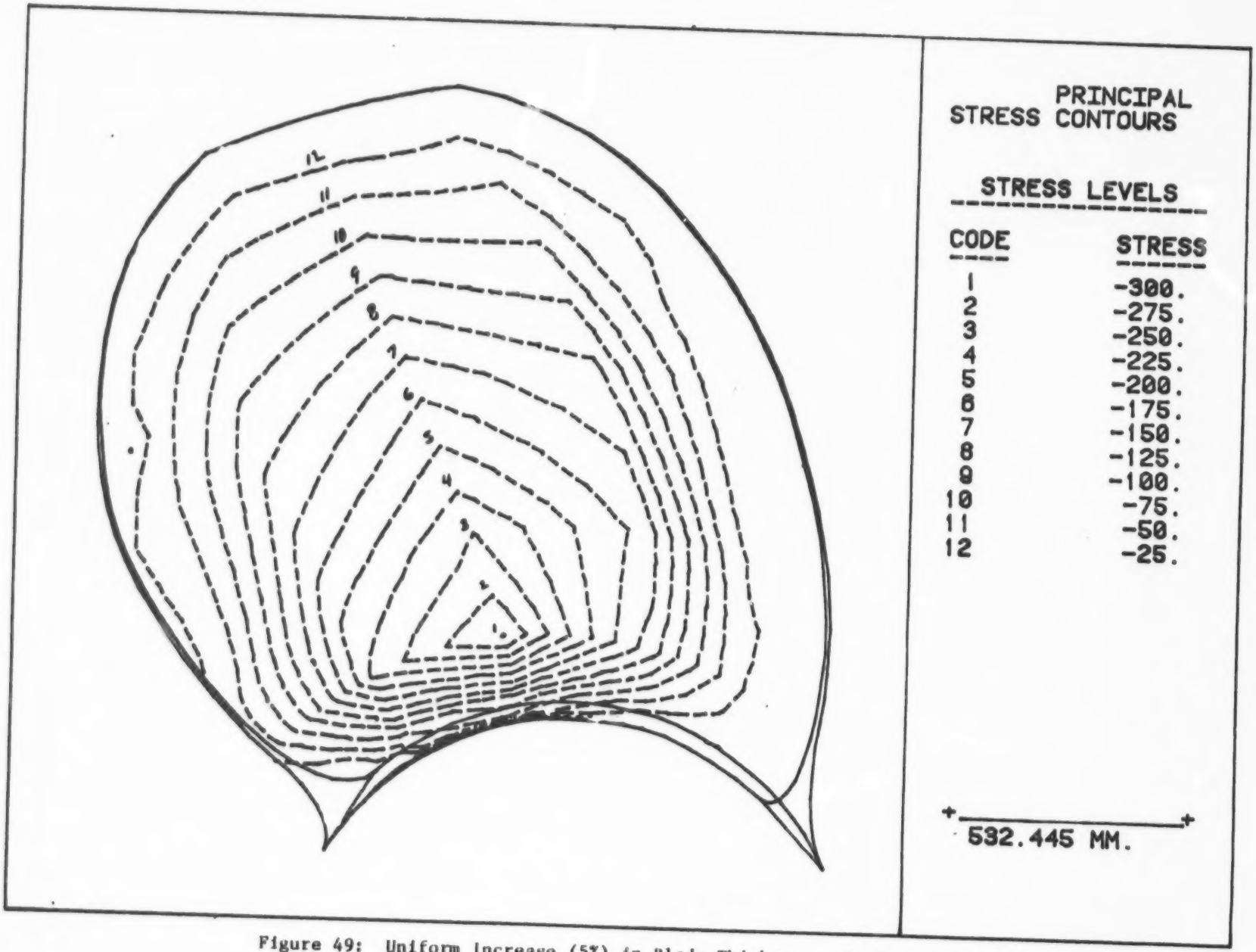


Figure 49: Uniform Increase (5%) in Blade Thickness - Load Case L3-A

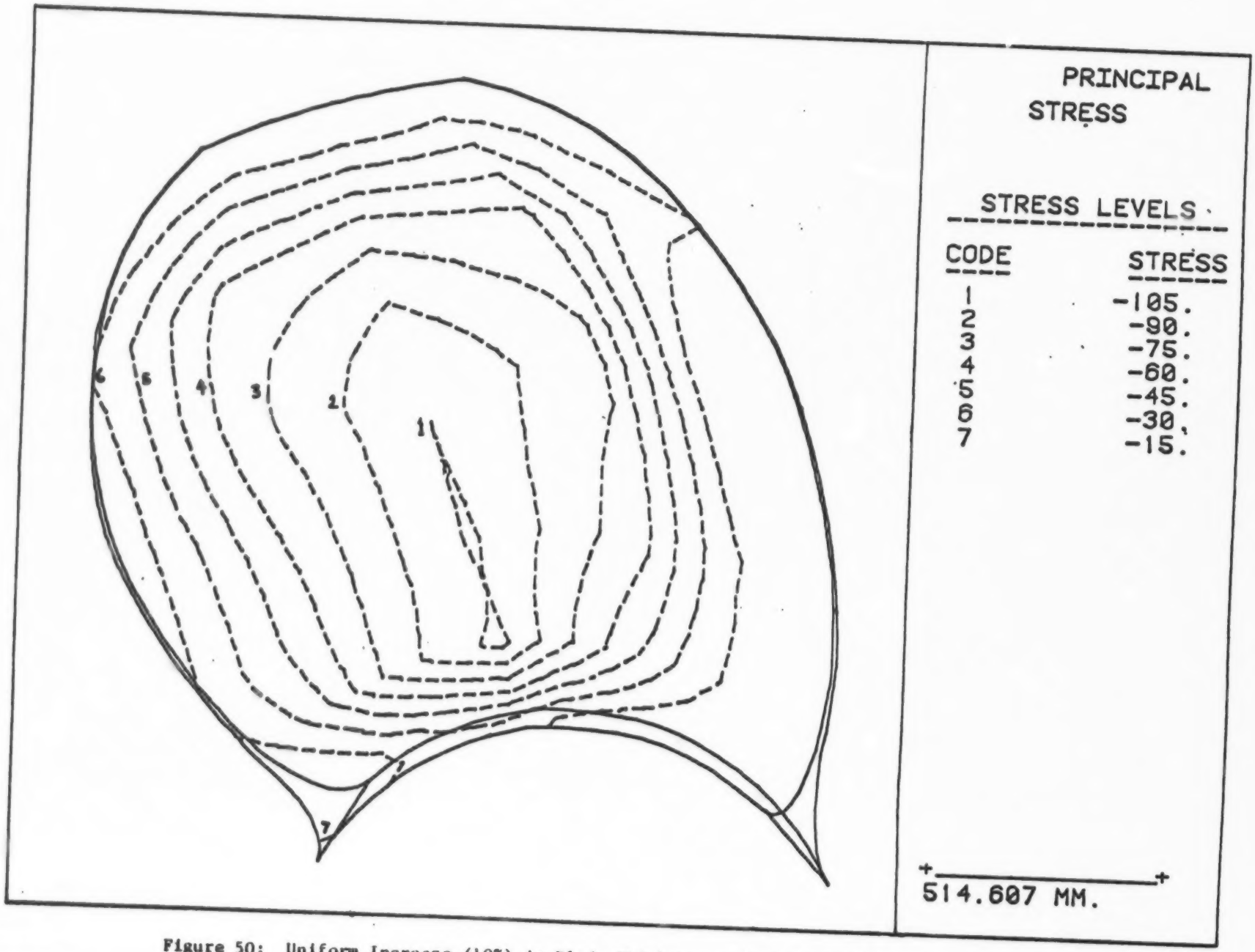


Figure 50: Uniform Increase (10%) in Blade Thickness - Load Case L1-A

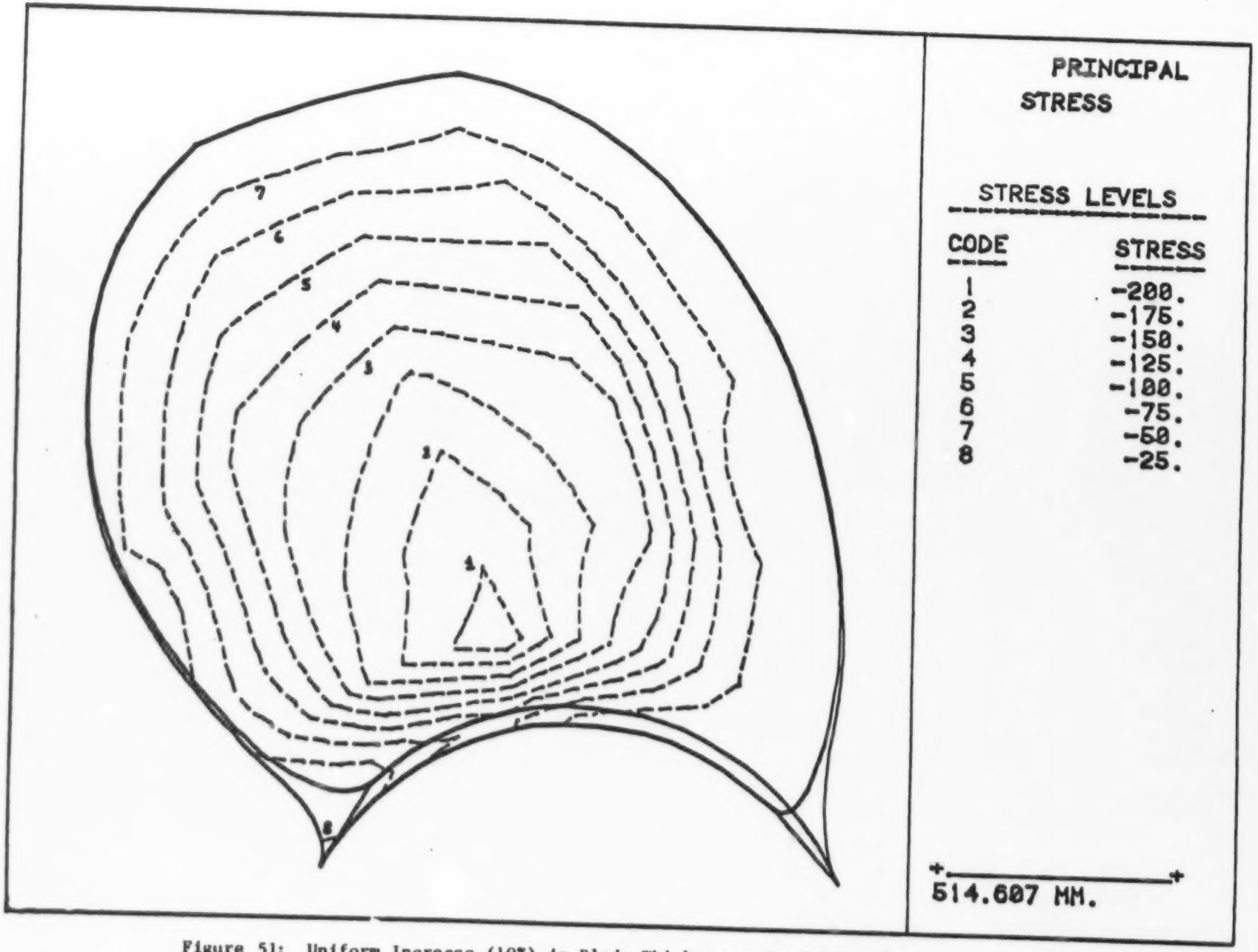


Figure 51: Uniform Increase (10%) in Blade Thickness - Load Case L2-A

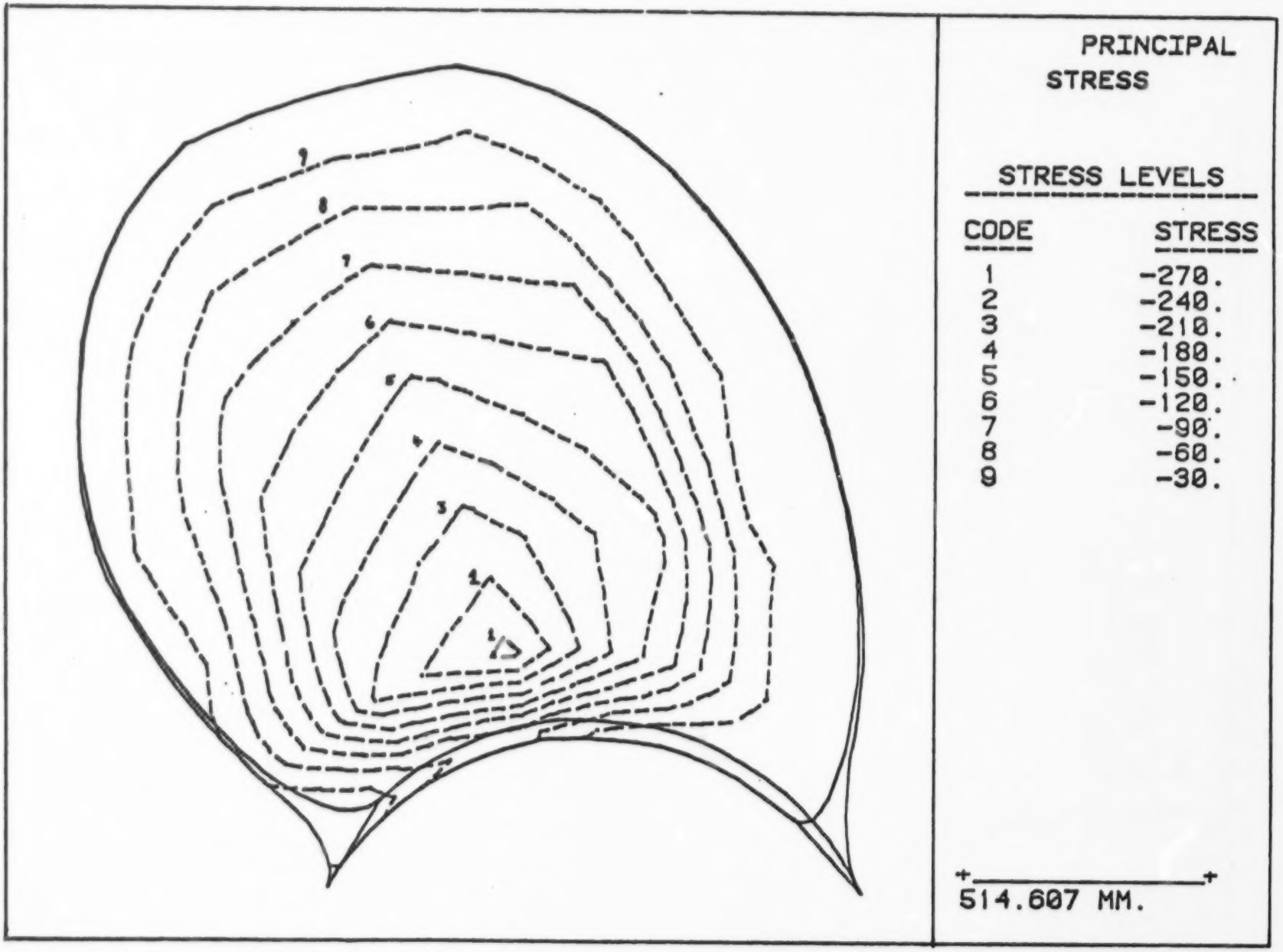


Figure 52 Uniform Increase (10%) in Blade Thickness - L3-A

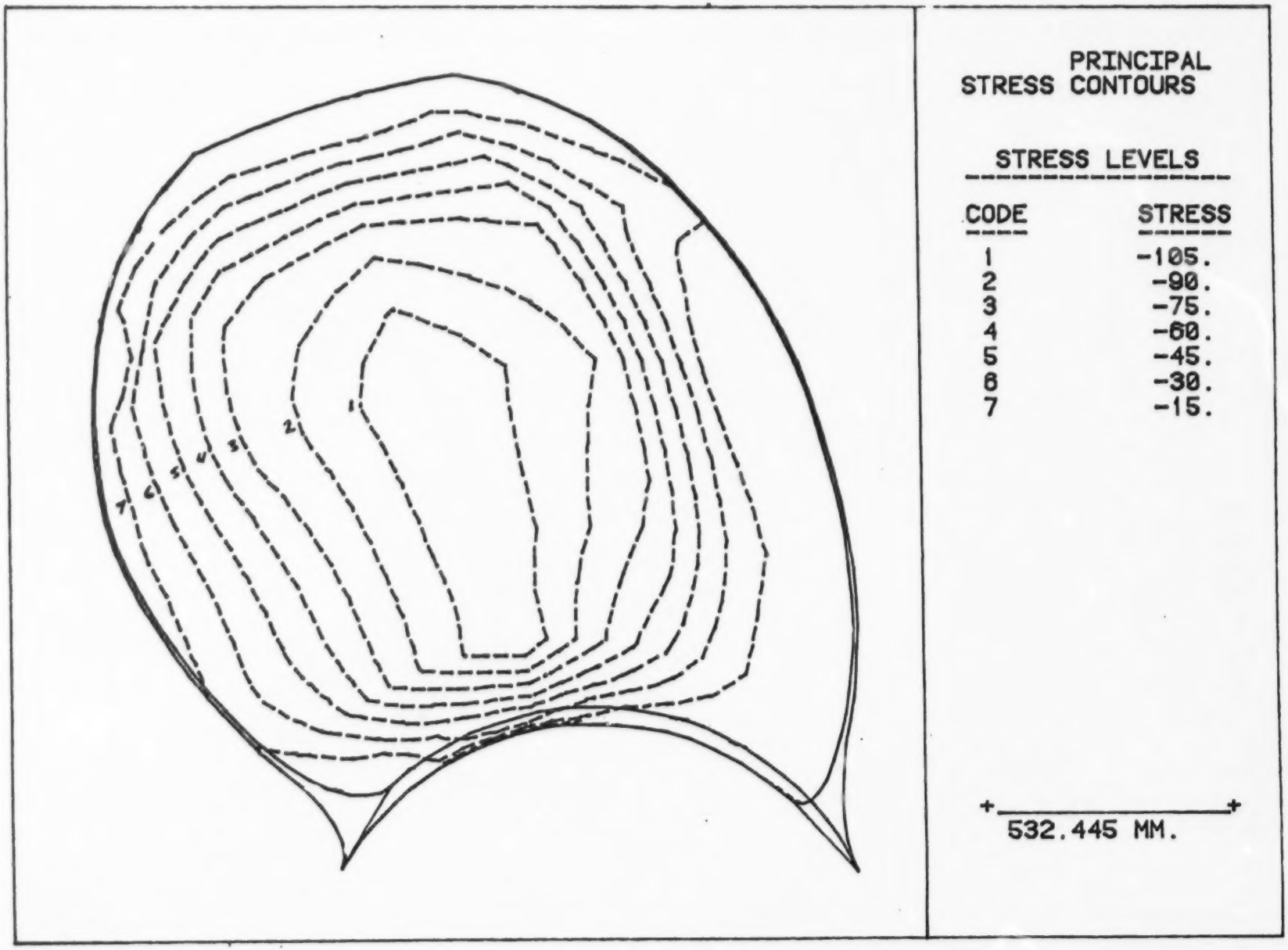


Figure 53: Linear Variation (5 - 0%) in Increase in Blade Thickness
Load Case L1-A

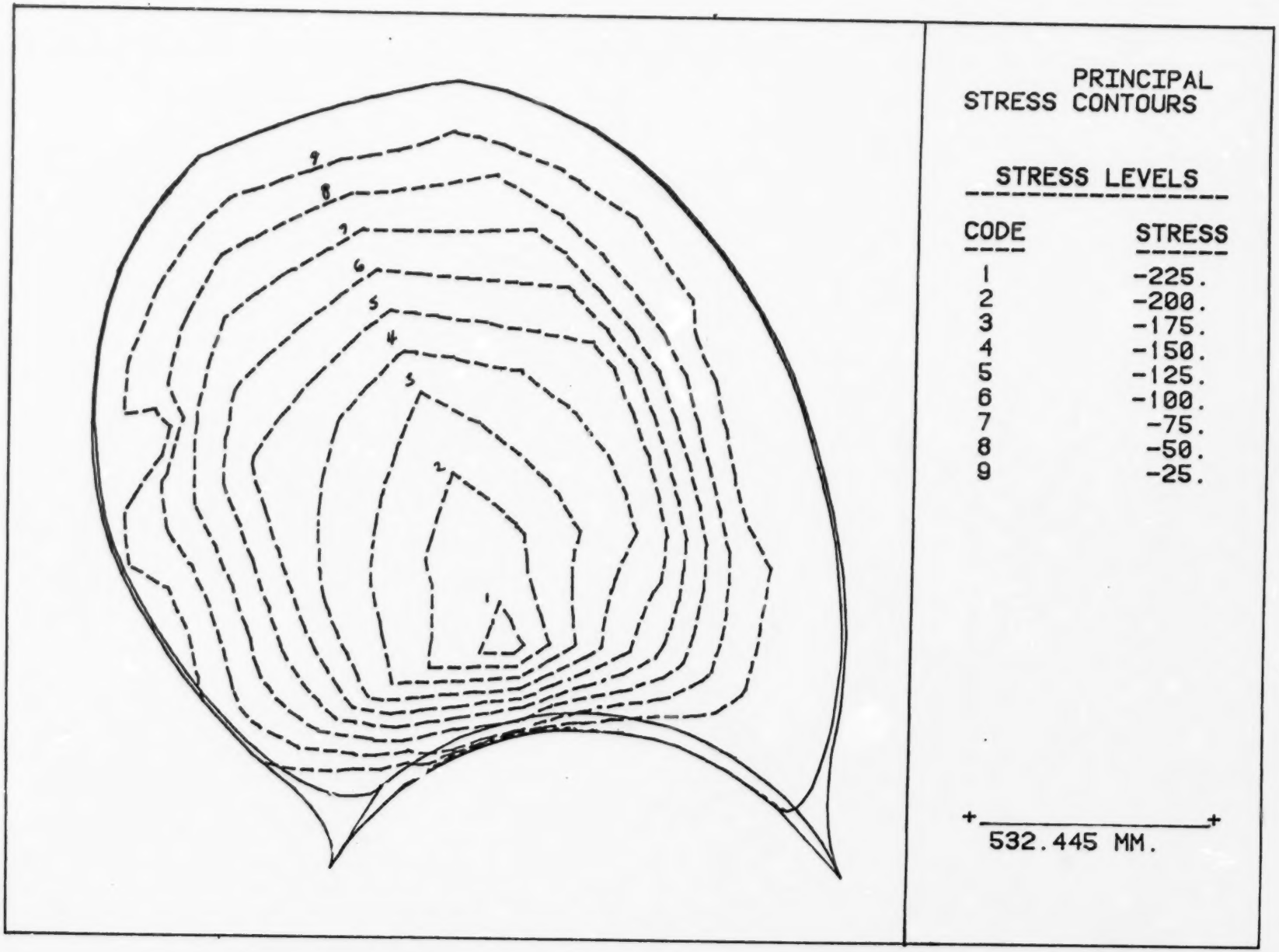


Figure 54: Linear Variation (5 - 0%) in Increase in Blade Thickness
Load Case L2-A

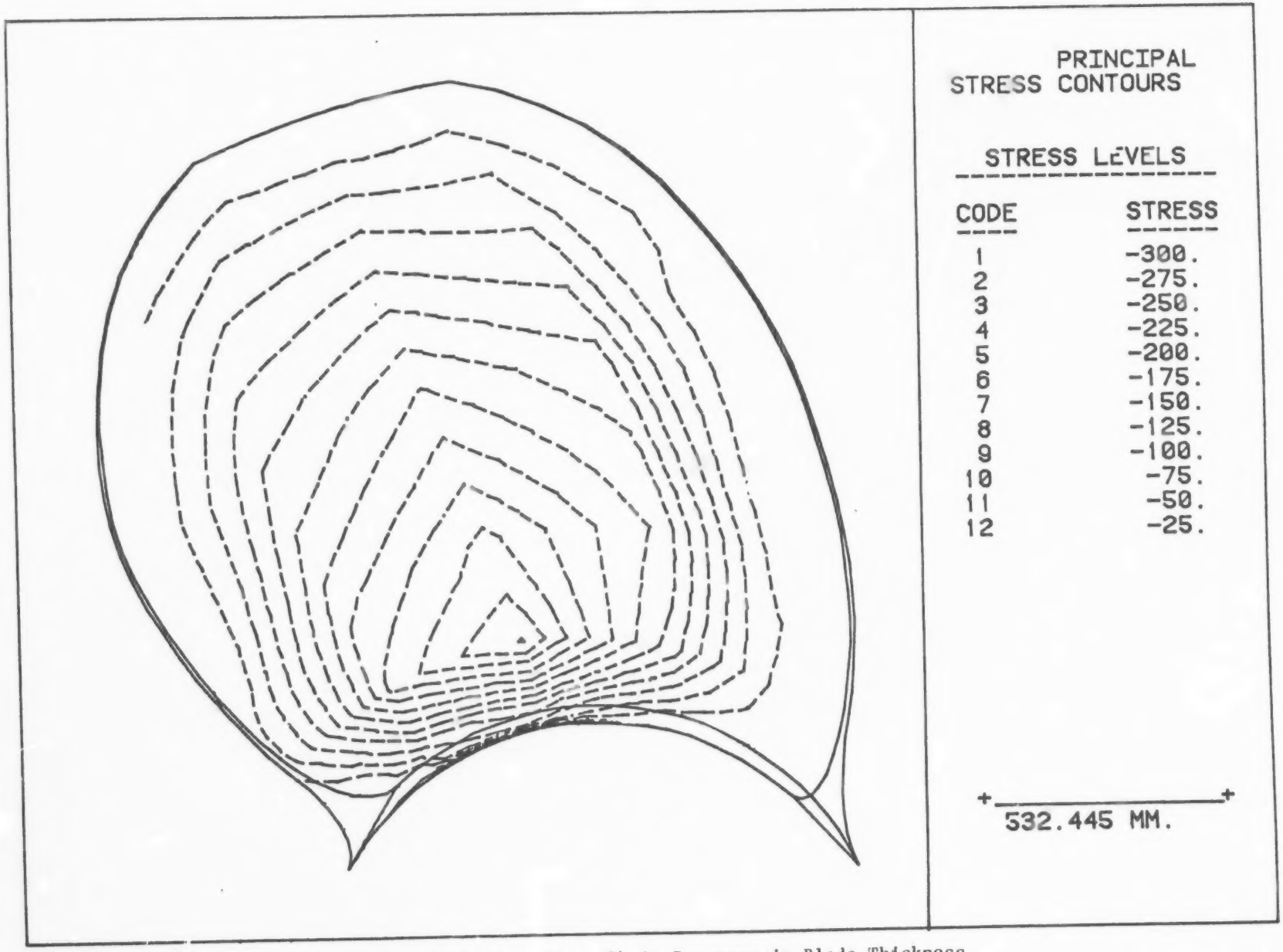


Figure 55: Linear Variation (5 - 0%) in Increase in Blade Thickness
Load Case L3-A

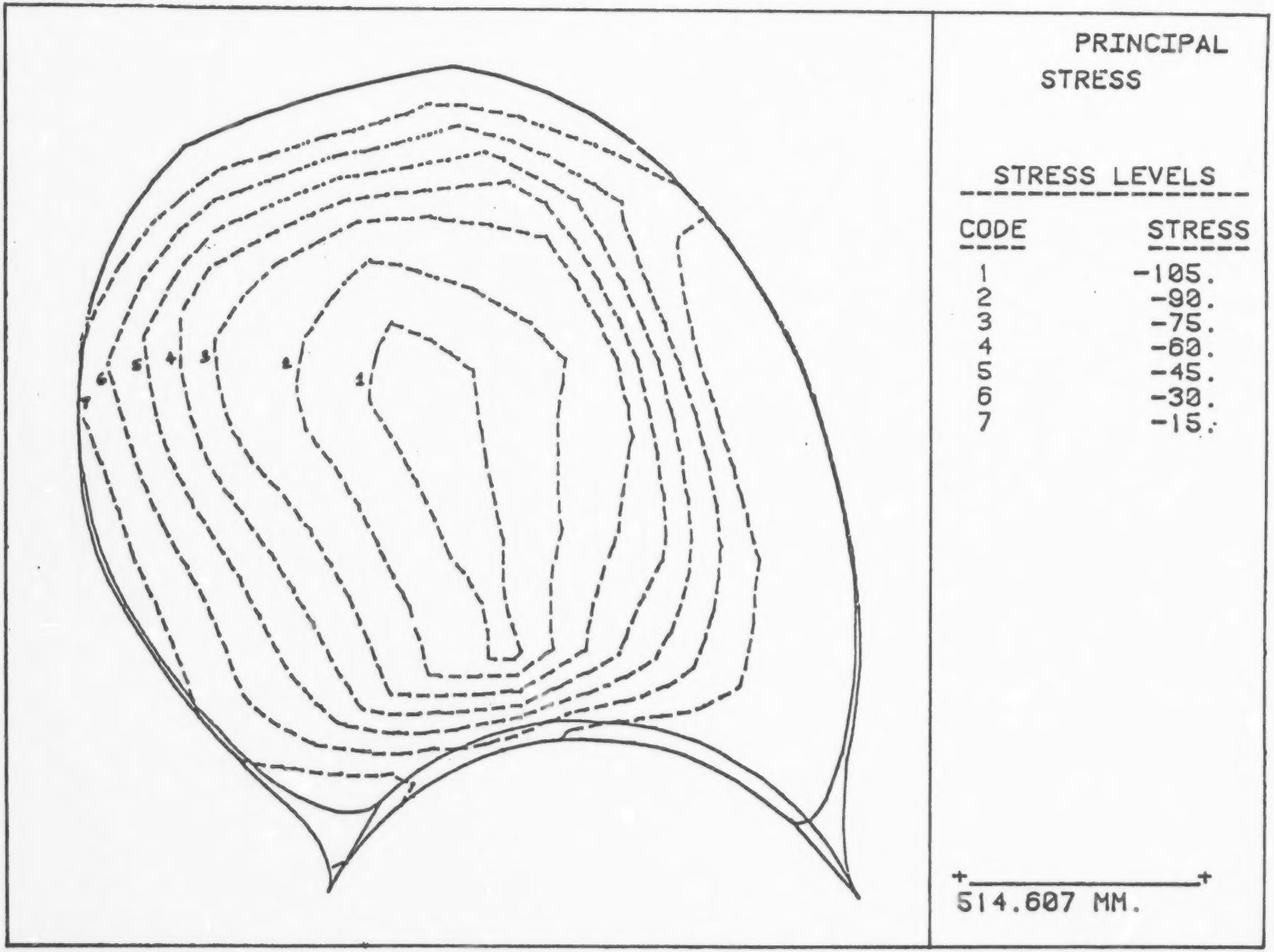


Figure 56: Linear Variation (10-0%) in Increase in Blade Thickness - Load L1-A

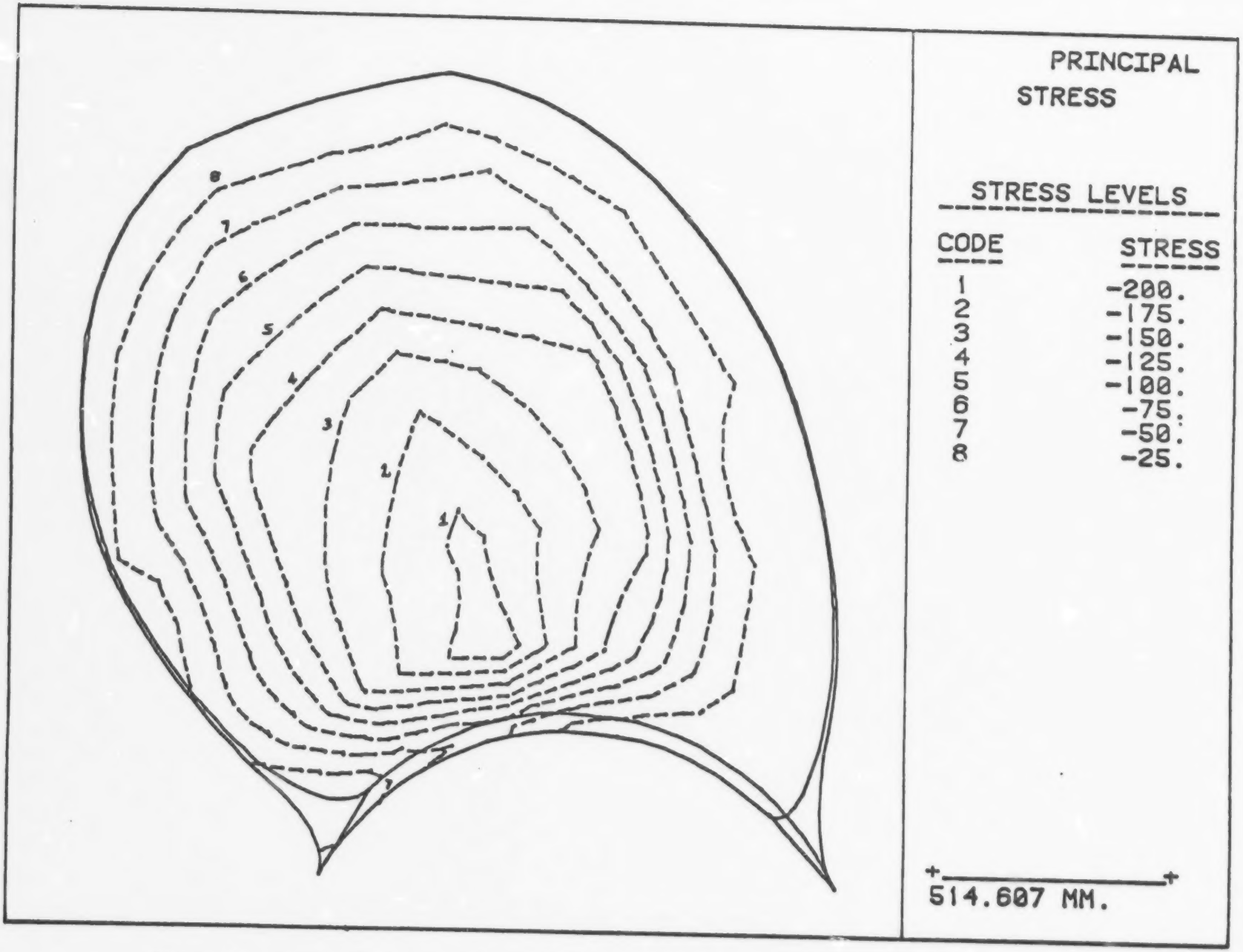


Figure 57: Linear Variation (10-0%) in Increase in Blade Thickness - Load L2-A

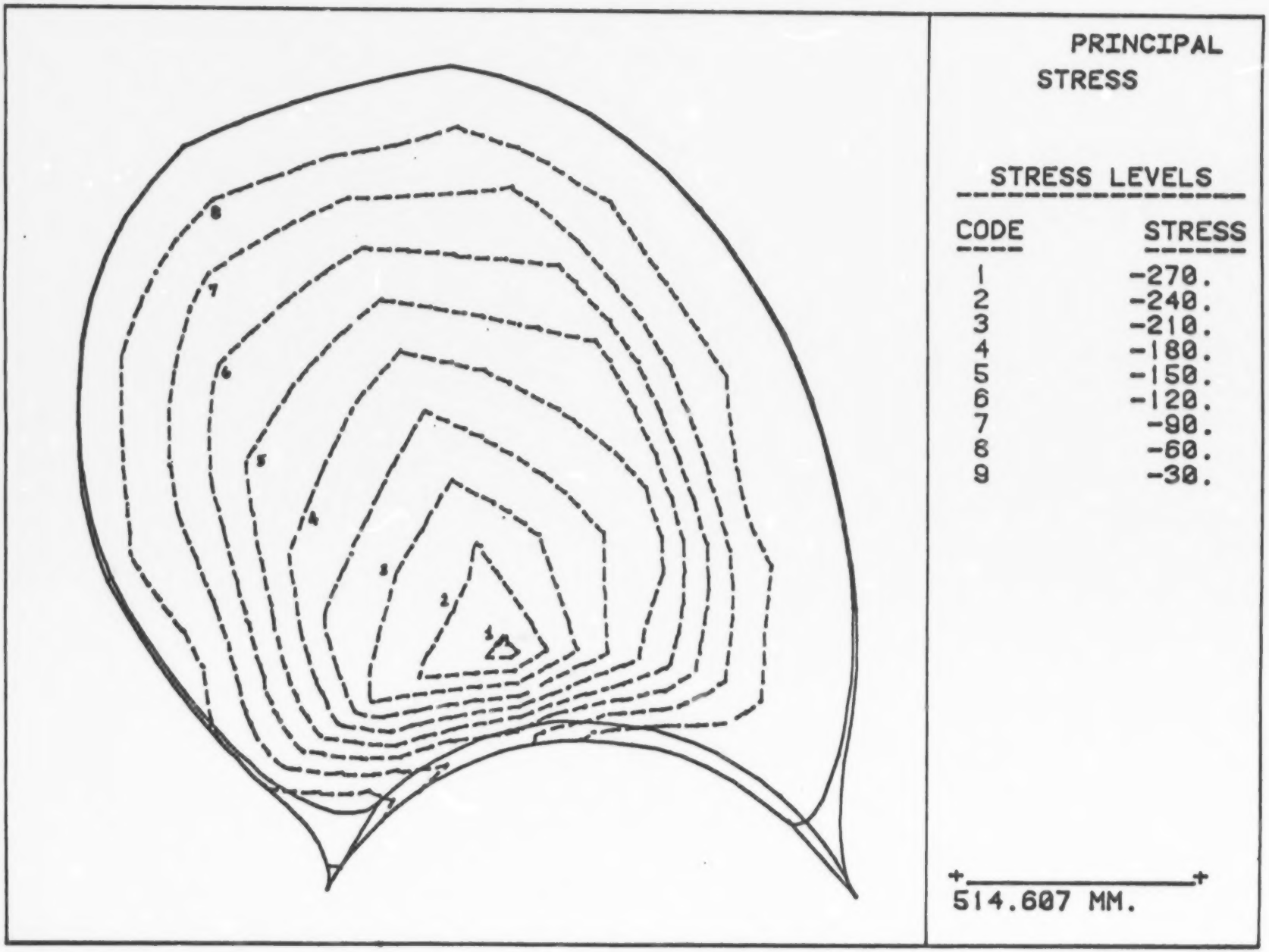


Figure 58: Linear Variation (10-0%) in Increase in Blade Thickness - Load Case L3-A

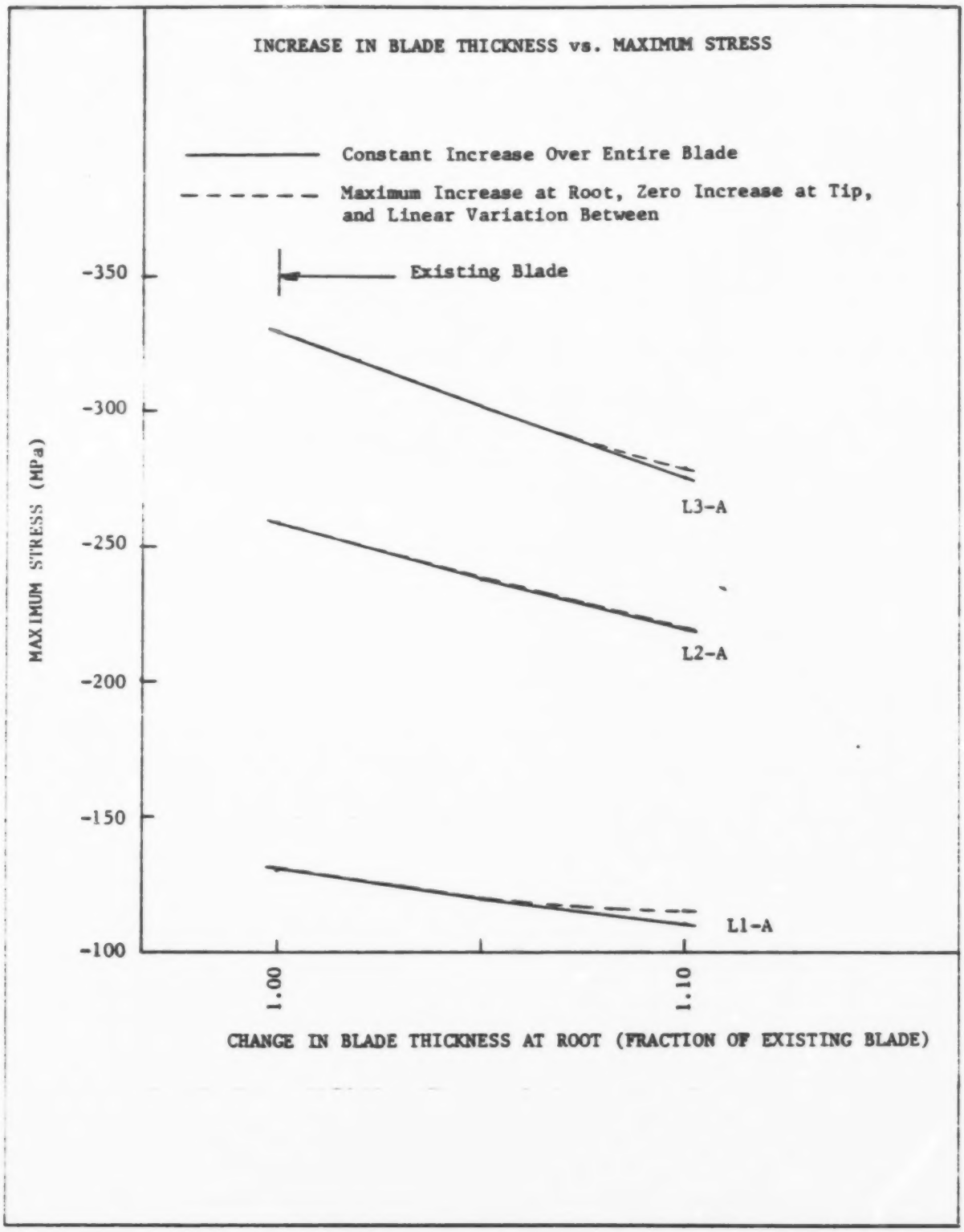


Figure 59: Effect of Blade Thickness on Maximum Stress

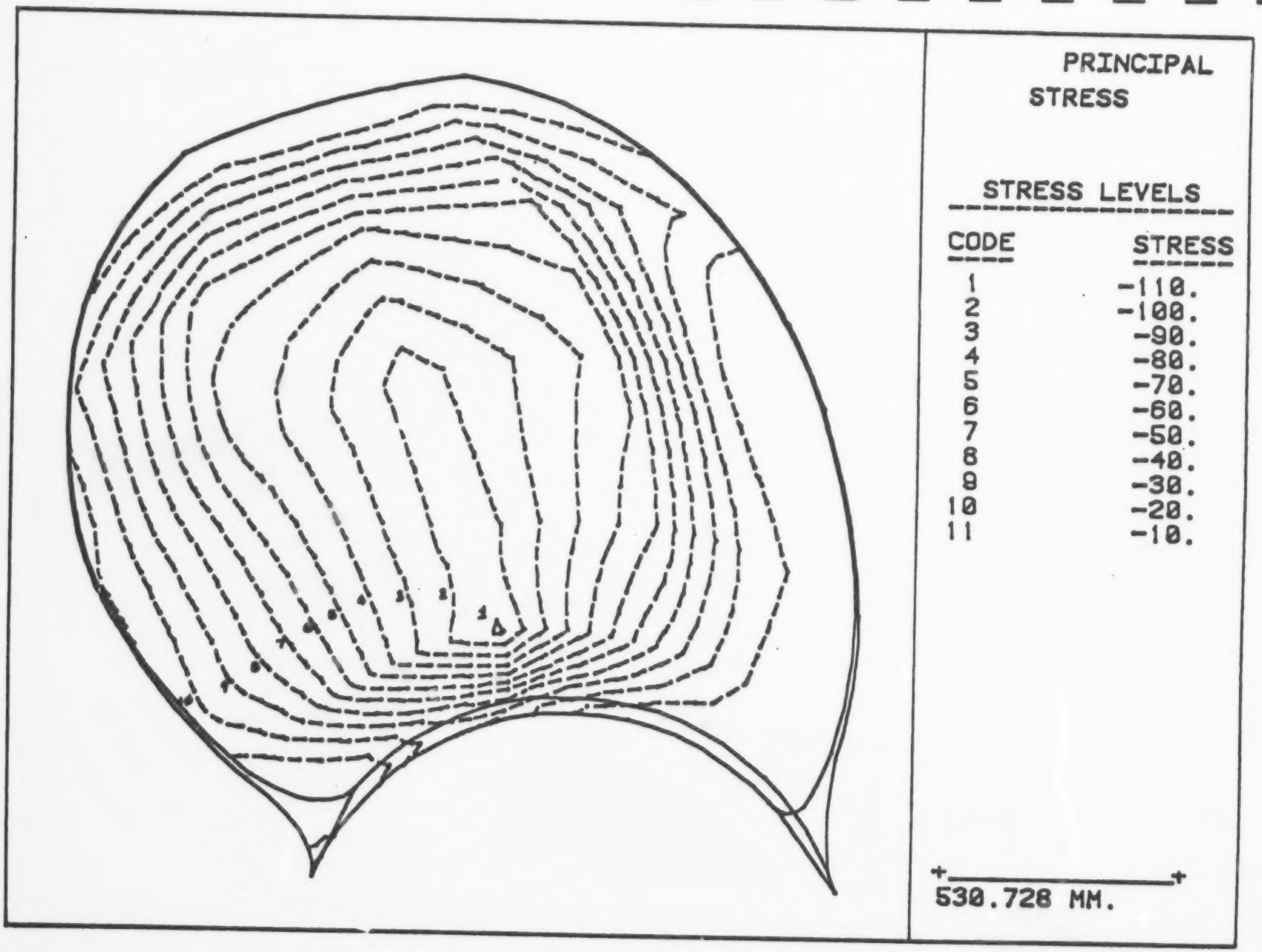


Figure 60: 10% Increase in Chord and Maximum Thickness - Load Case L1-A.

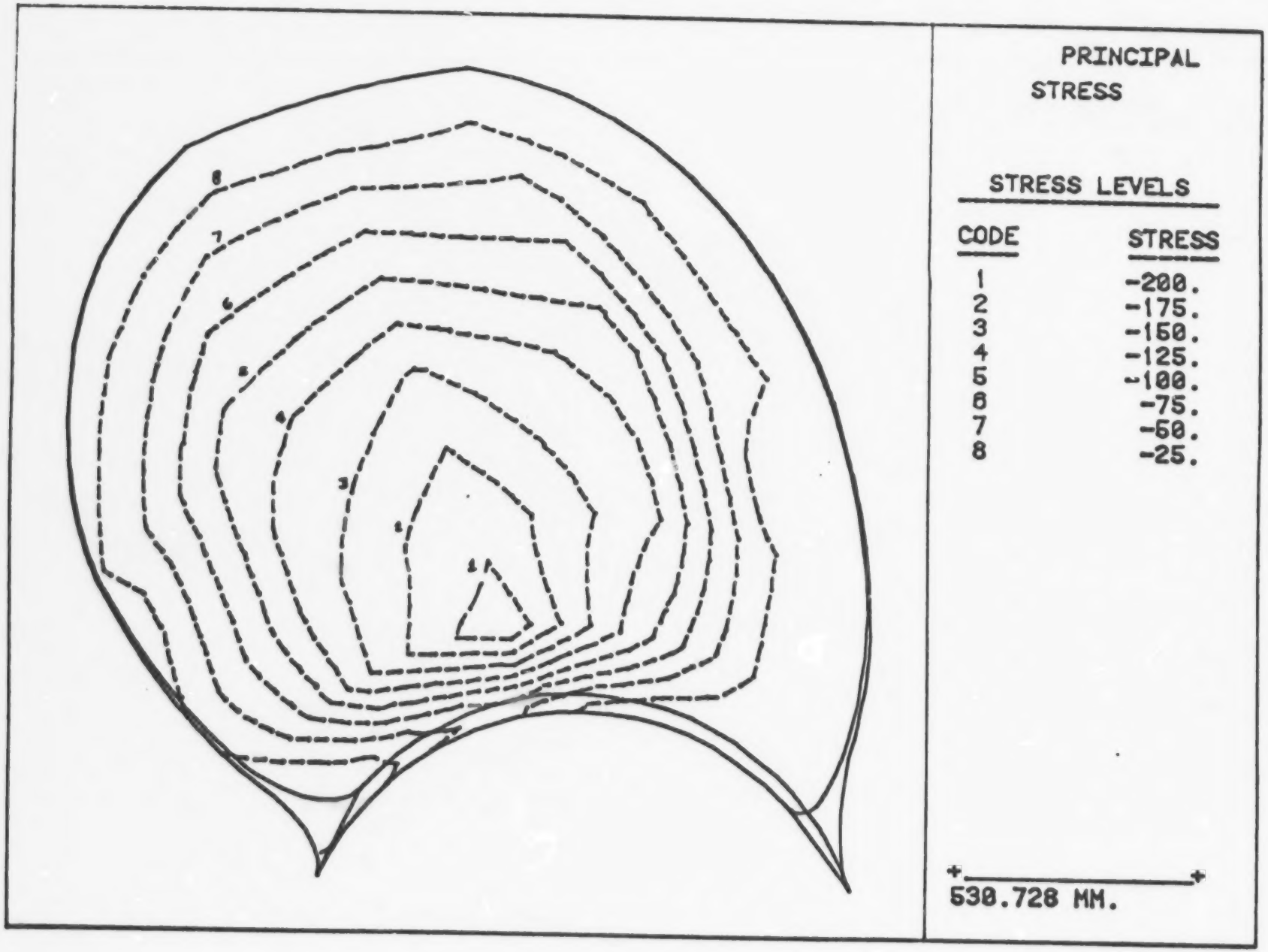


Figure 61: 10% Increase in Chord and Maximum Thickness - Load Case L2-A

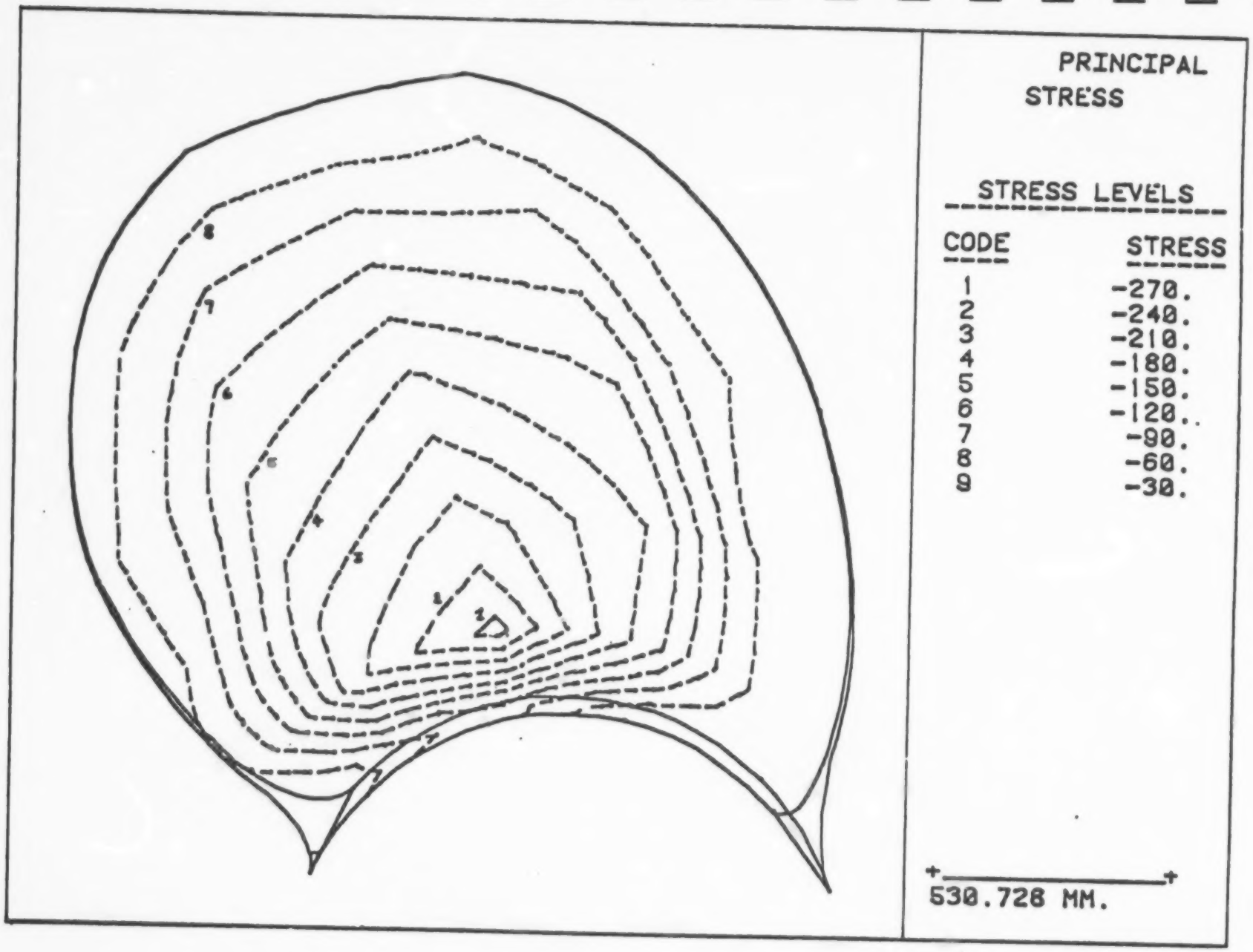


Figure 62: 10% Increase in Chord and Maximum Thickness - Load Case L3-A

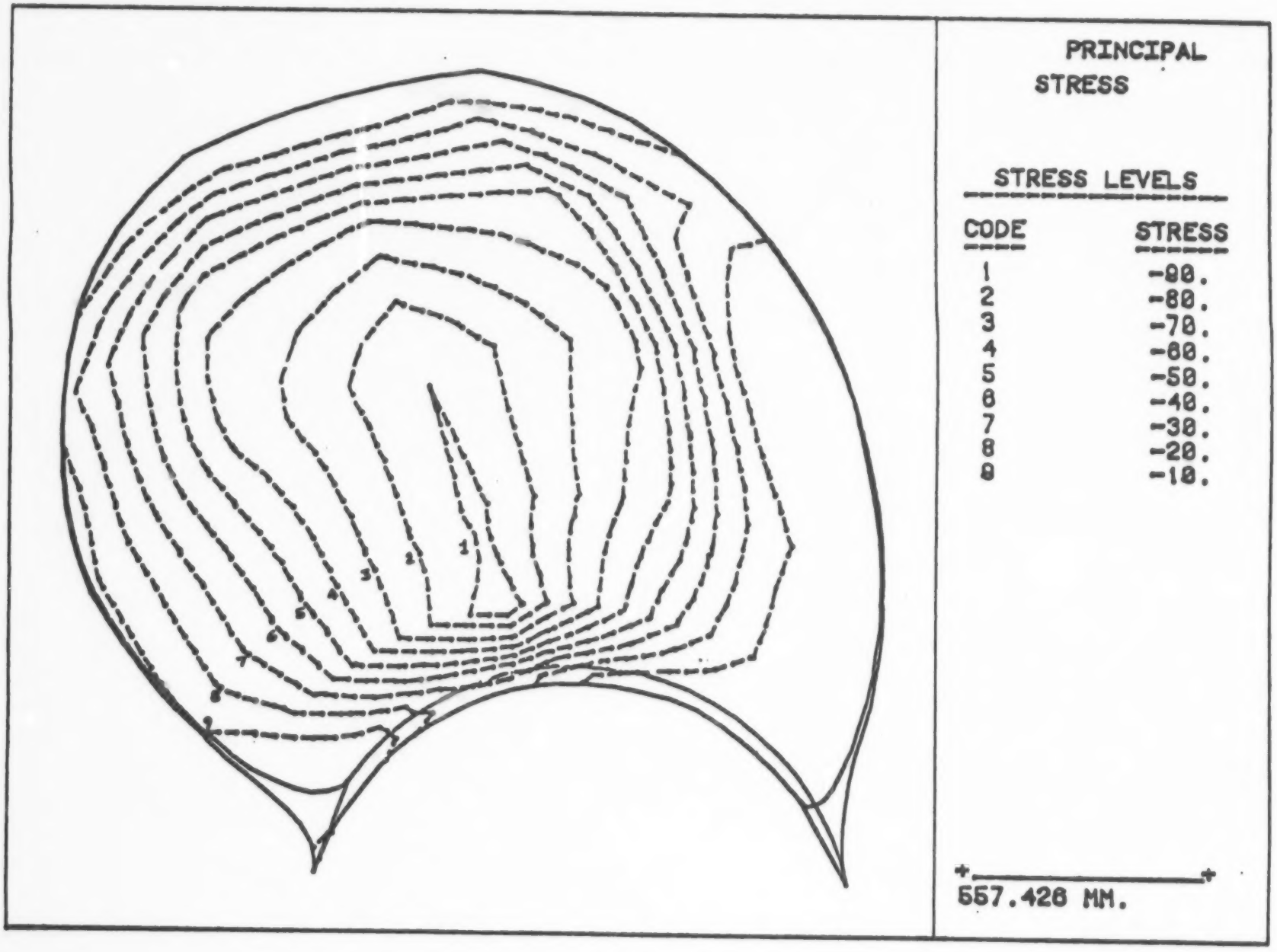


Figure 63: 20% Increase in Chord and Maximum Thickness - Load Case L1-A

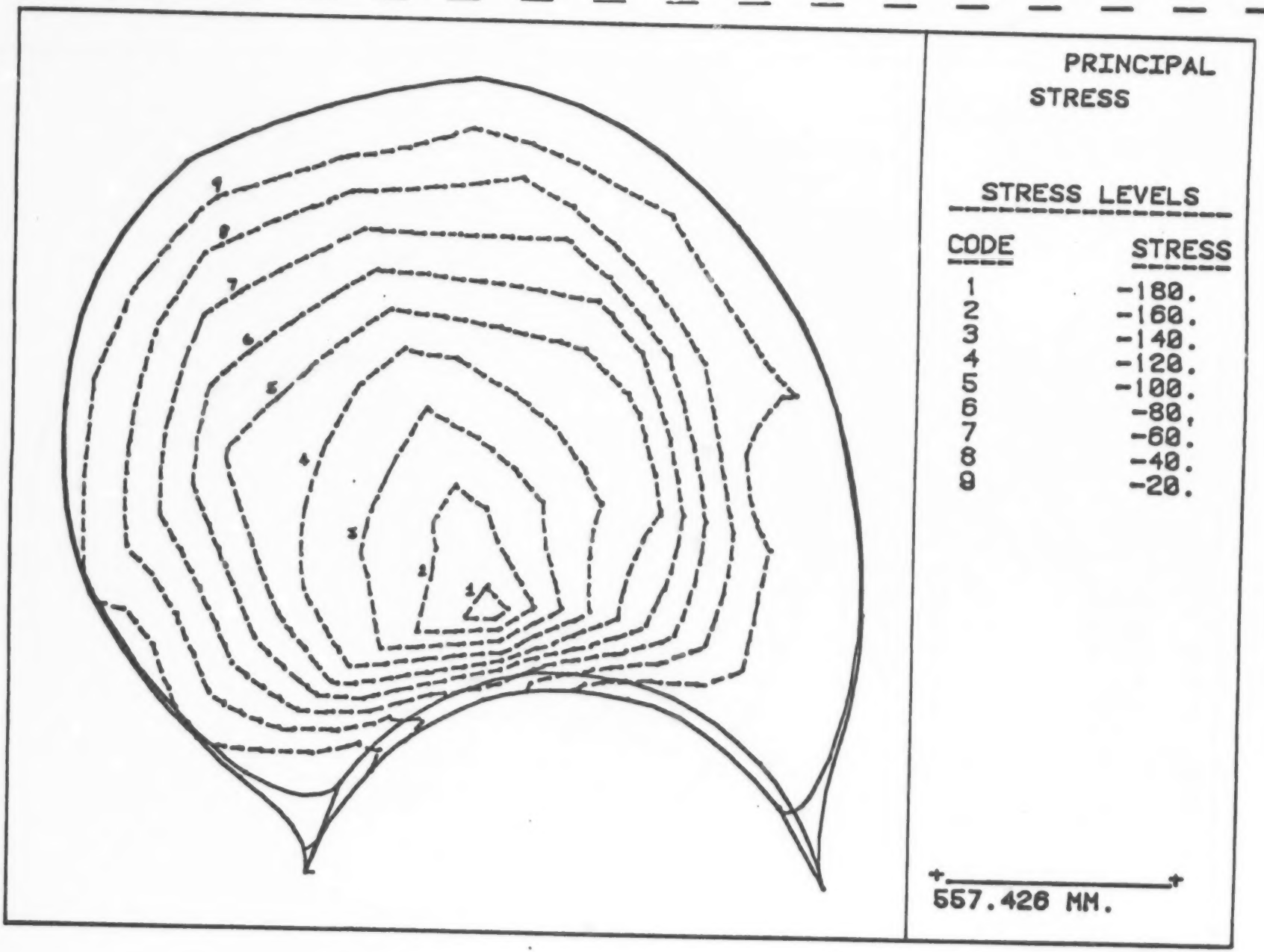


Figure 64: 20% Increase in Chord and Maximum Thickness - Load Case L2-A

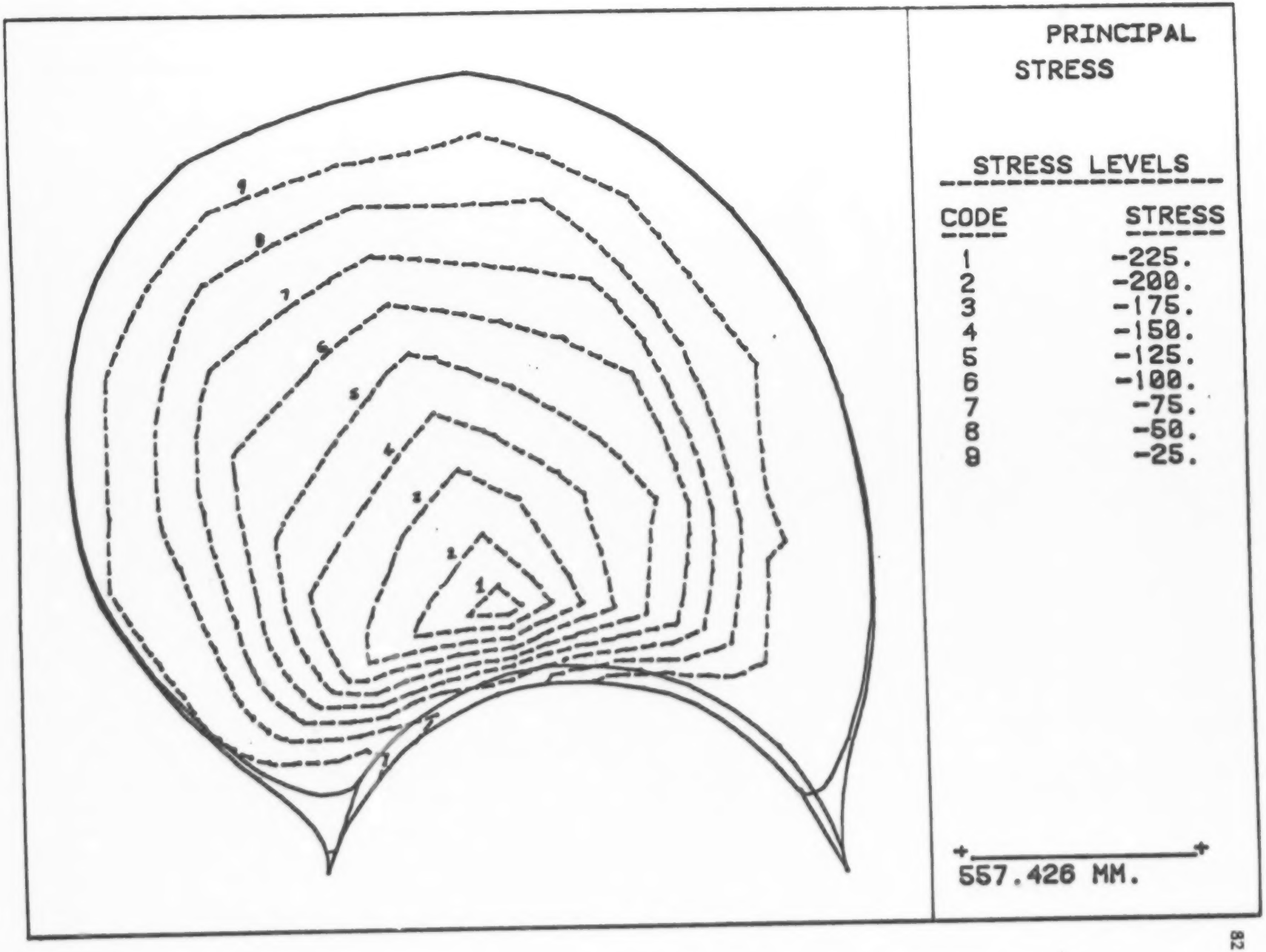


82

...ure ... 20... ...ncr... in ... rd ... Max... Th...ess... ...oad... se I...

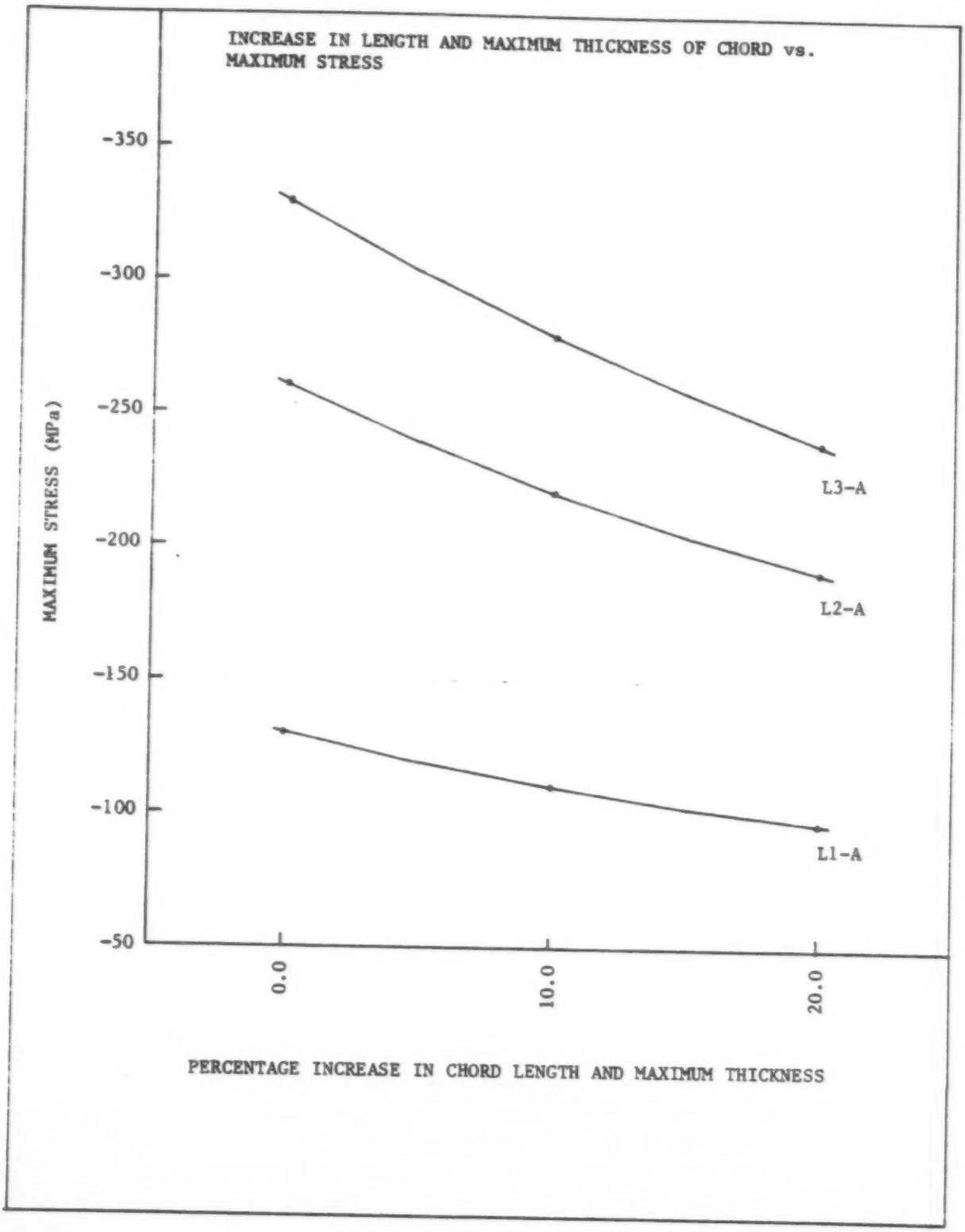


Figure 66: Effect of Length and Maximum Thickness of Chord on Maximum Stress

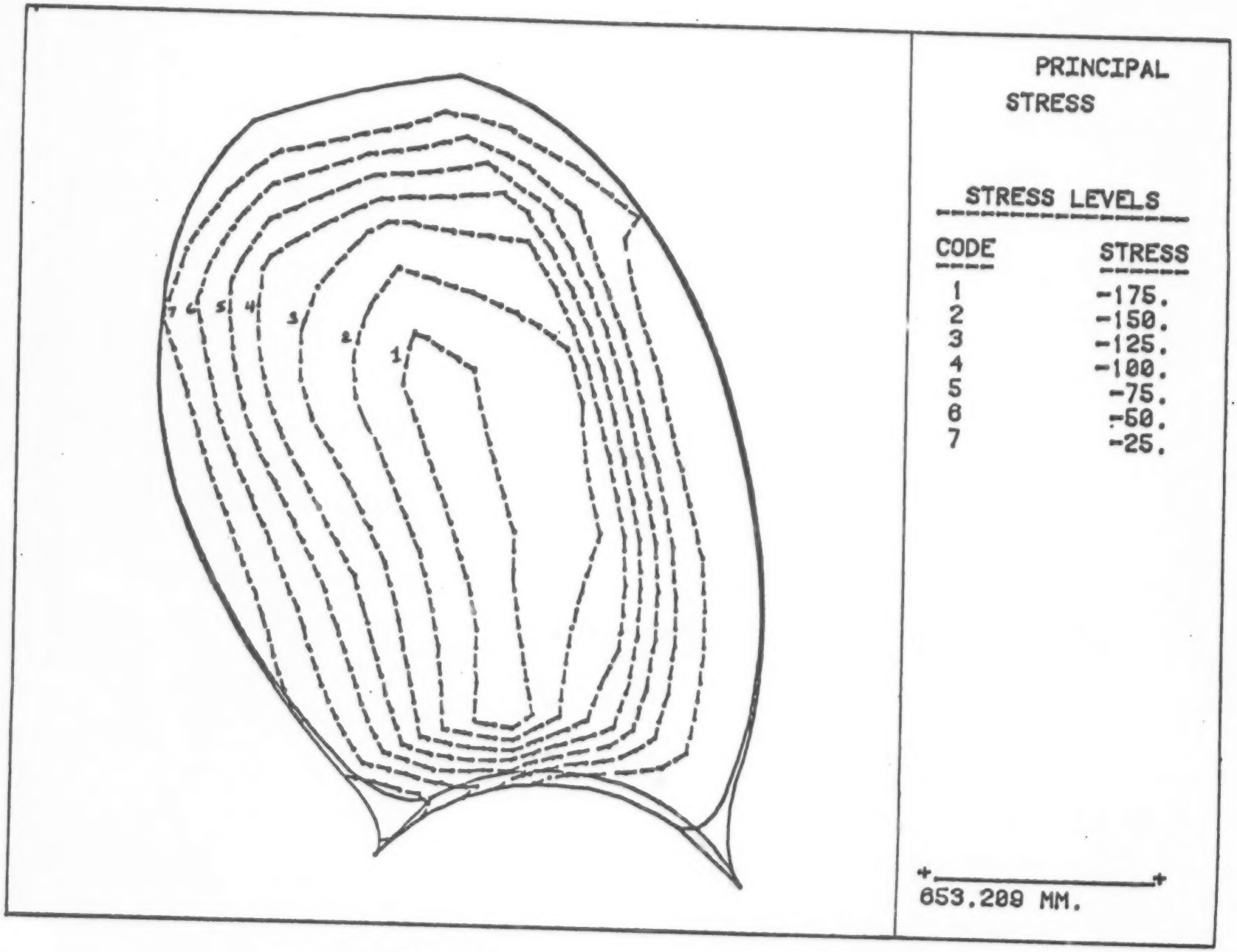


Figure 67: 25% Increase in Blade Diameter - Load Case 11-A

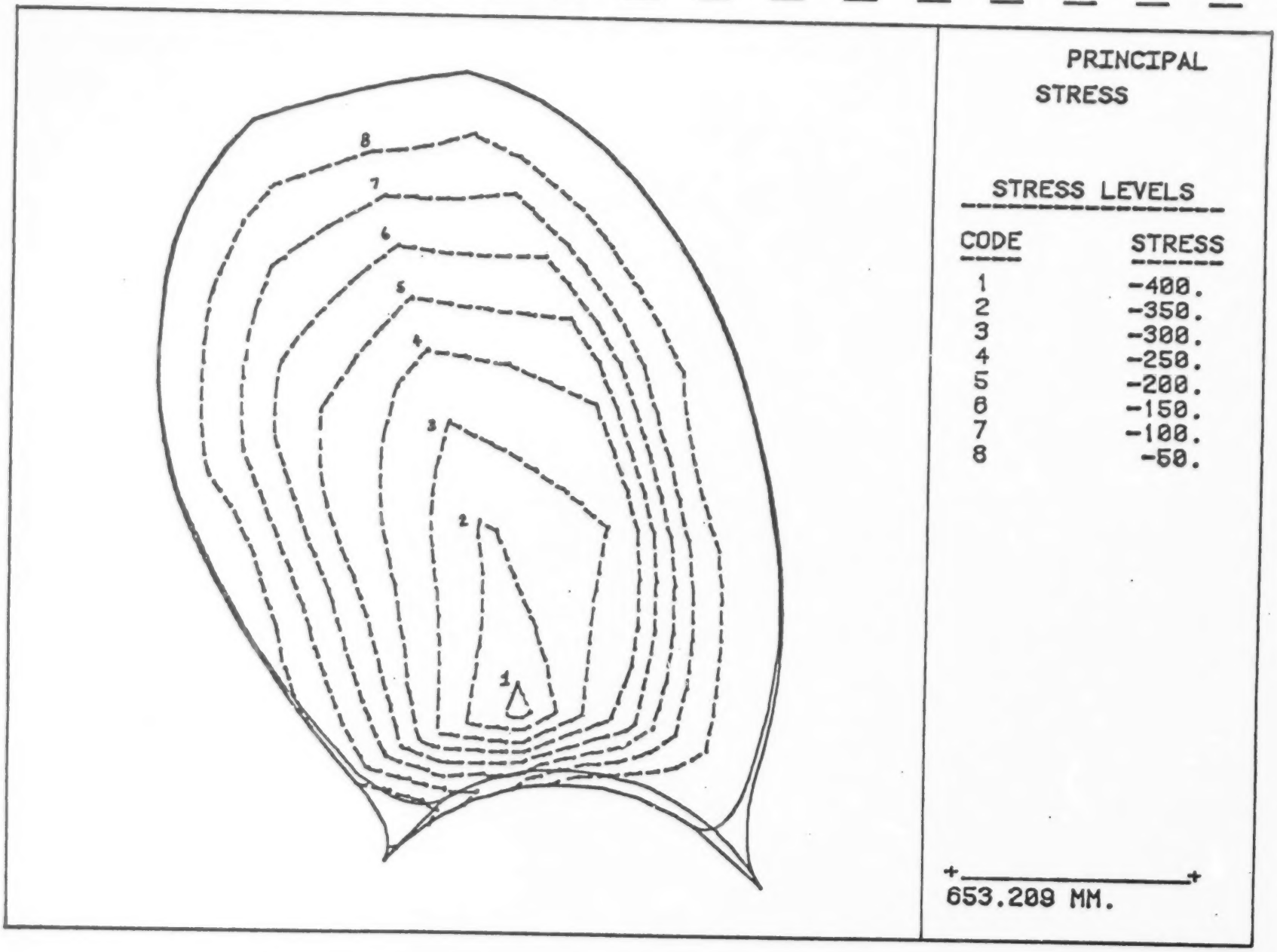


Figure 68: 25% Increase in Blade Diameter - Load Case L2-A

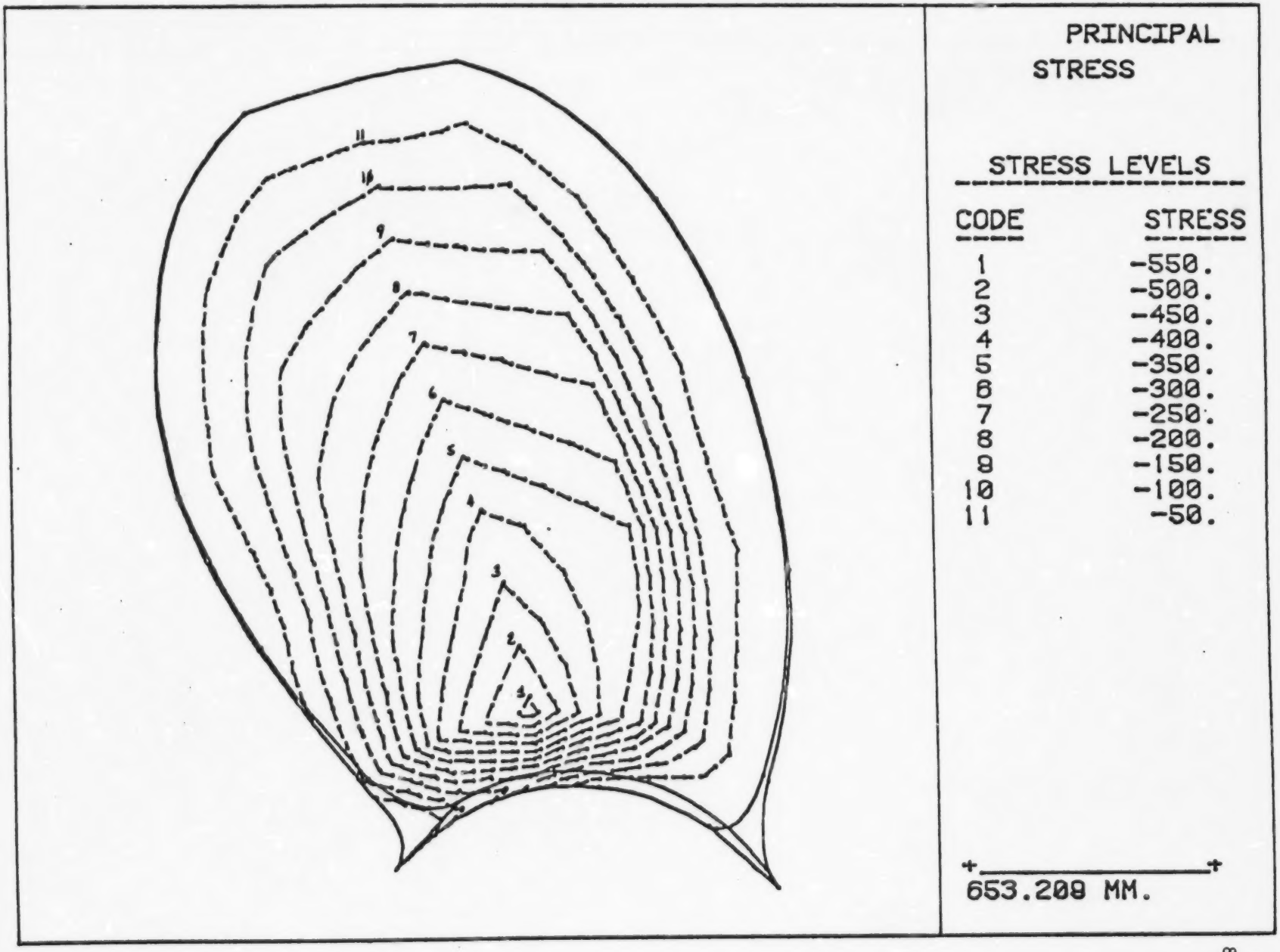




Figu 67: ure% I: 2ease ncr Rl[illegible] ir[illegible]ade net[illegible] Lo ase A

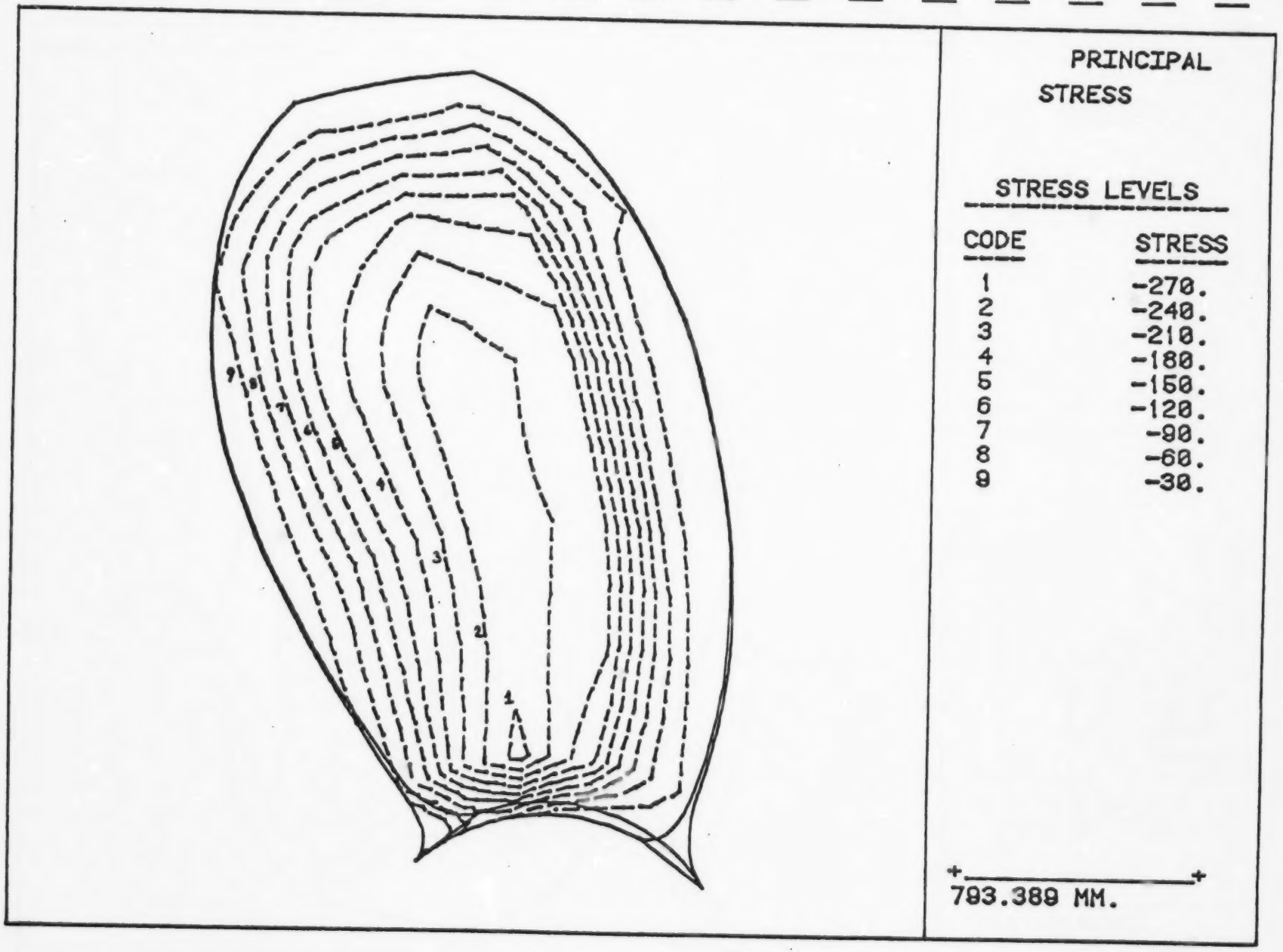


Figure 70: 50% Increase in Blade Diameter - Load Case L1-A

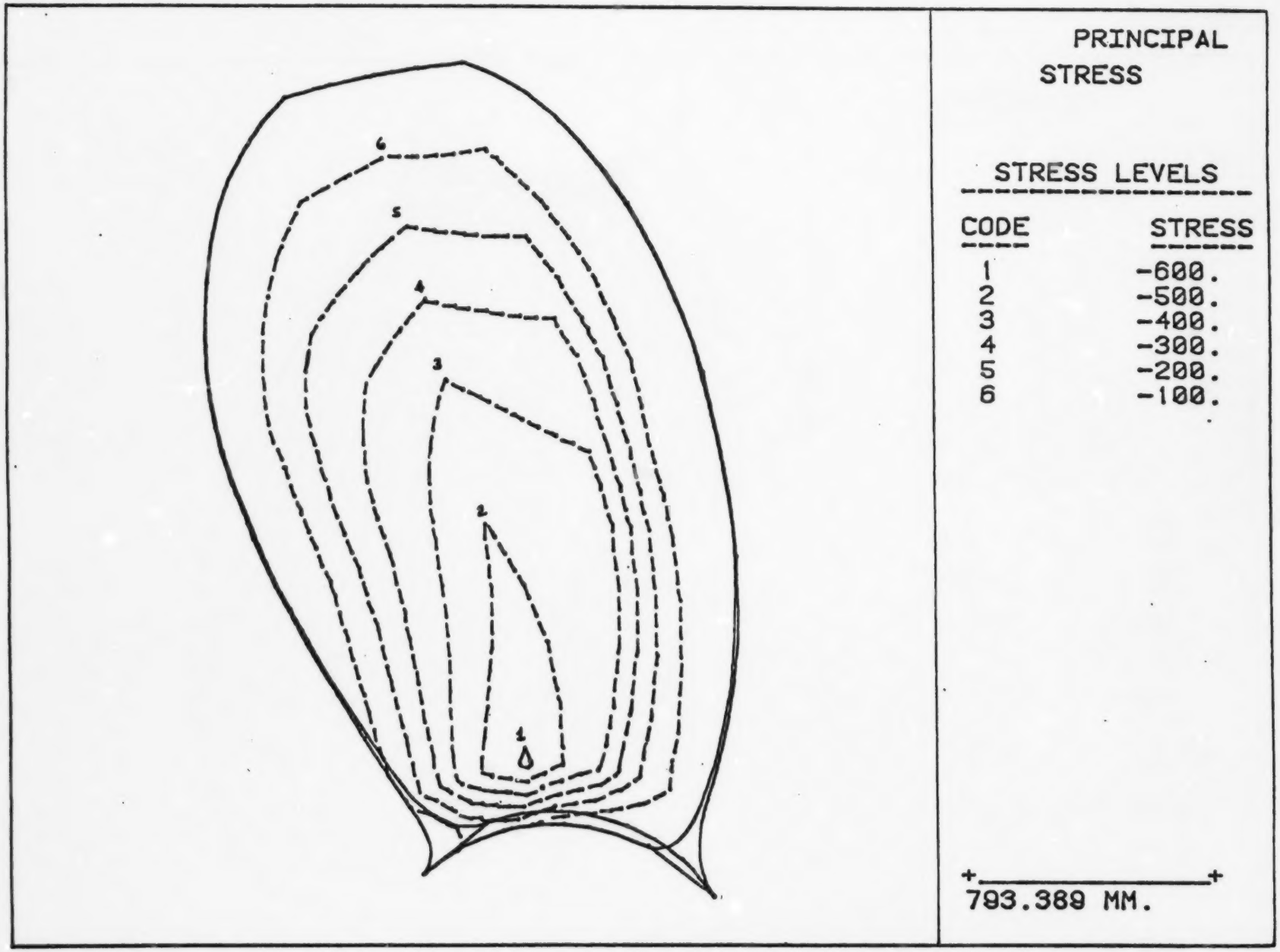


Figure 71: 50% Increase in Blade Diameter - Load Case L2-A

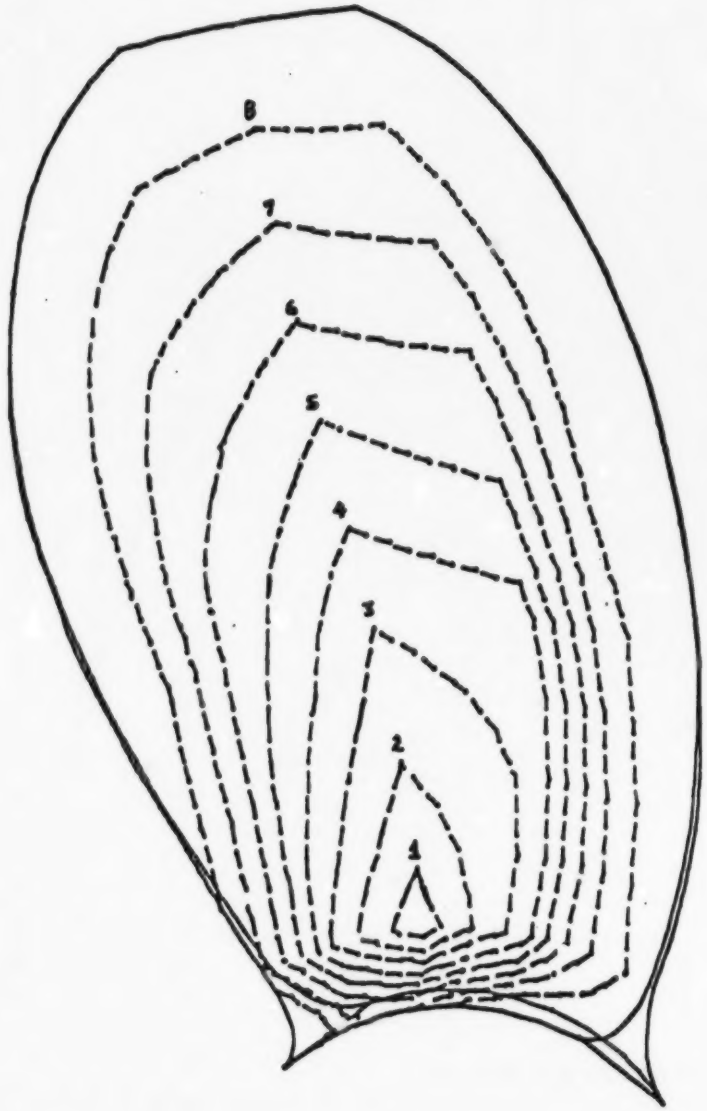


PRINCIPAL
STRESS

STRESS LEVELS

| CODE | STRESS |
|---|---|
| 1 | -800. |
| 2 | -700. |
| 3 | -600. |
| 4 | -500. |
| 5 | -400. |
| 6 | -300. |
| 7 | -200. |
| 8 | -100. |

793.389 MM.

Figure 72: 50% Increase in Blade Diameter - Load Case L3-A

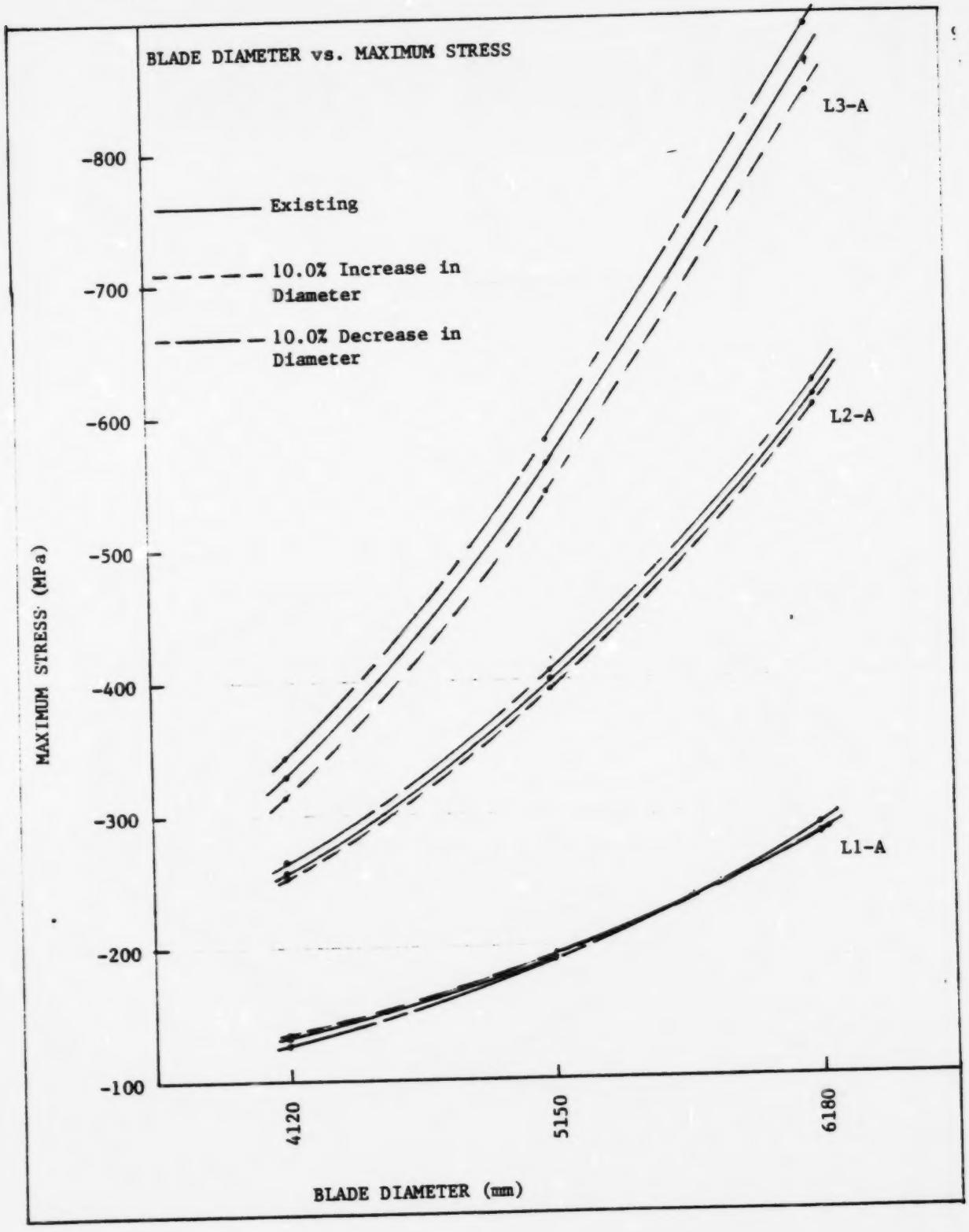


Figure 73: Effect of Blade Diameter on Maximum Stress

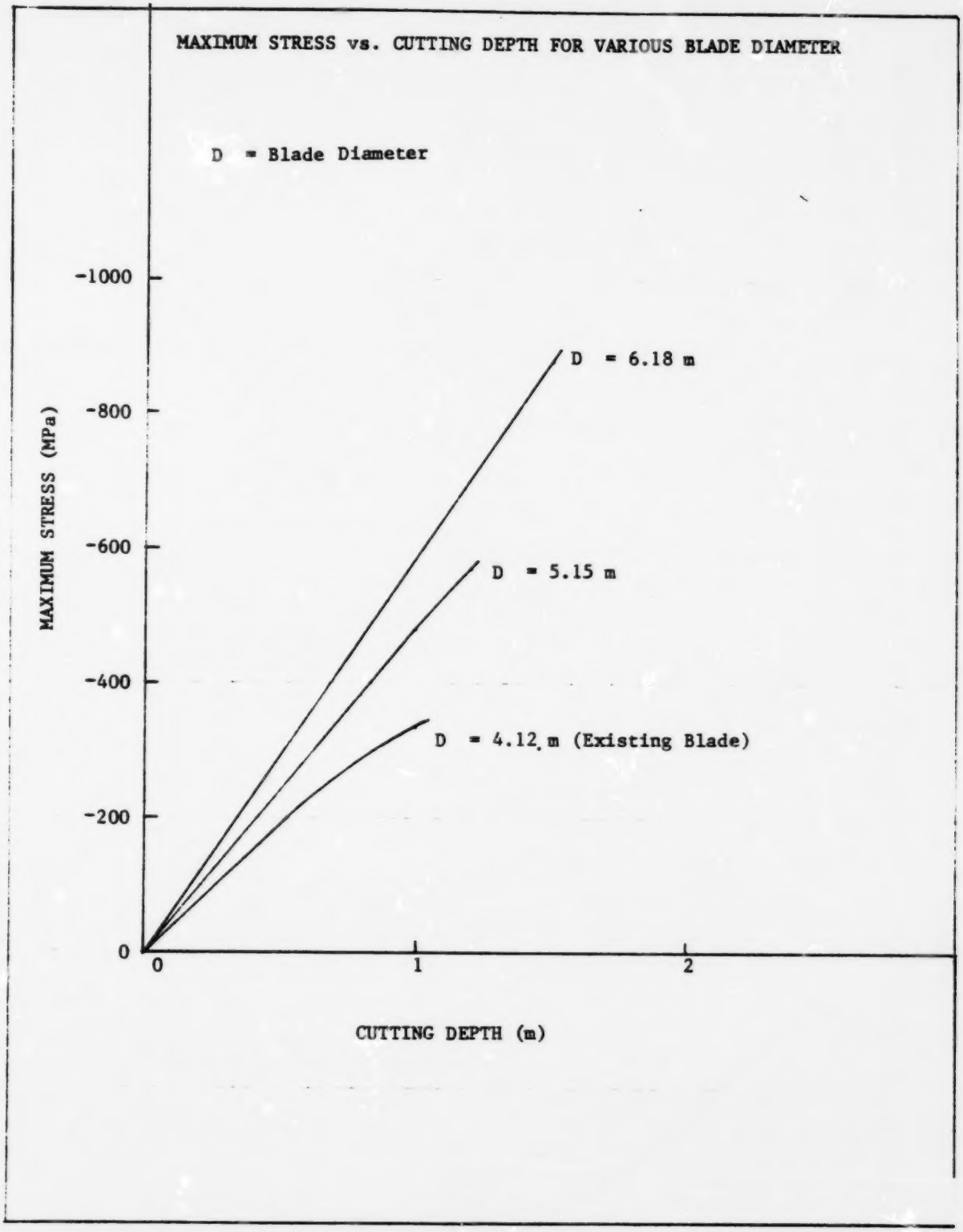


Figure 74: Maximum Stress Versus Cutting Depth for Various Blade Diameters

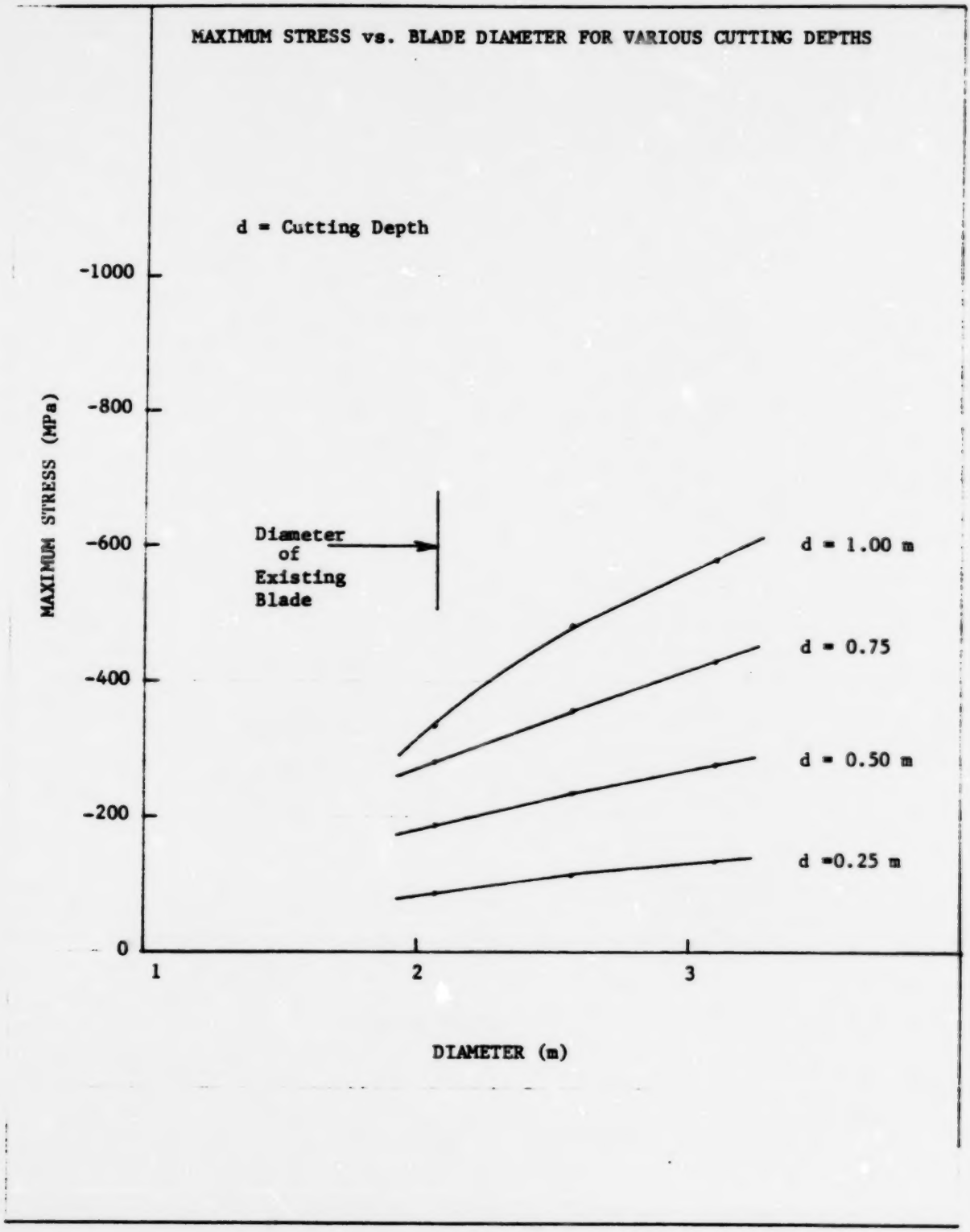


Figure 75: Maximum Stress Versus Blade Diameter for Various Cutting Depths

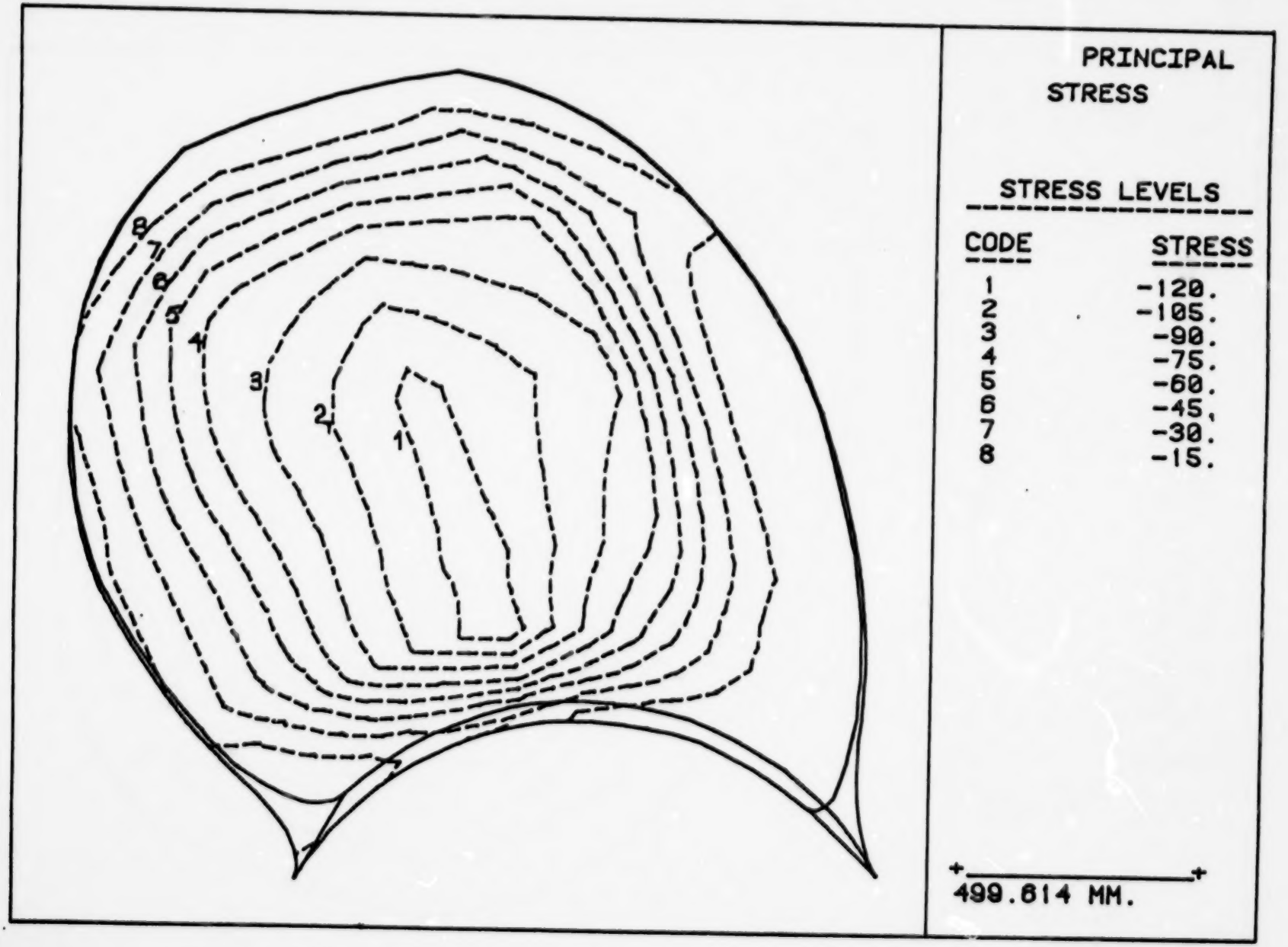


Figure 76: 10% Increase in Hub Diameter - Load Case L1-A

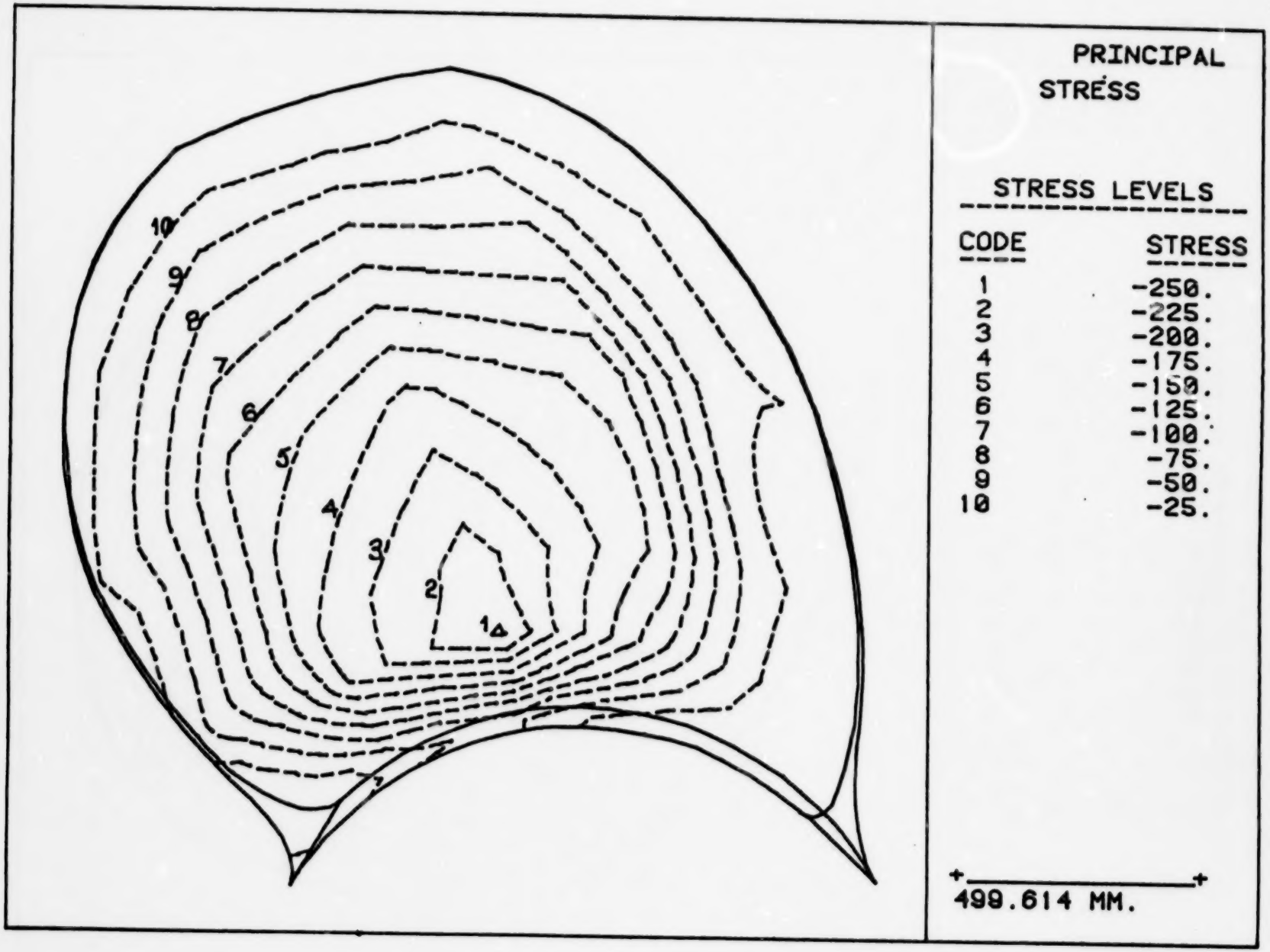


Figure 77: 10% Increase in Hub Diameter - Load Case L2-A

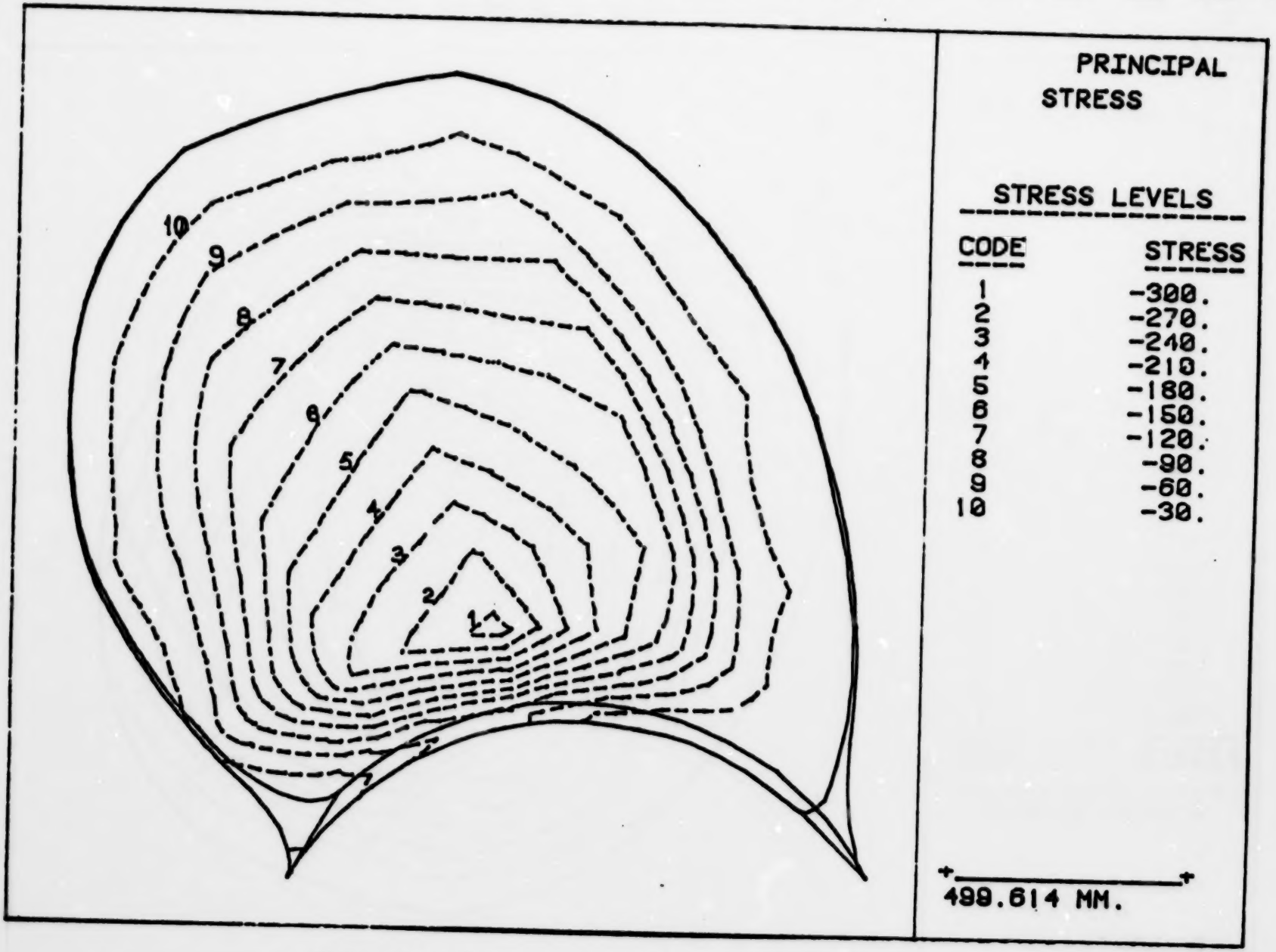


Figure 78: 10% Increase in Hub Diameter - Load Case L3-A

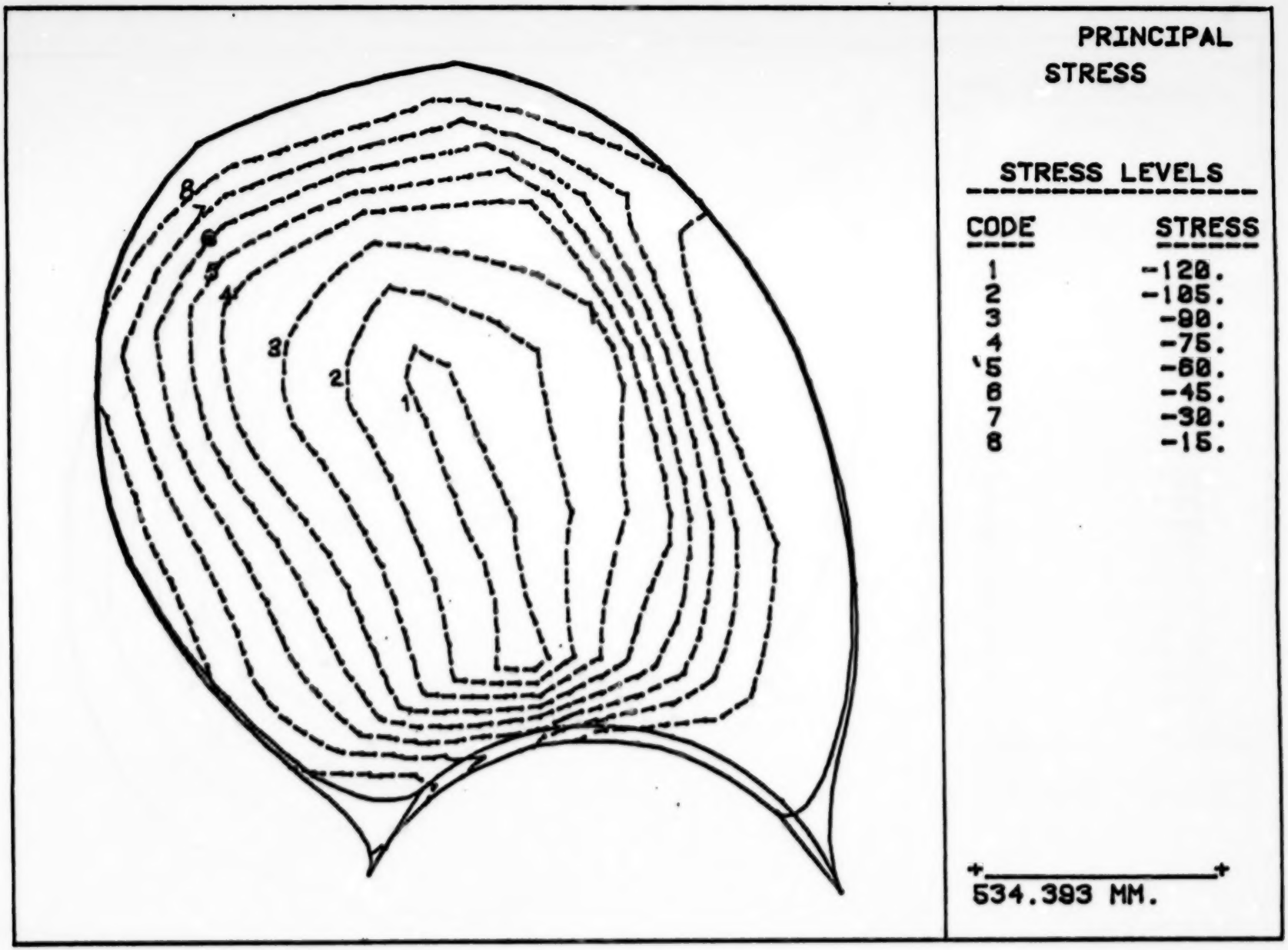


Figure 79: 10% Decrease in Hub Diameter - Load Case L1-A

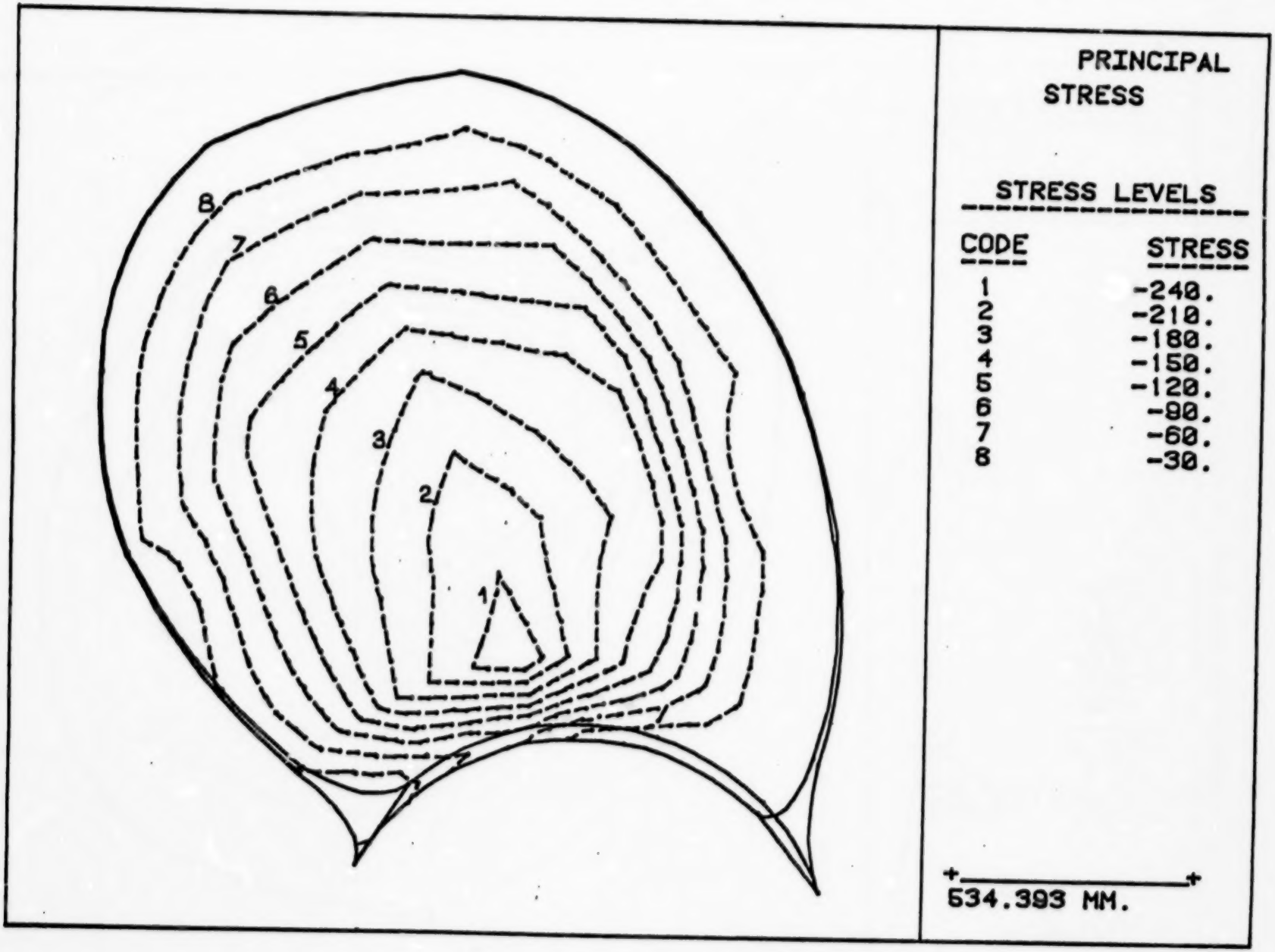


Figure 80: 10% Decrease in Hub Diameter - Load Case L2- A.

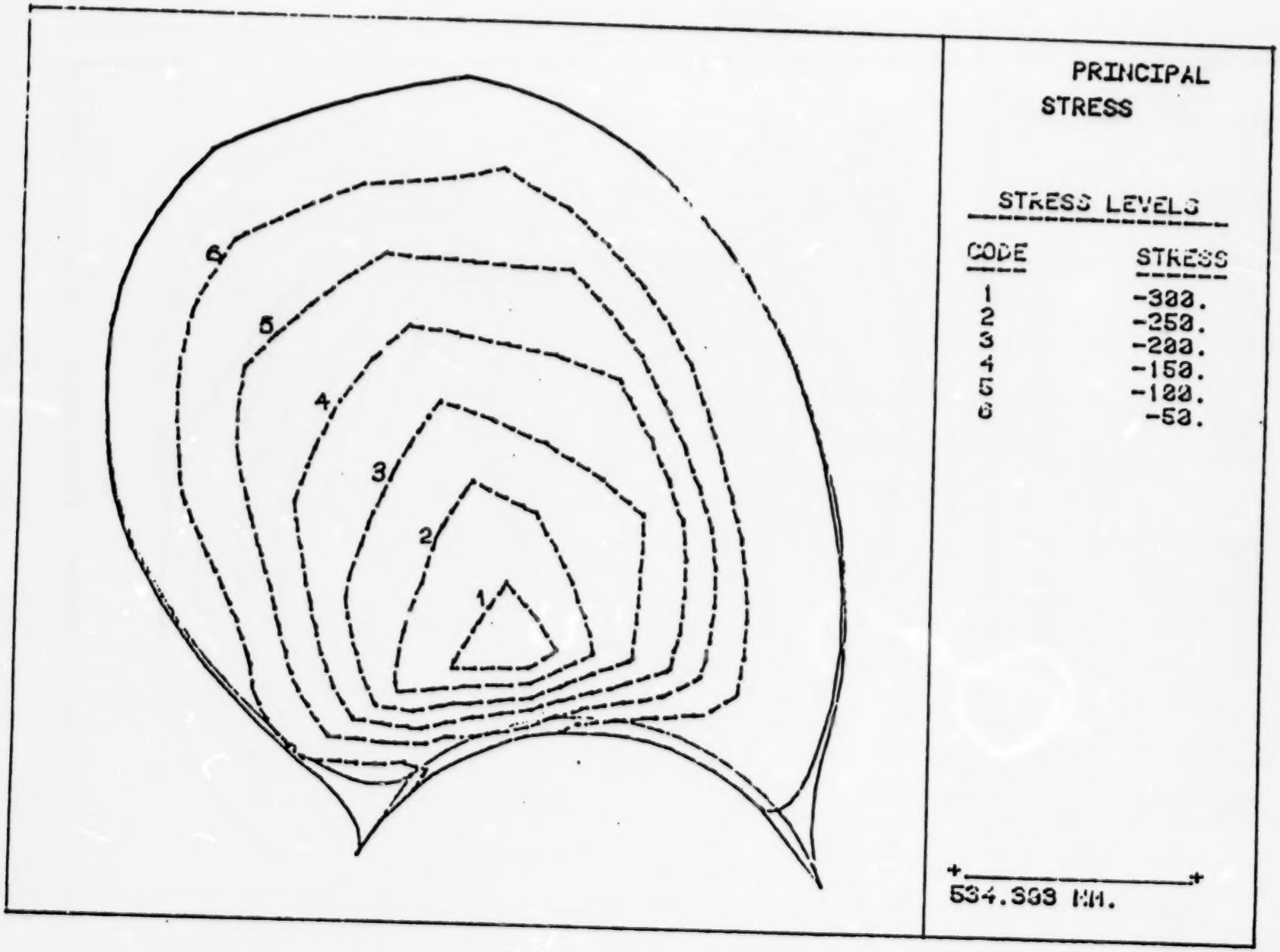


Figure 81: 10% Decrease in Hub Diameter - Load Case L3-A

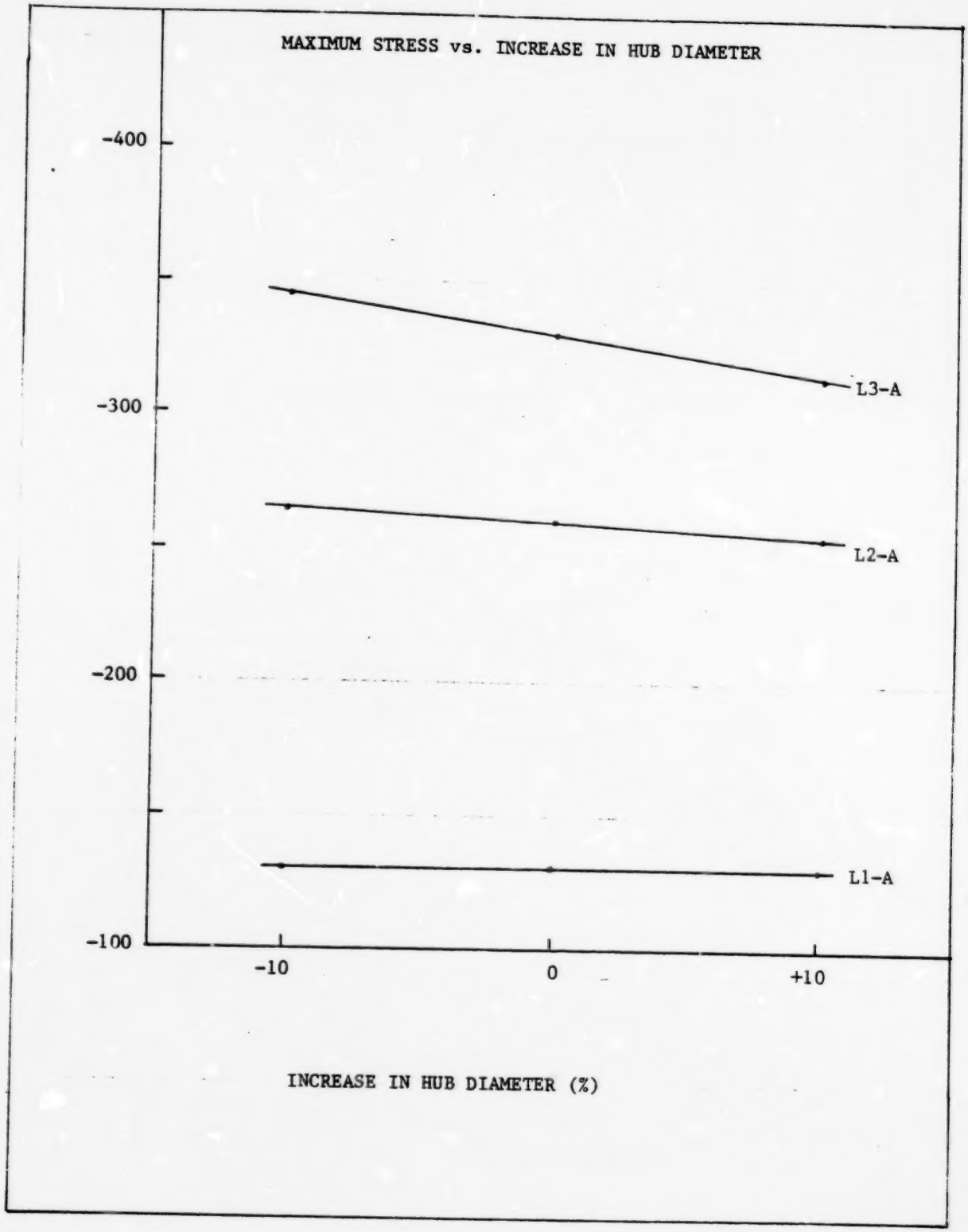


Figure 82: Effect of Hub Diameter on Maximum Stress

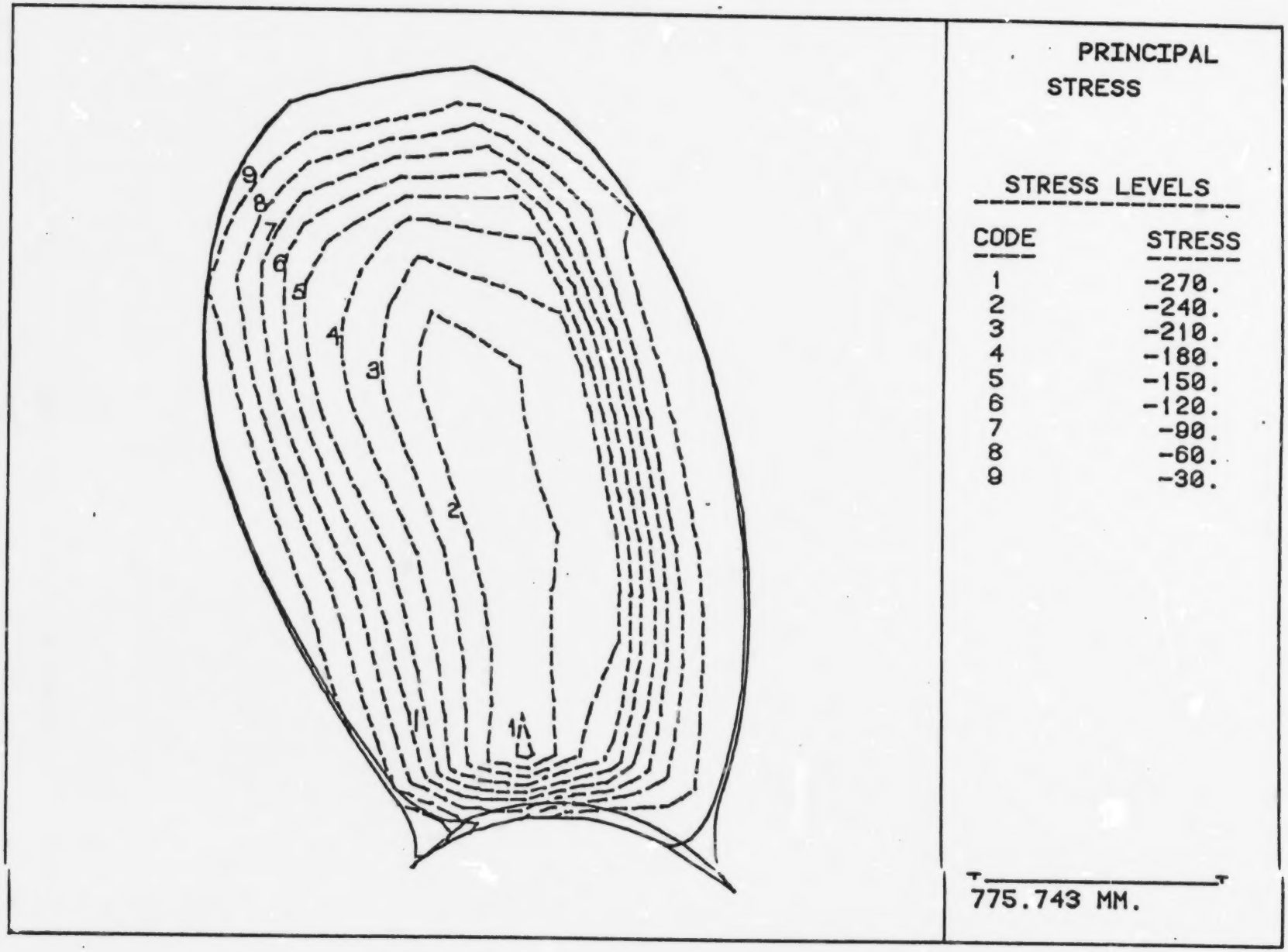


Figure 83: 50% Increase in Blade Diameter, 10% Increase in Hub Diameter - Load Case L1-A

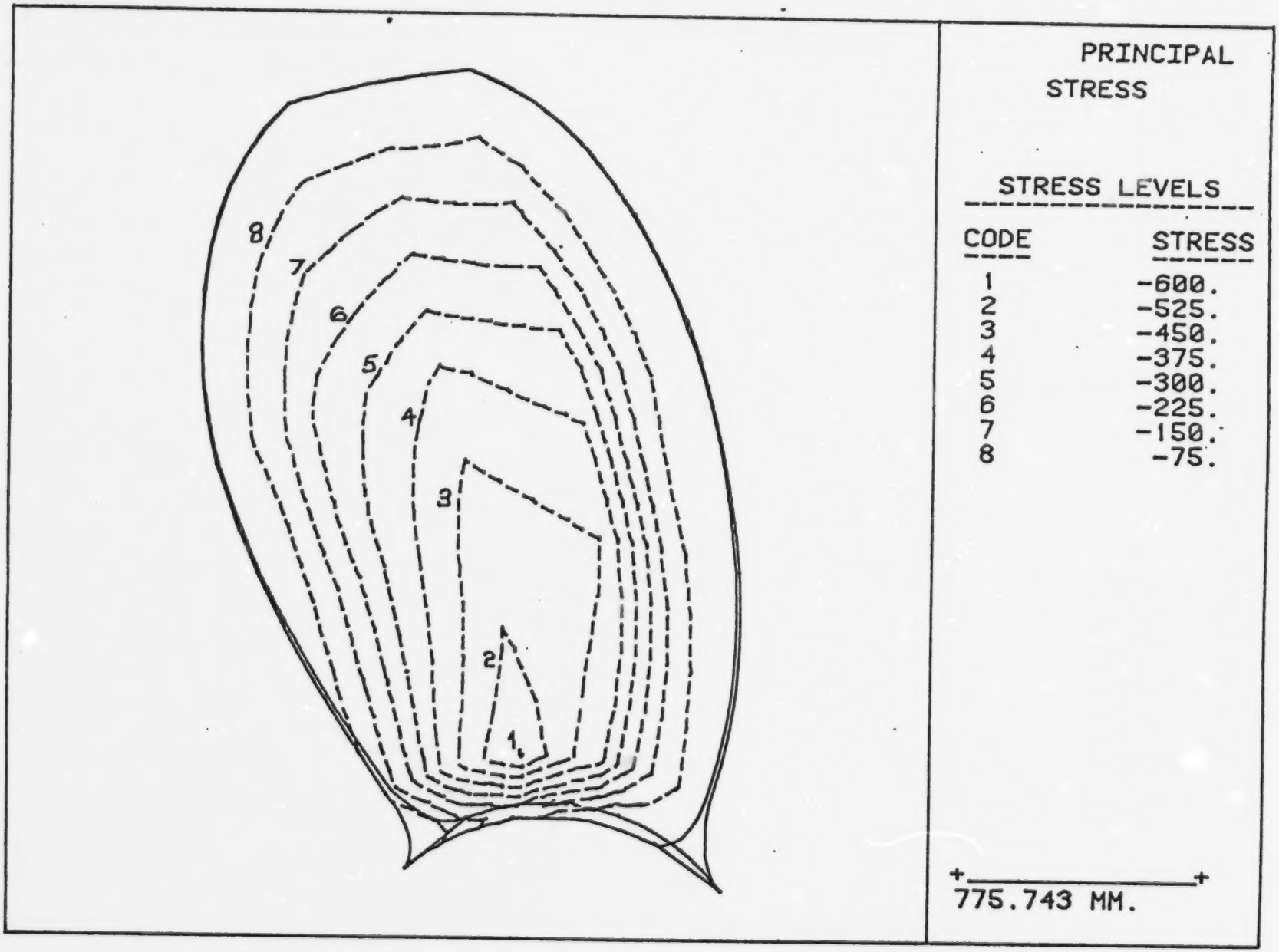


Figure 84: 50% Increase in Blade Diameter, 10% Increase in Hub Diameter - Load Case L2-A

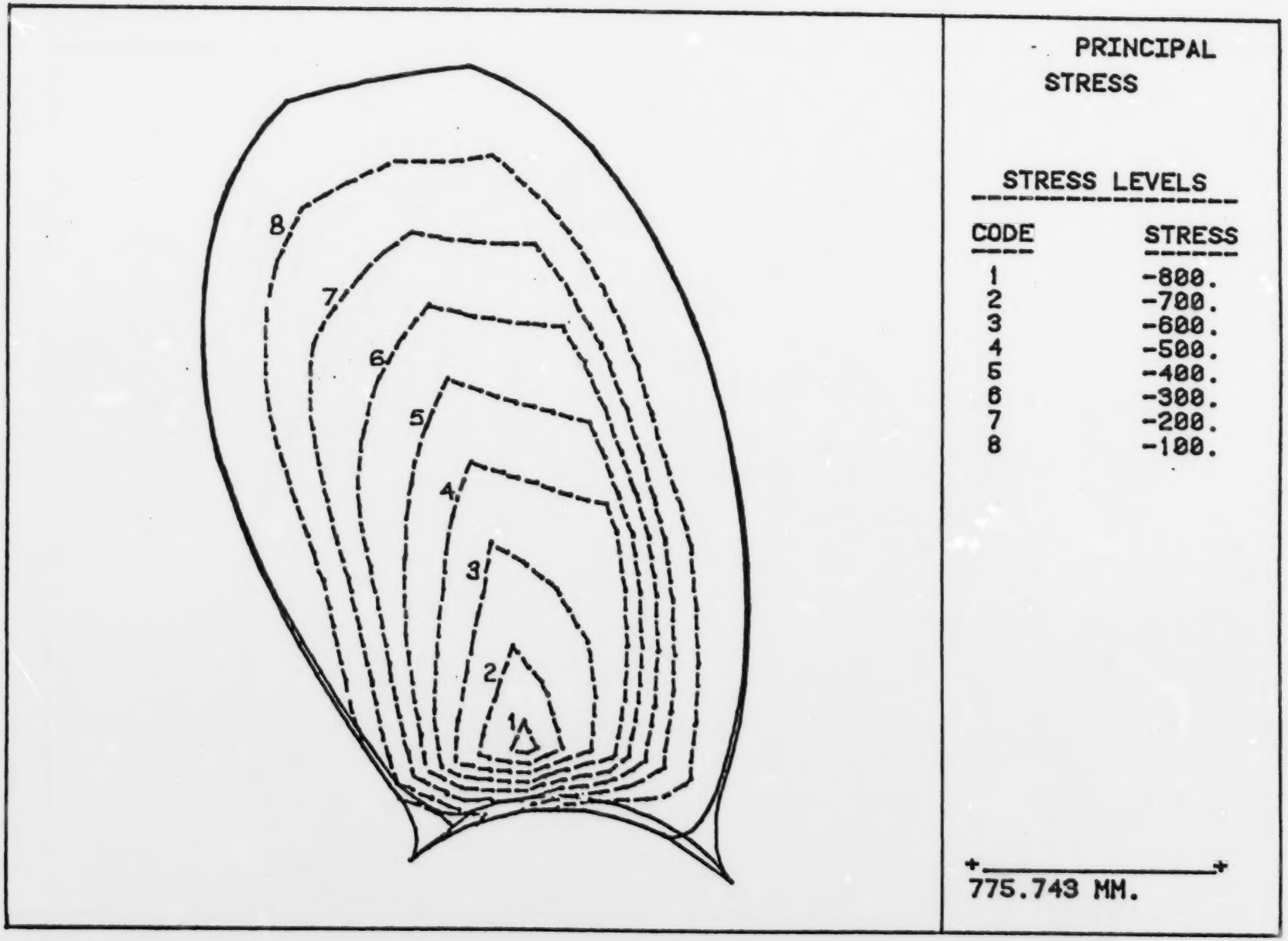


Figure 85: 50% Increase in Blade Diameter, 10% Increase in Hub Diameter - Load Case L3-A

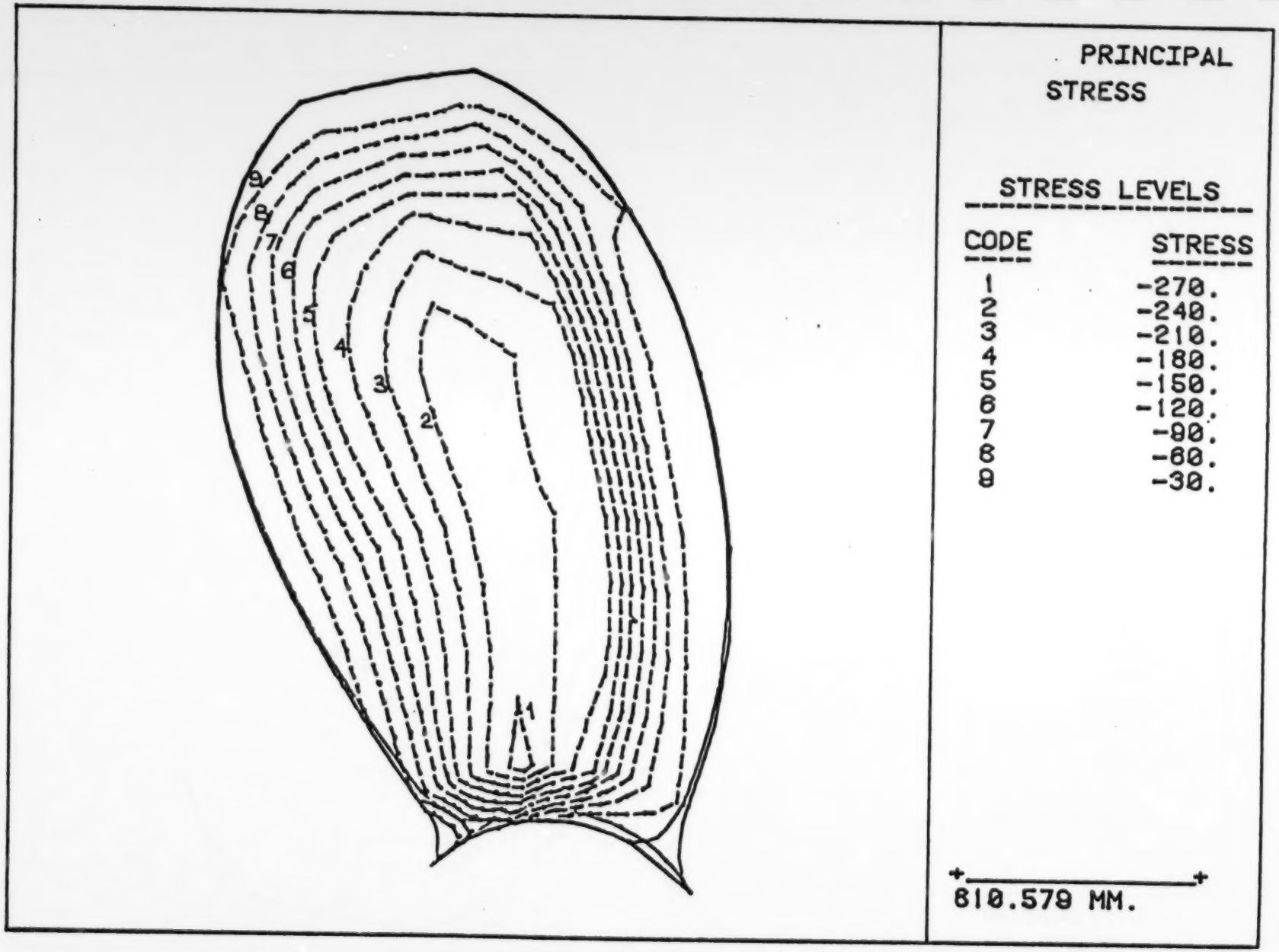


Figure 86: 50% Increase in Blade Diameter, 10% Decrease in Hub Diameter - Load Case L1-A

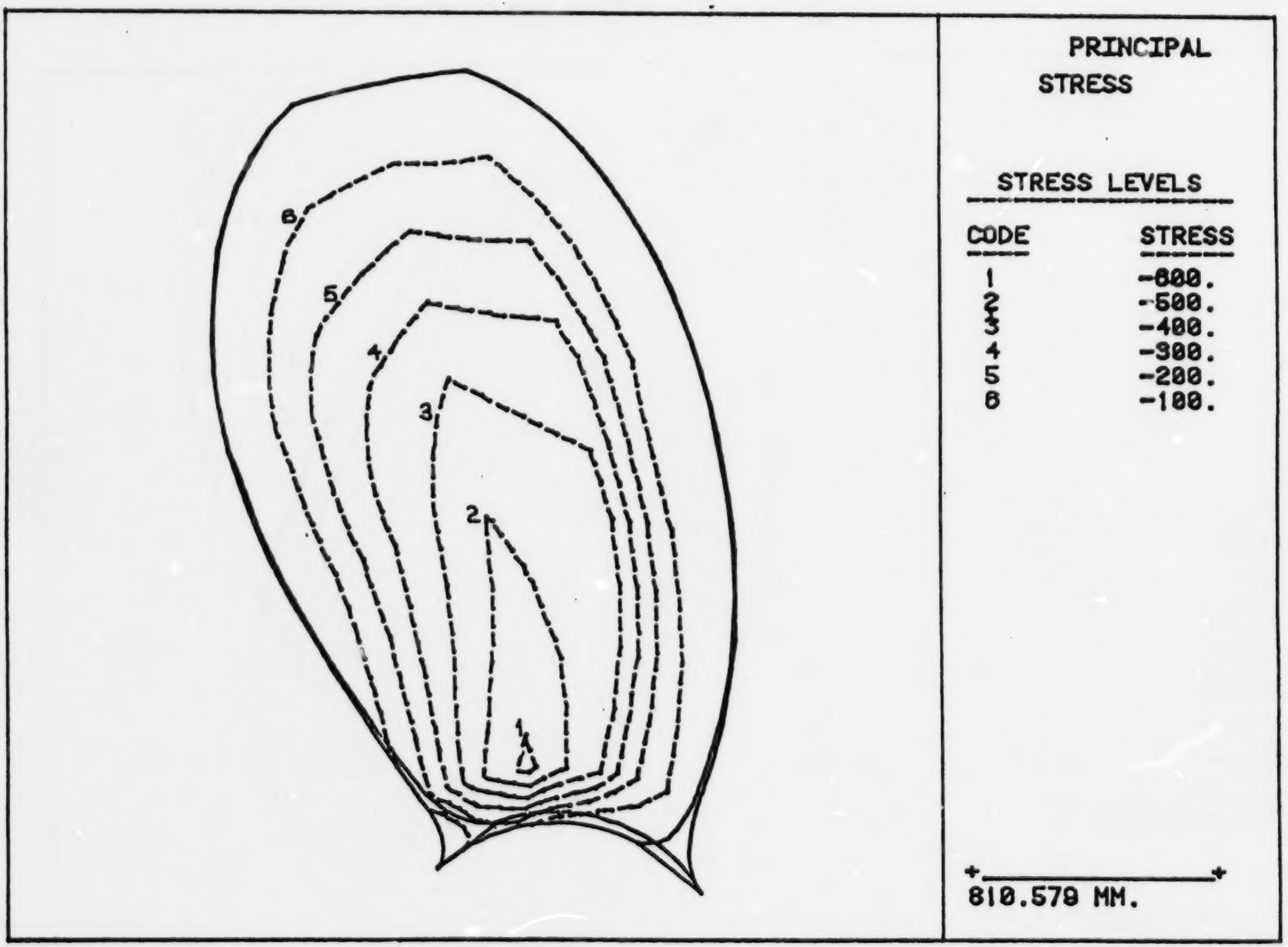


Figure 87: 50% Increase in Blade Diameter, 10% Decrease in Hub Diameter - Load Case L2-A

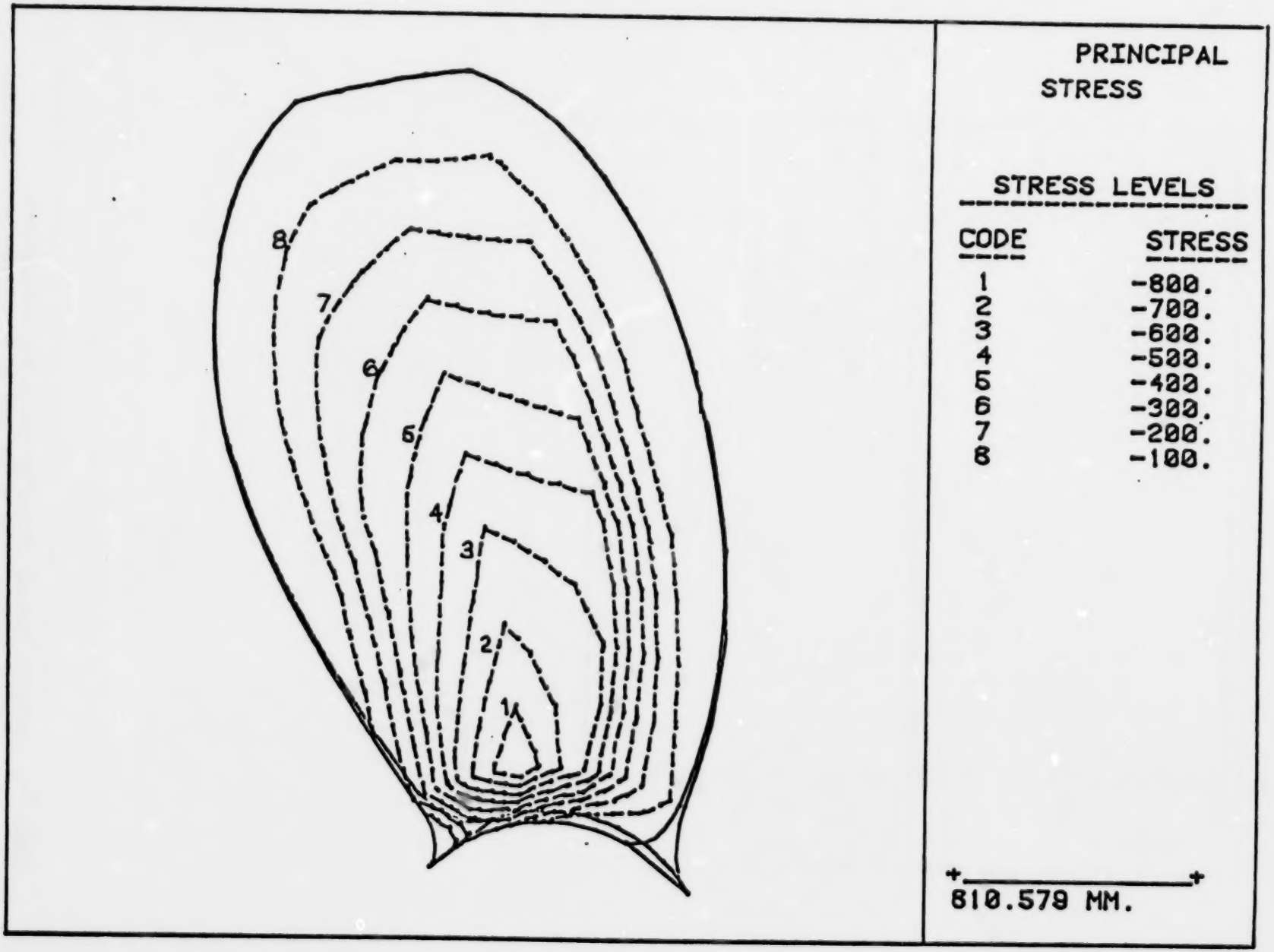


Figure 88: 50% Increase in Blade Diameter, 10% Decrease in Hub Diameter - Load Case L3-A

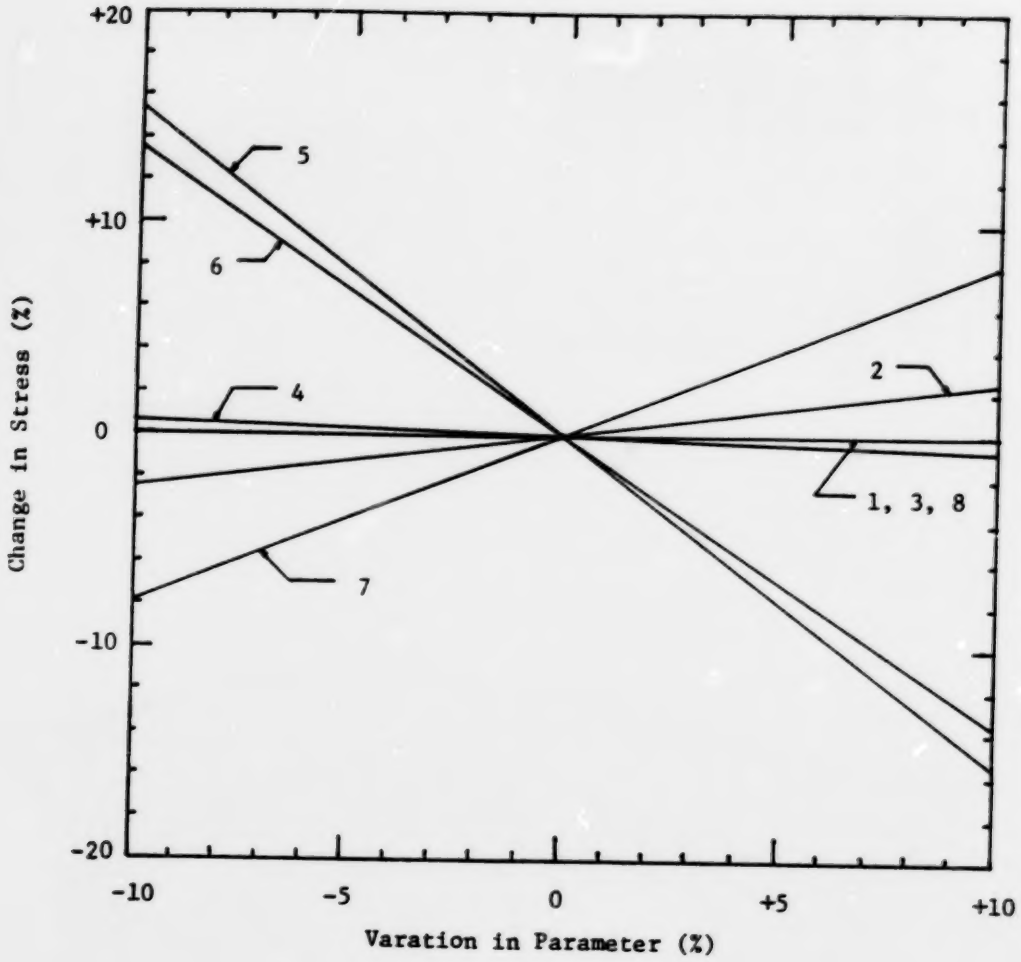


LEGEND:
1 - Rake
2 - Skew
3 - Rotation about spindle axis
4 - P/D ratio
5 - Thickness
6 - Thickness and chord length
7 - Blade diameter
8 - Hub diameter

Figure 89: Change in Maximum Stress vs. Variation in Parameters (Cutting depth of 0.34 meters and uniform Pressure of 1.83 MPa)

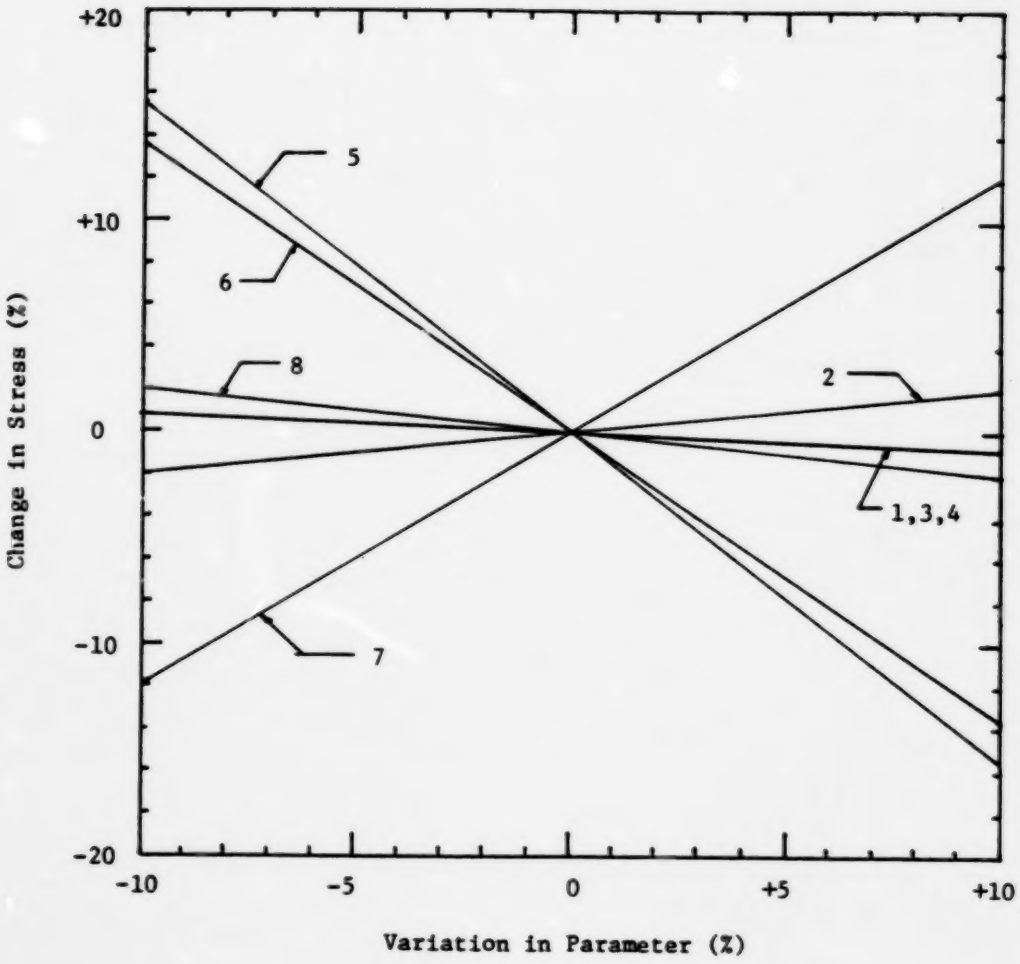


LEGEND:
1 - Rake
2 - Skew
3 - Rotation about spindle axis
4 - P/D ratio
5 - Thickness
6 - Thickness and chord length
7 - Blade diameter
8 - Hub diameter

Figure 90: Change in Maximum Stress vs. Variation in Parameters
(Cutting Depth of 0.67 meters and uniform Pressure of 1.83 MPa)

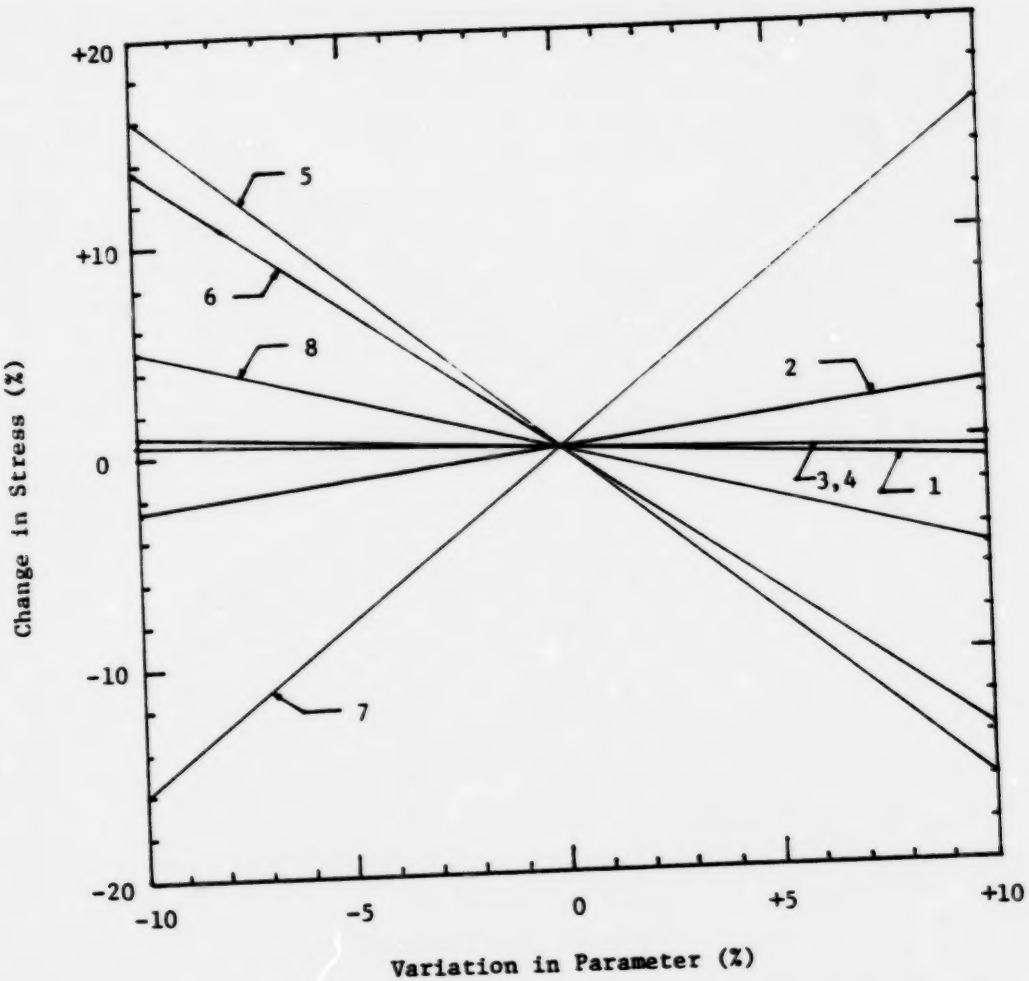


LEGEND:
1 - Rake
2 - Skew
3 - Rotation about spindle axis
4 - P/D ratio
5 - Thickness
6 - Thickness and chord length
7 - Blade diameter
8 - Hub diameter

Figure 91: Change in Maximum Stress vs. Variation in Parameters (Cutting Depth of 1.0 meter and uniform pressure of 1.83 MPa)

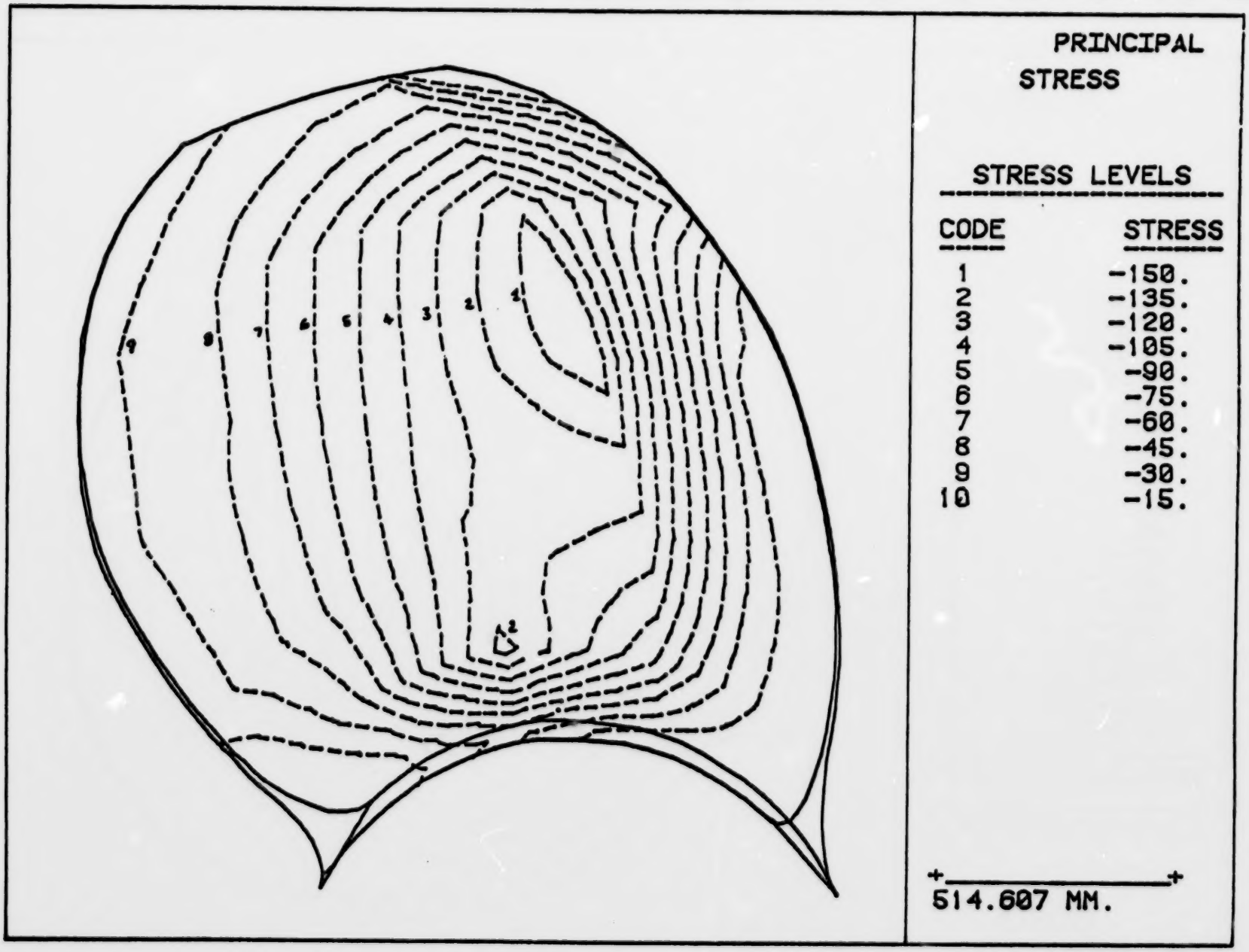


Figure 92: Existing Blade - Load Case L1-B

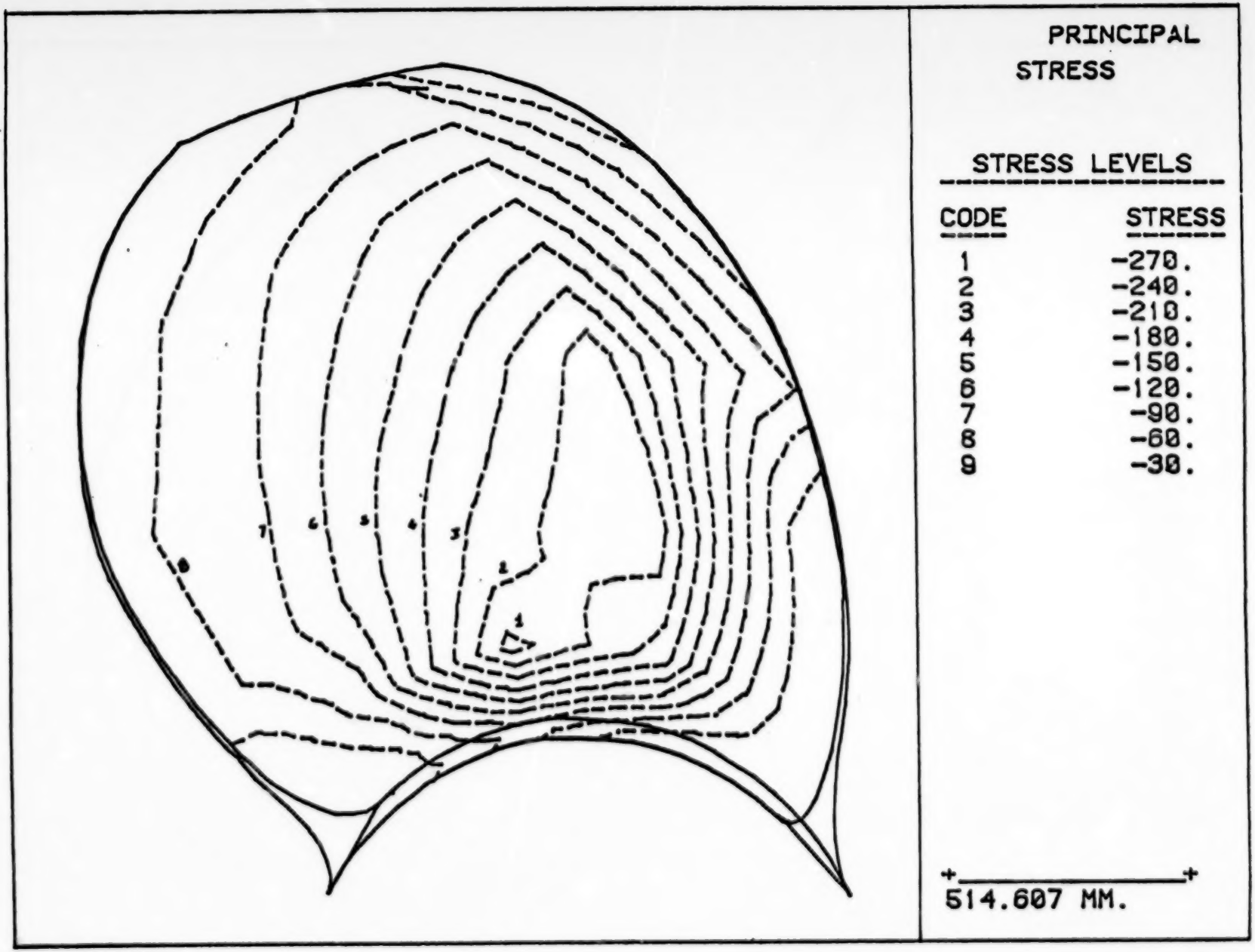


ure E ing ide oad e L

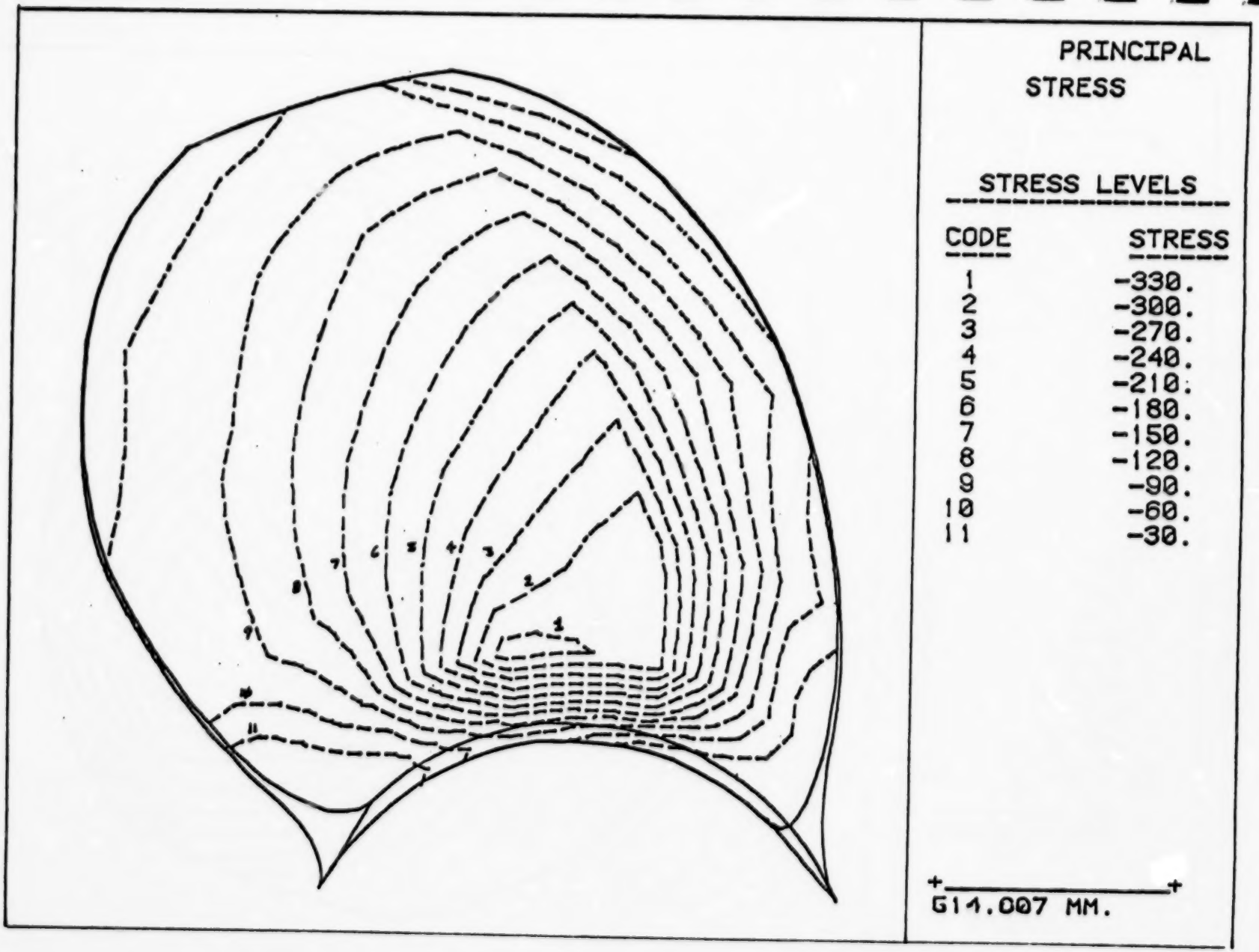


Figure 94: Existing Blade - Load Case L3-B

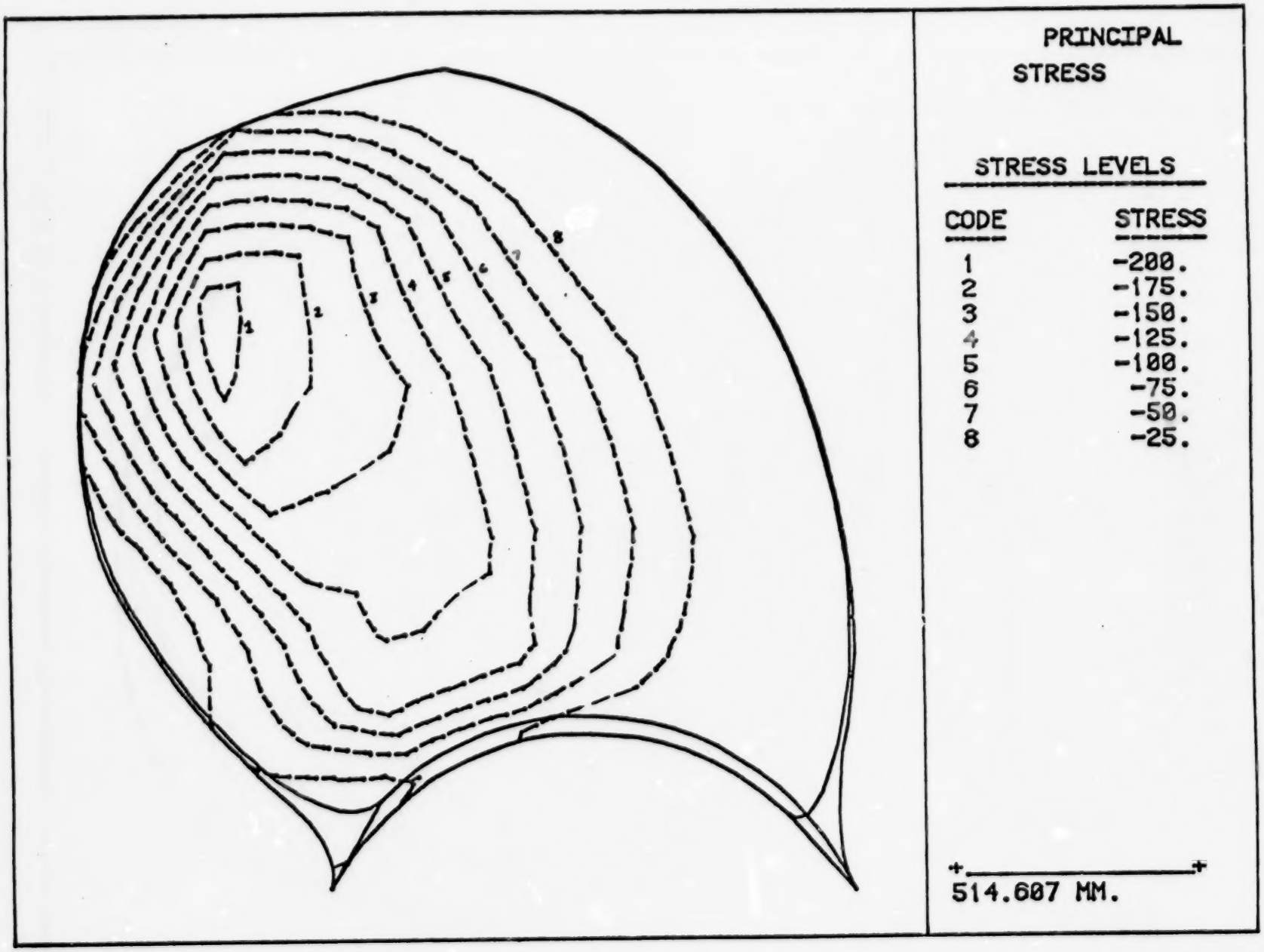


Figure 95: Existing Blade - Load Case L1-C

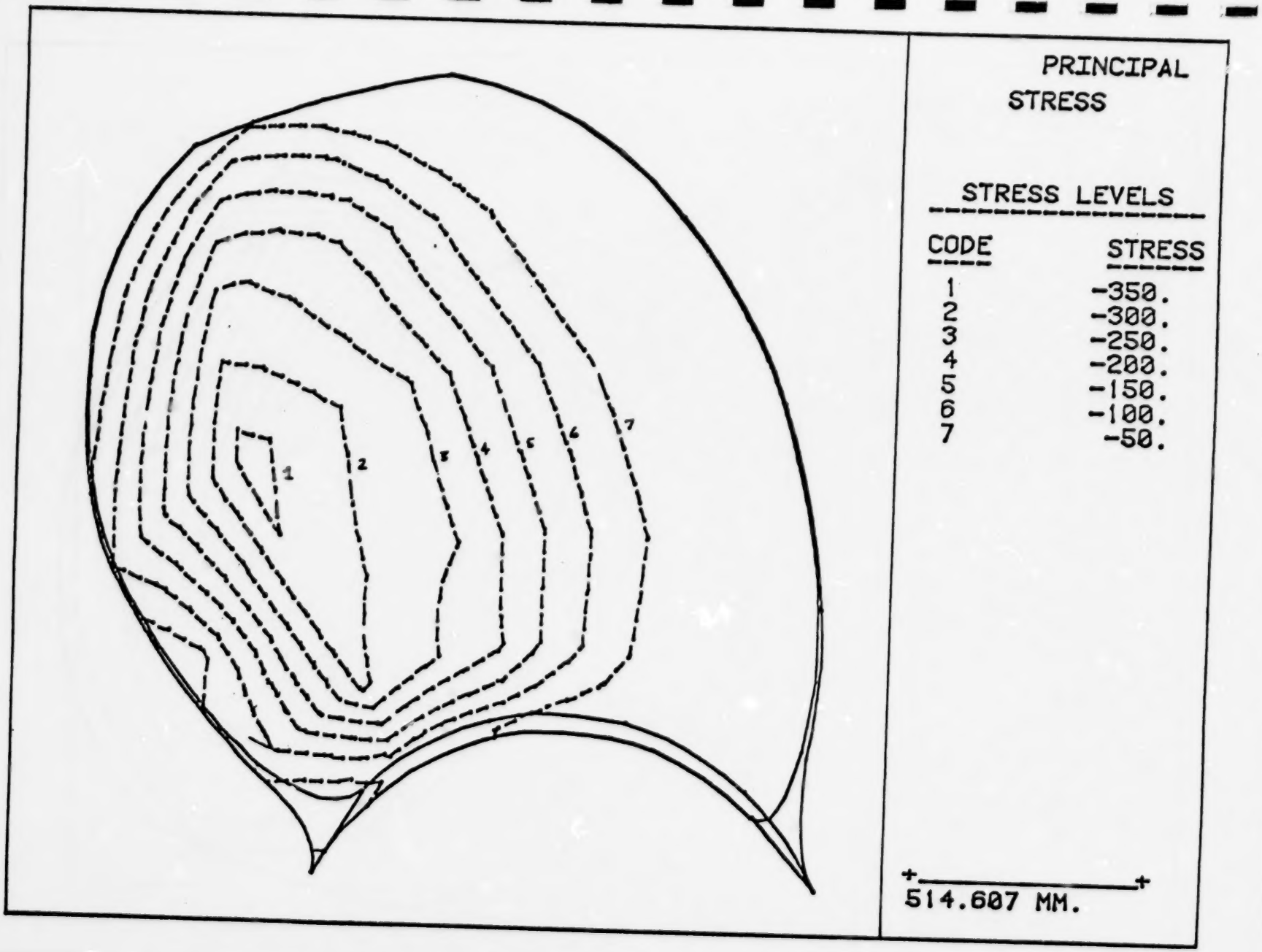


Figure 96: Existing Blade - Load Case L2-C

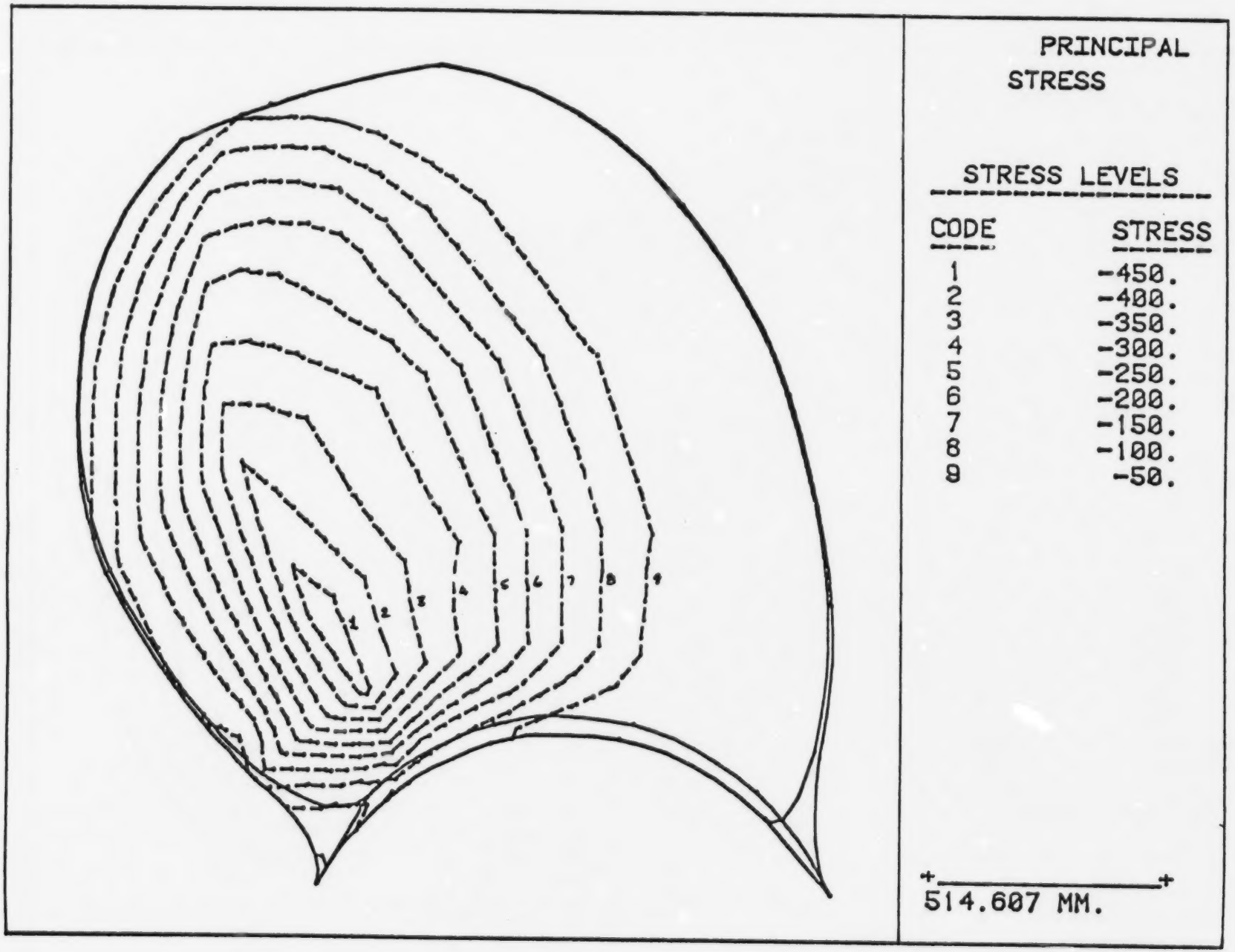
PRINCIPAL
STRESS
STRESS LEVELS
CODE STRESS
1 -450.
2 -400.
3 -350.
4 -300.
5 -250.
6 -200.
7 -150.
8 -100.
9 -50.
514.607 MM.

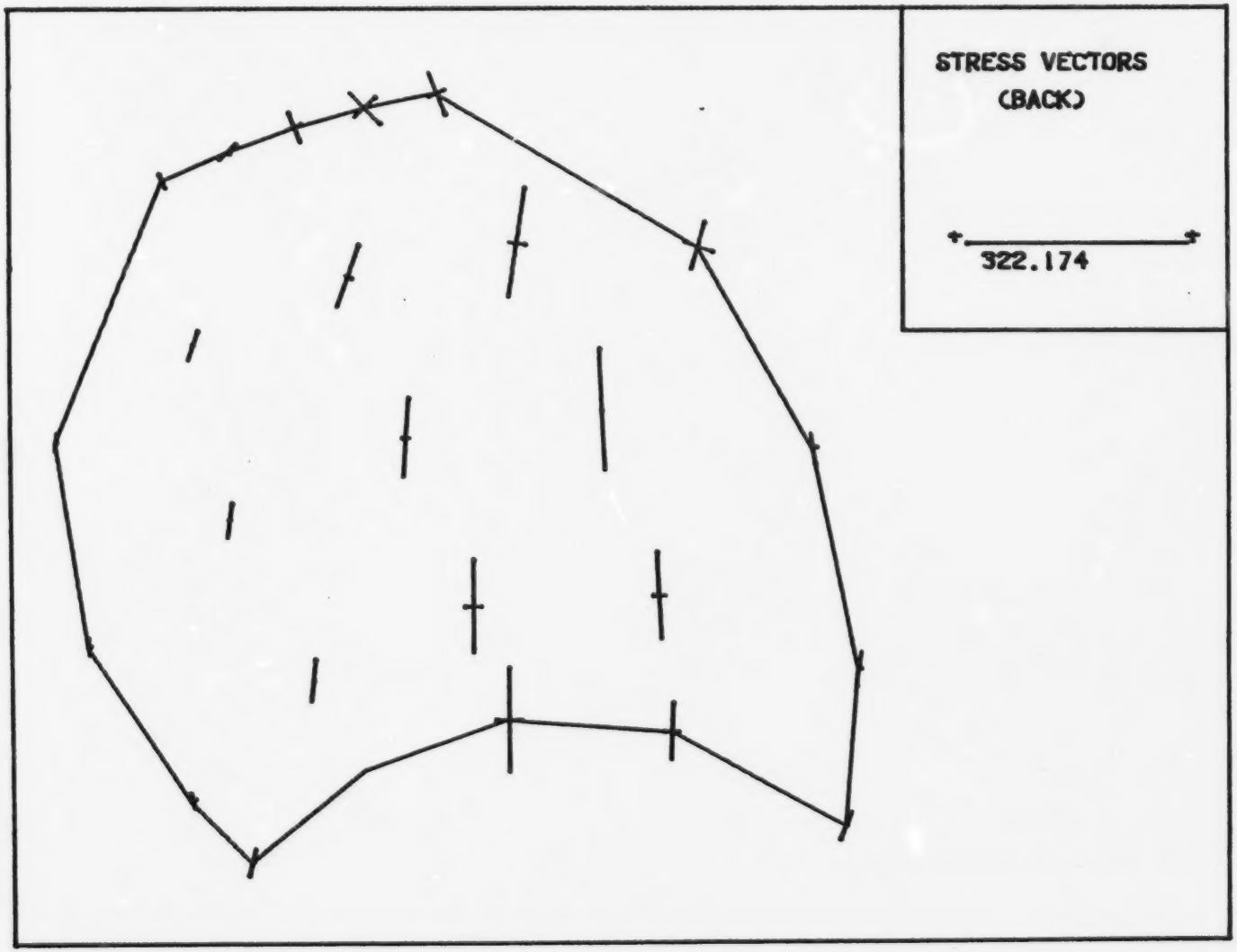


Figure 98: Principal Stress Directions for Load Case L1-B (Existing Blade)

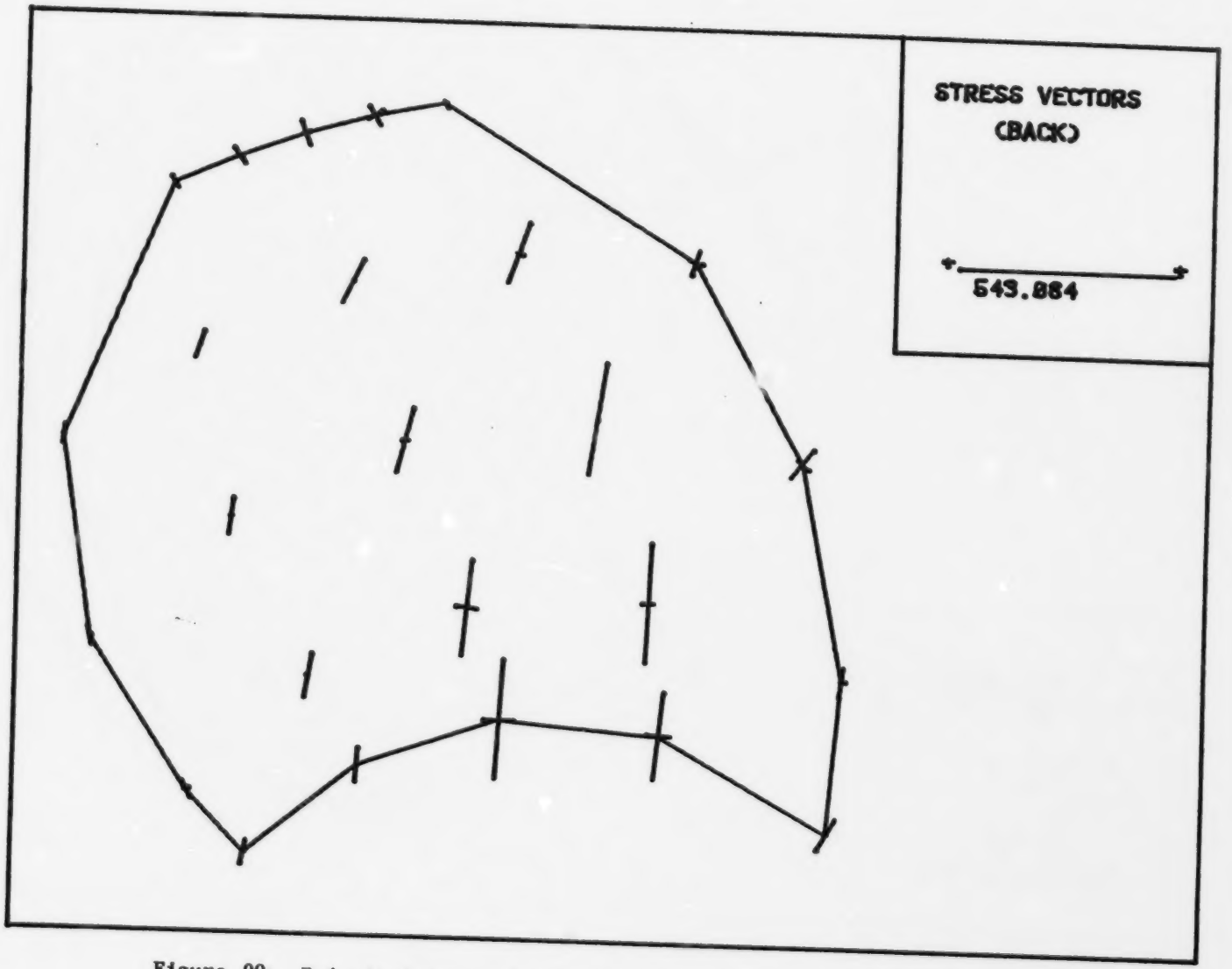


Figure 99: Principal Stress Directions for Load Case L2-B

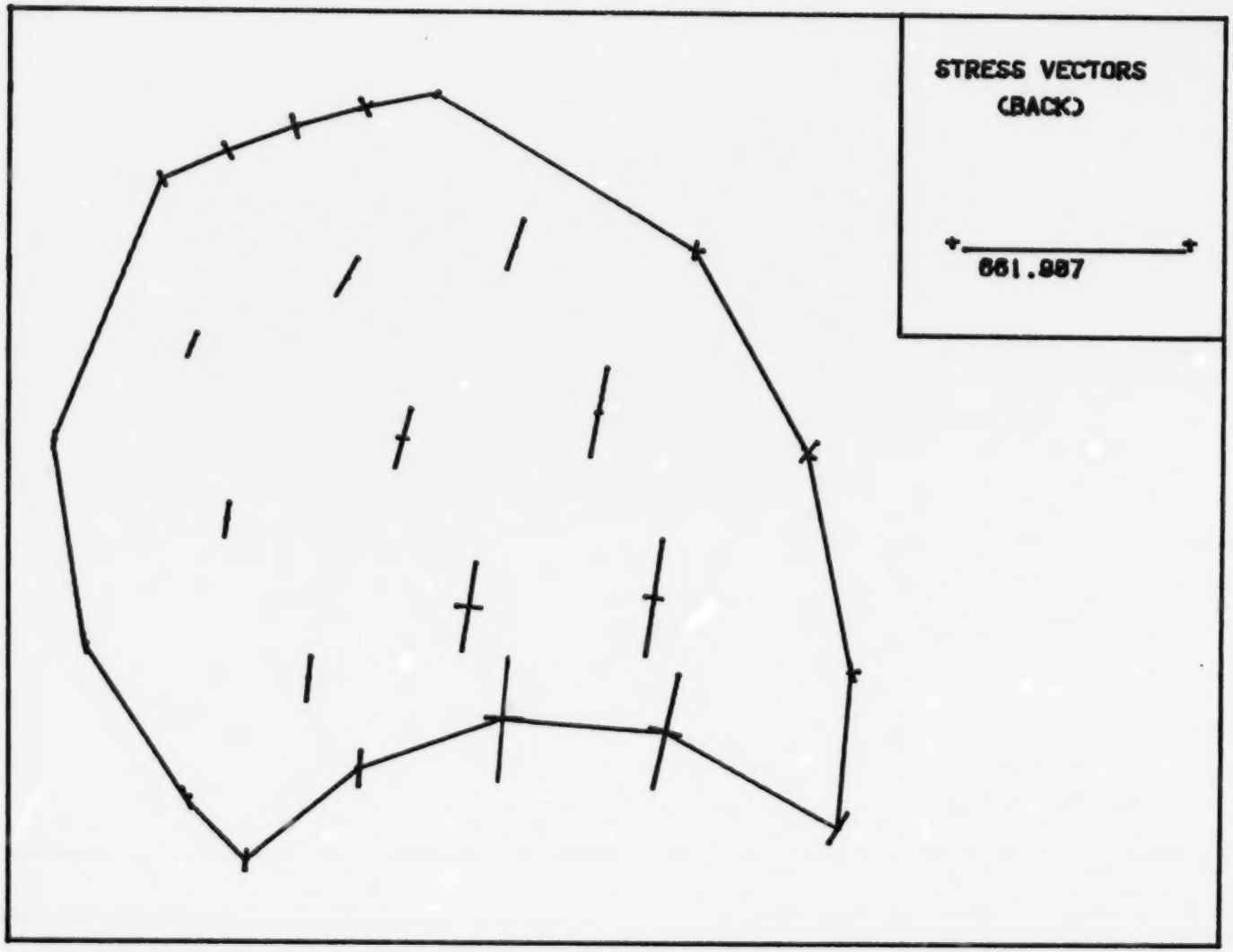


Figure 100: Principal Stress Directions for Load Case L3-B (Existing Blade)

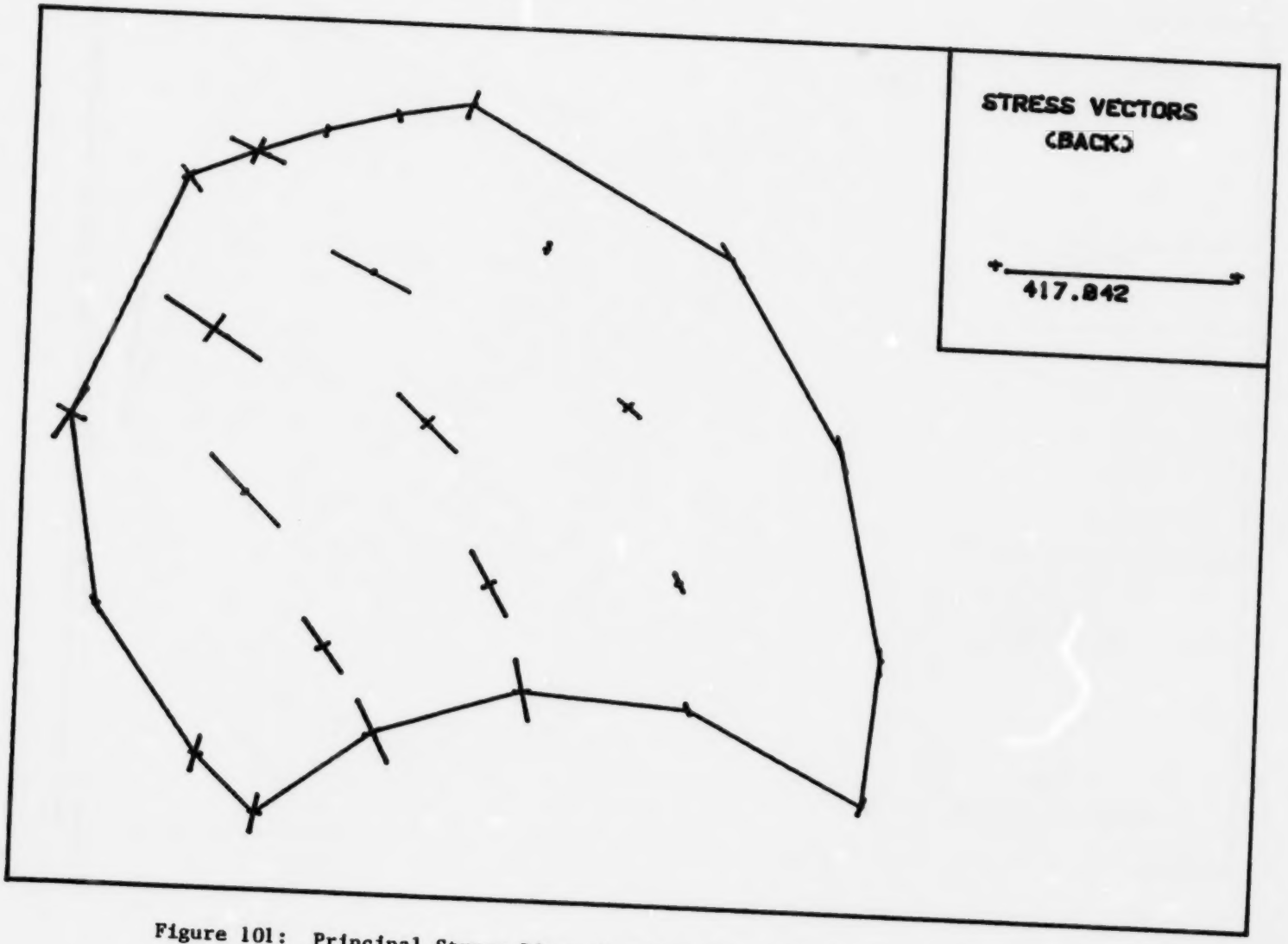


Figure 101: Principal Stress Directions for Load Case L1-C (Existing Blade)

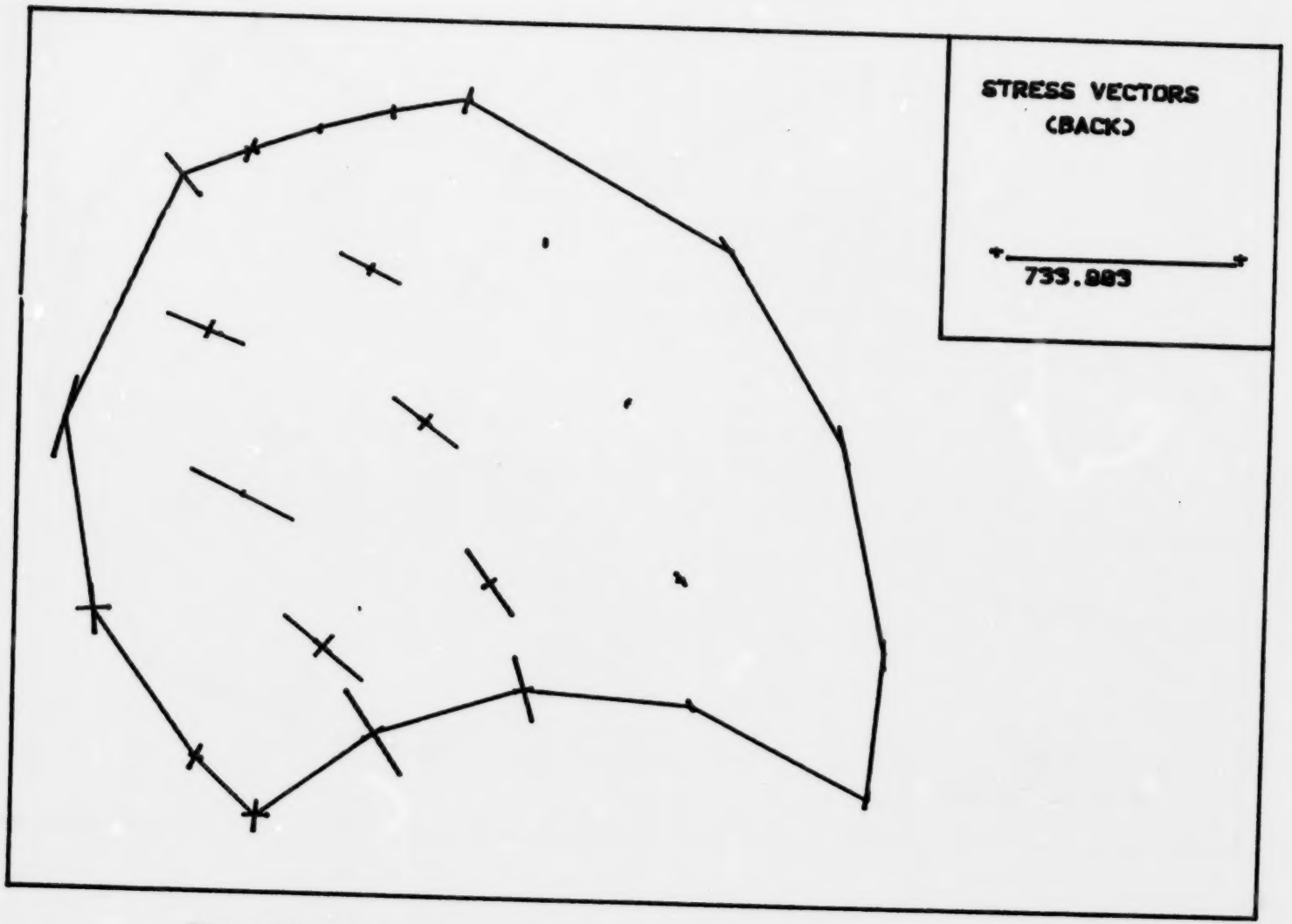


Figure 102: Principal Stress Directions for Load Case L2-C (Existing Blade)

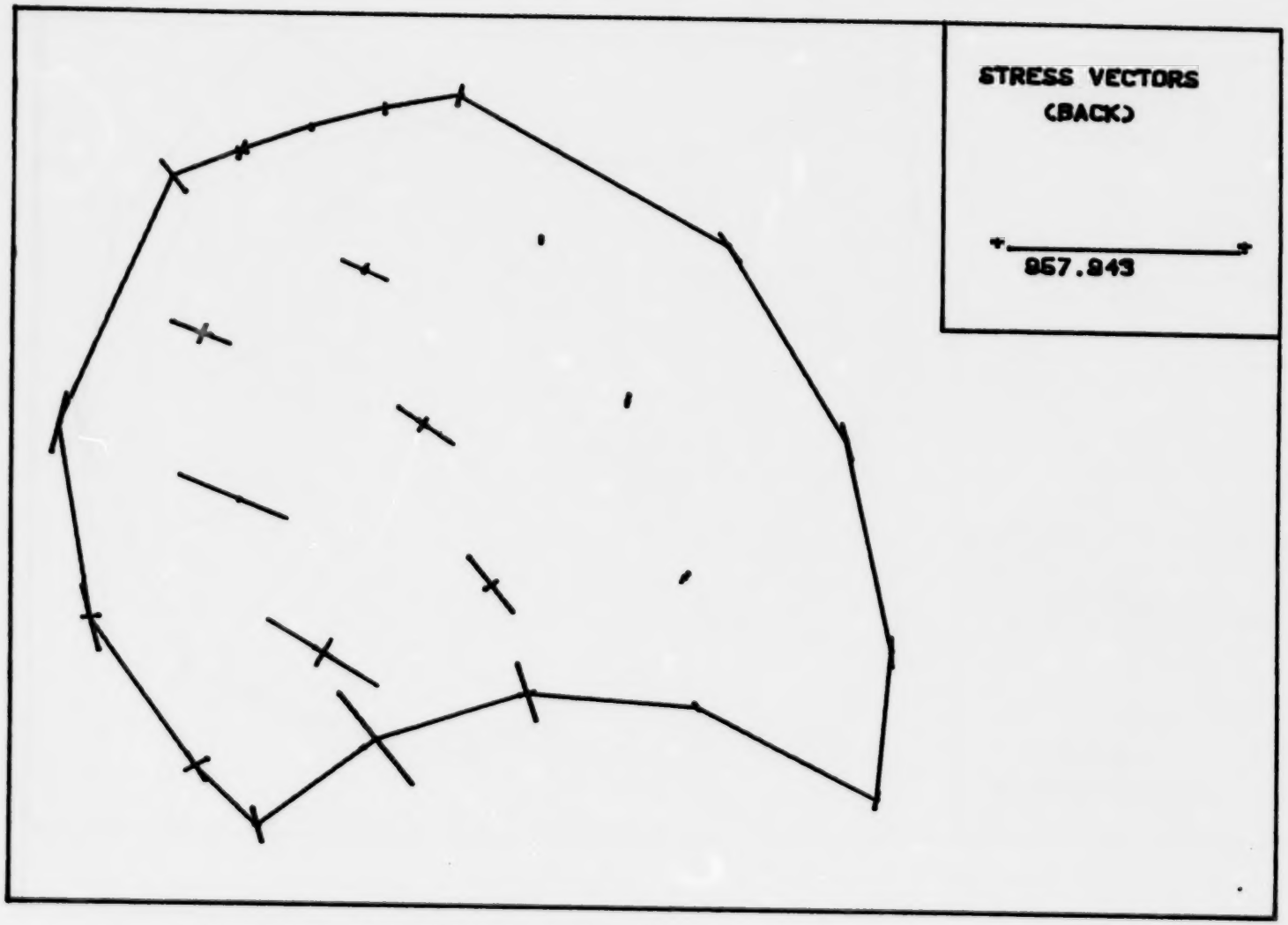


Figure 103: Principal Stress Directions for Load Case L3-C (Existing Blade)

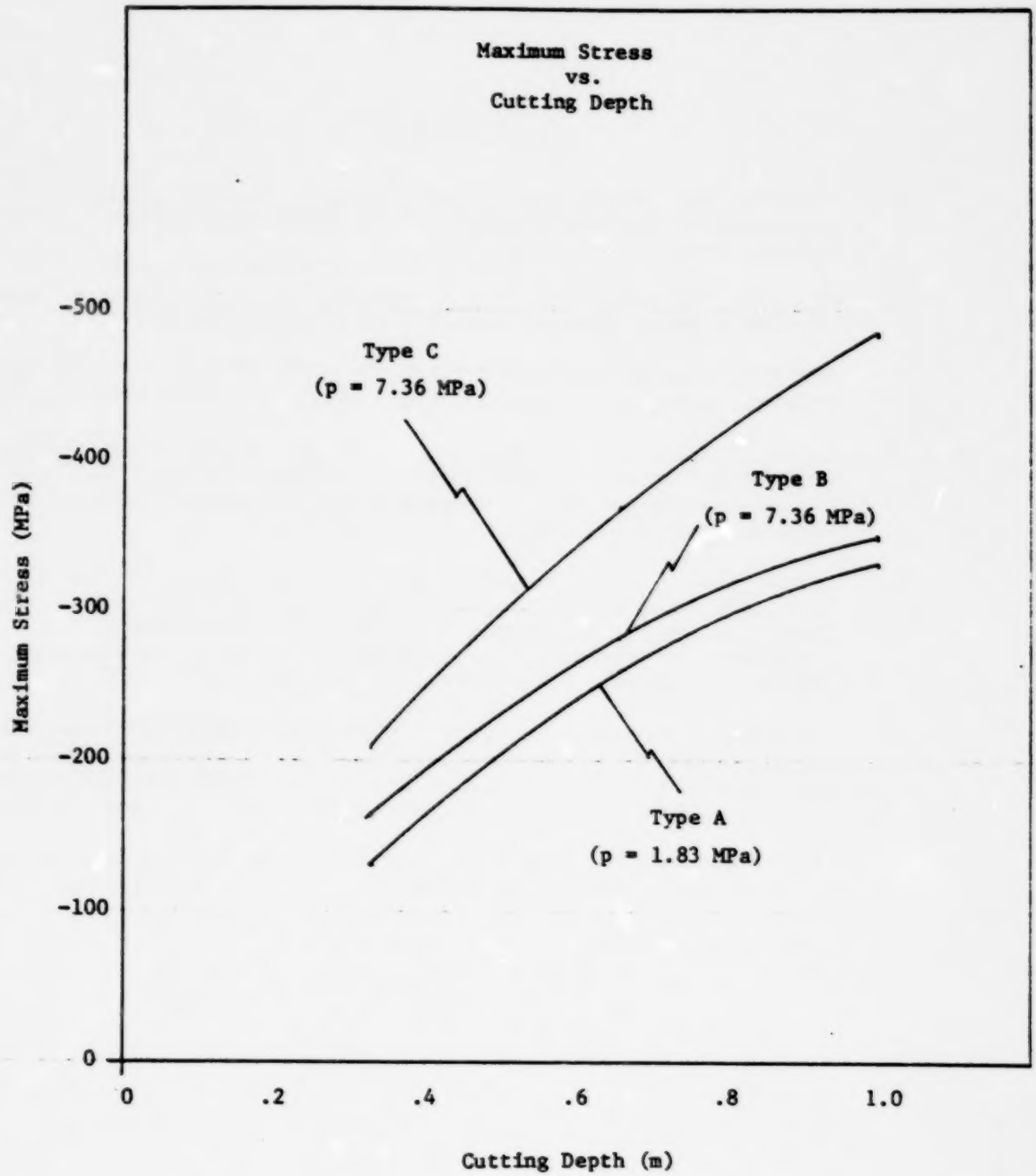


Figure 104: Variation of Maximum Stress with Cutting Depth.

## REFERENCES


1. Propeller/Ice Interaction Finite Element Stress Analysis: An Investigation into the Problem of Predicting Propeller/Ice Interaction Forces; MARTEC Ltd., May, 1982.

2. Propeller Vibration and Stress Analysis by Finite Element Methods (PVAST); Users Manual; MARTEC Ltd., June, 1980.

3. C.C.G.S. Pierre Radison/C.C.G.S. Franklin Propeller; Drawing No. 23809M2, Burrard Drydock Co. Ltd. (1976).

4. Noble, P.G., and V. Bulat. A Study of Ice Class Rules for Propellers, Arctec Canada Limited, Calgary, Alberta and Kanata, Ontario, presented at the Propellers' 81 Symposium, Virginia Beach, Virginia, May 26-27, 1981.

5. Gabel, D.G., M.G. Parsons, and M.J. Kaldjian. Finite Element Structural Analysis for Displacements Occurring in the Hub of a Polar Class Icebreaker Controllable Pitch Propeller Operating in Ice. The University of Michigan, The Department of Naval Architecture and Marine Engineering, Report No. 217, September 1979.

6. Frederking, R., and G. Timco. Mid-winter Mechanical Properties of Ice in the Southern Beaufort Sea, POAC 81, Procedings of the Sixth International Conference on Port and Ocean Engineering Under Arctic Conditions, held at Quebec, Canada on 27-31 July 81, pp. 225-234.

7. Michel, B., and N. Toussaint. Mechanisms and theory of indentation of ice plates. Journal of Glaciology, Vol. 19, No. 81, pp 285-301 (1977).

## NOMENCLATURE

| | |
|---|---|
| X | Cartesian coordinate (positive in starboard direction) |
| Y | Cartesian coordinate (spindle axis) |
| Z | Cartesian coordinate (propeller shaft axis; positive aft) |
| Fx, Fy, Fz | Pressure resultants (forces) in the X, Y and Z directions, respectively |
| Mx, My, Mz | Pressure resultants (moments) about the X, Y and Z axis, respectively |
| P | Pitch |
| D | Propeller diameter |
| R | Propeller radius |
| p | Pressure applied to blade |
| d | Cutting depth |

POOR

QUALITY

ORIGINAL